UNIVERSITÀ DEGLI STUDI DI FIRENZE

DIPARTIMENTO DI SCIENZE E TECNOLOGIE AMBIENTALI E FORESTALI

DOTTORATO IN SCIENZE GENETICHE

XXII CICLO (2007-2009)

SSD BIO/18

STUDIES ON CATALYTIC RNA MOLECULES RELEVANT TO THE RNA WORLD HYPOTHESIS

GIULIA TALINI

Tutor	Coordinatore
Prof. Enzo Gallori	Prof. Raffaello Giannini

Alla mia famiglia

Table of contents

1. Introduction

1.1. RNA world hypothesis

The central dogma of molecular biology (Crick, 1970) states that information is transferred from DNA to proteins through an RNA intermediate, with the possibility of reverse transfer from RNA to DNA (added after the discovery of reverse transcriptase enzyme). This dogma could become a paradox in terms of the origin of life. Indeed, there is a crucial feedback in this system: to replicate and transcribe DNA, functionally active proteins are required, but production of these proteins requires accurate replication, transcription, and translation of nucleic acids. In other words the replication of nucleic acids depends on protein enzyme activities and viceversa. Thus it is logic to wonder what came first, the DNA or the protein, the gene or the product: it is the so-called "egg and chicken paradox".

It is clear that the only mechanism that can evolve a complex biochemical system from simpler ones is the natural selection through replication and mutations. Based on this idea, an autoreplicating polymer was required in the primordial era to transfer the genetic information and to evolve through a Darwinian process. The only polymers with these characteristics are nucleic acids. Watson-Crick base-pairing provided a very plausible mechanism by which a polynucleotide could direct the synthesis of its complement from mononucleotides or short oligonucleotides, whereas no equivalent mechanism was known for the replication of a polypeptide.

However other theories have been proposed. For instance a 'Protein World' (Lee *et al.*, 1996; Oparin, 1965), for which the first polymers were made of amino acids, and proteins preceded RNA and DNA in the rise of complexity during evolution; a 'Lipid World' (Luisi and Varela, 1989; Segre *et al.*, 2001), that would have borne from the spontaneous aggregation of amphiphilic molecules in reproducing catalytic micelles (Bachmann *et al.*, 1991) or vescicles (Walde *et al.*, 2002). Many examples of other self-replicating systems have been suggested, like clay minerals (Cairns-Smith, 1966), hexanucleotides (Günter von, 1986), and small organic molecules with non biological base-pairs (Nelsestuen, 1980; Tjivikua *et al.*, 2002).

In the years 1967-1968, (Crick, 1968; Orgel, 1968; Woese, 1967), independently, proposed RNA as the best candidate for the central role in primordial replicating systems.

The discovery of ribozymes, RNA molecules with catalytic activity (Cech *et al.*, 1981; Guerrier-Takada *et al.*, 1983), let to an increase in the interest in the idea that an ‘’RNA-world” (Gilbert, 1986) preceded the DNA/RNA/PROTEIN world. In fact, RNA contains in itself both of the two functions performed separately by DNA and proteins in present cells: the ability to transfer genetic information (DNA), and to carry out catalytic activity (proteins). These characteristics make RNA an exceptional molecule, the most plausible molecule that the earlier form of life on earth could use as the only genetically encoded component of biological catalysis (Gesteland, 2006).

In the last years, biochemists have come to appreciate the remarkable structural and functional versatility of RNA. Despite containing only four different chemical subunits, RNA folds into a variety of complex tertiary structures, analogous to structured proteins, and catalyses a broad range of chemical transformations. The ability to assume particular structures is probably the secret of the catalytic activity of RNA.

1.2. Ribozymes

The discovery of a vast repertory of naturally occurring ribozymes in contemporary cells, and the crucial importance of their reactions, largely lend support to the credibility of an RNA World and to speculations that nucleic acids were the original biocatalysts (Gesteland, 2006). Roles for RNA catalysis in the modern protein world can be found in the regulation of gene expression and in protein synthesis (Nissen *et al.*, 2000; Teixeira *et al.*, 2004; Winkler *et al.*, 2004), demonstrating that RNA plays a central role in all fundamental processes in present-day cells. All these findings strongly suggest not only that an RNA World could have existed, but also that it still lurks within modern living forms.

Some of these ribozymes, the so called hammerhead ribozymes, are also found in viroids, the smallest RNA plant pathogens known (see section 1.3). These

catalytic RNA molecules are considered relics of a RNA world (Diener, 2003; Flores *et al.*, 2005; Tabler and Tsagris, 2004).

The popularity of the RNA world hypothesis, has in turn, stimulated ribozyme research, aimed in large part at testing the feasibility of various RNA-based catalytic activities. The main methodology used to develop ribozymes with desired activities is *in vitro* selection. SELEX ("Systematic Evolution of Ligands by EXponential amplification") mimics the Darwinian evolution of ribozymes thought to have occurred in the primeval RNA World (Johnston *et al.*, 2001). This technique, described primarily in 1990 (Ellington and Szostak, 1990; Tuerk and Gold, 1990), uses large populations of random RNA or DNA sequences as raw material for the selection of rare functional molecules.

1.2.1. Natural ribozymes

According to the RNA World hypothesis, "ancient" RNA should be able to encode and replicate faithfully genetic information as well as to catalyze the synthesis of essential chemical building blocks.

Probably during evolution these primitive RNA-based metabolisms needed more sophisticated biocatalysts stimulating the transition from primordial RNA catalysis to protein-based enzymatic catalysis.

It is possible that the vast number of ribozymes in extant viruses and organisms ranging from bacteria to humans may derive from such an RNA-dominated era (Gesteland, 2006) and can be considered "relics" of the ancient RNA world. If true, these molecules could reflect their evolutionary origin and open new windows on the ancient world. Therefore by studying natural ribozymes it is possible to retrace the evolutionary steps leading to modern-day cells and to the distinction between the roles of DNA, RNA and proteins that are known today.

Certainly, in the steps that have led to the modern-day world, these molecules have adapted to new strategies. This made the ancient ribozymes modify and lose some of their primordial functions on the basis of new more complex and evolved mechanisms (interactions with protein, DNA, etc.). Nevertheless some functions of the ancient ribozymes have been maintained, which, if studied in depth, could give us an idea of the activities that the "primitive" RNA carried out.

Since the discovery of ribozymes (Cech *et al.*, 1981; Guerrier-Takada *et al.*, 1983), numerous natural RNA motifs endowed with catalytic activity have been

described. With the only exception of the ribosome, whose peptidyl transferase activity keeps it distinct from other ribozymes, naturally occurring ribozymes carry out a phosphoryl transfer, catalyzing the cleavage or ligation of the RNA phosphodiester backbone.

Transfer of phosphate group can be catalyzed by ribozymes through two types of chemical reactions (Fig. 1.1) differing in their products. On this basis, natural ribozymes can be classified into two different groups, i.e. 1) the self-cleaving RNAs, which include the hammerhead (Blount and Uhlenbeck, 2005), hairpin (Fedor, 2000), hepatitis delta virus (HDV) (Shih and Been, 2002), Varkud satellite (VS) (Lilley, 2004) and *glmS* ribozymes (Winkler *et al.*, 2004); and 2) the self-splicing ribozymes, which are the group I and II introns, the Group I-like cleavage ribozyme (GIR1 branching ribozyme (Pyle, 2005) and ribonuclease (RNase) P (Table 1.1).

Self-cleaving ribozymes catalyze a reversible phosphodiester cleavage reaction yielding a termini 5'-hydroxyl and a 2′–3′-cyclic-phosphate group; such ribozymes use an internal nucleophile, the 2'-oxygen of the ribose moiety at the cleavage site (Fig. 1.1. a). Self-splicing ribozymes catalyze phosphodiester cleavage and ligation reactions that produce 5′-phosphate and 3′-hydroxyl termini; as opposed to the first group, the second group accepts external nucleophiles (Fig. 1.1. b).

Another class of natural ribozymes are the mammalian ribozymes (Table 1.1), here kept separated from the others ribozymes because of their peculiarity to be the only ones found in mammals. This group comprises HDV and two other ribozymes recently discovered: the co-transcriptional cleavage (CoTC) ribozyme (Teixeira *et al.*, 2004) and the cytoplasmatic polyadenylation element-binding protein 3 (CPEB3) ribozyme (Salehi-Ashtiani *et al.*, 2006). The CoTC ribozyme catalyzes a reaction that produce 3'-OH and 5'-P ends, as the self-splicing ribozymes. On the other hand, the CPEB3 ribozyme is structurally and biochemically related to the HDV ribozyme, and its self-cleaving chemistry proceeds as that of self-cleaving ribozymes.

The features, the catalytic strategies, and the mechanisms of cleavage of the majority of naturally occurring ribozymes have been discussed in detail in recent reviews (Cochrane and Strobel, 2008; Fedor and Williamson, 2005).

Table 1.1 summarizes the main characteristics of all natural ribozymes.

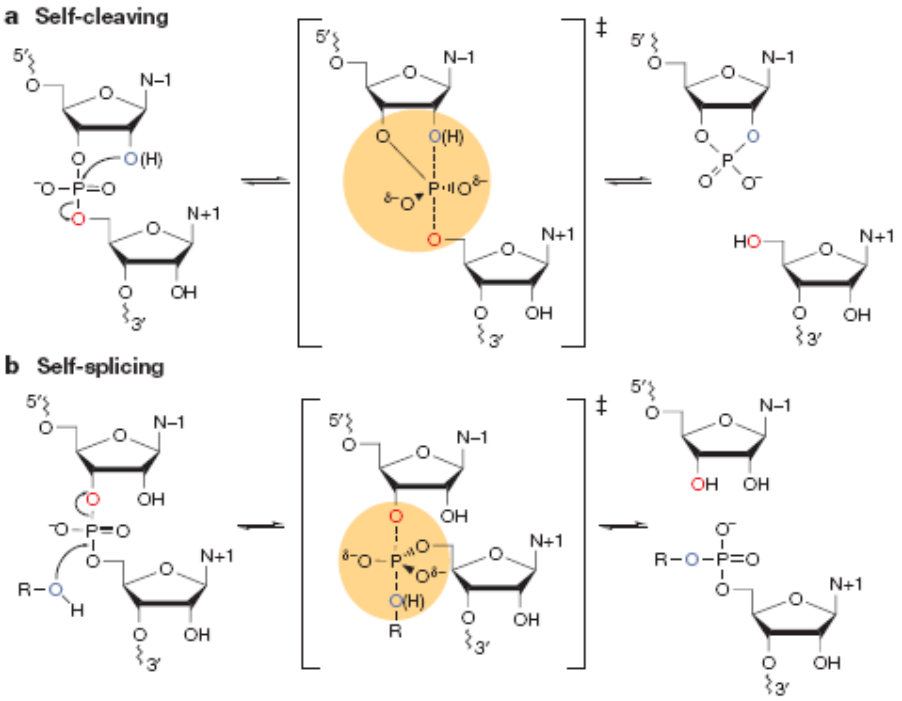

Fig. 1.1. The reactions of self-cleaving (a) and self-splicing (b) ribozymes

a) **Self-cleaving RNAs catalyze a reversible cleavage reaction in which the 2' hydroxyl is the attacking nucleophile (part a, blue) and the bridging 5' oxygen (part a, red) is the leaving group.**
b) **Phosphodiester-cleavage reactions mediated by RNase P and self-splicing introns involve the SN2-type in-line attack of an exogenous nucleophile on phosphorus. The three possible nucleophiles for introns and RNase P are represented by ROH in part b, and the oxygen nucleophile is in blue. The bridging 3' oxygen (part b, red) is the leaving group.**

The symbol ‡ indicates the transition states.

Reaction	Class	Members	Main functions	Distribution
Phosphoryl transferase	Self-cleaving Ribozymes	Hammerhead	Processing of multimeric transcripts during rolling-circle replication	Viroids, plant viral satellite RNA, eukaryotes (plants, crickets, amphibians, schistosomes) *In the genomic RNA of four different plant viroids, in nine satellite RNAs, in a circular RNA of cherry and in a retroviroid-like element of carnation plants. Three active hammerhead domains isolated from animal RNAs: a transcript from a satellite DNA of newts, the RNA encoded in Schistosoma satellite DNA and in a DNA satellite from Dolichopoda cave crickets*
Phosphoryl transferase	Self-cleaving Ribozymes	Hairpin	id	RNA satellites of plant viruses *In the minus strand of the tobacco ringspot virus satellite RNA, in chicory yellow mottle virus, and arabis mosaic virus*
Phosphoryl transferase	Self-cleaving Ribozymes	VS	id	Satellite RNA of *Neurospora* spp. mitochondria
Phosphoryl transferase	Self-cleaving Ribozymes	HDV	id	Human *In the genomic and antigenomic forms of HDV, a small satellite RNA virus that superinfects patients with hepatitis B, increasing the disease symptoms of HBV (Hepatitis B virus)*
Phosphoryl transferase	Self-cleaving Ribozymes	*glmS*	Gene control (cleavage of the mRNA of the *glmS* gene in Gram-positive bacteria)	Gram-positive bacteria *Part of the 5' UTR (5' untranslated region) of the mRNA that encodes glucosamine-6-phosphate (GlcN6P) synthetase*
Phosphoryl transferase	Self-splicing Ribozymes	Group I Introns	Self-splicing	Organelles (fungi, plants, protists), bacteria, bacteriophages, mitochondria (animals)
Phosphoryl transferase	Self-splicing Ribozymes	Group II Introns	Self-splicing	Organelles (fungi, plants, protists), bacteria, archaea
Phosphoryl transferase	Self-splicing Ribozymes	GIR1	Cleavage of the 5' end of the I-*Dir*I (*Didymium iridis*) mRNA	Myxomycete *Didymium iridis.*
Phosphoryl transferase	Self-splicing Ribozymes	RNase P	tRNA processing	*Archaea, Bacteria* and *Eukarya*
Phosphoryl transferase	Mammalian Ribozymes	HDV	id	id
Phosphoryl transferase	Mammalian Ribozymes	CoTC	Transcription termination	Humans *3' flanking region of the β-globine gene*
Phosphoryl transferase	Mammalian Ribozymes	CPEB3	Splicing regulation	Mammals *On the second intron of the CPEB3 gene, which belongs to a family of genes regulating messenger RNA polyadenylation*
Peptidyl transferase		Ribosome	Amide-bond formation	*Archaea, Bacteria* and *Eukarya*

Table 1.1. Classification and main characteristics of naturally occurring ribozymes

1.2.1.1. Self-cleaving ribozymes

The group of self-cleaving ribozymes includes five different catalytic motifs that catalyze self-cleavage using the same mechanism and the same basic strategies as RNase A (Cochrane and Strobel, 2008), a trans-acting protein enzyme (Raines, 1998).

The hammerhead (Blount and Uhlenbeck, 2005), hairpin (Fedor, 2000), HDV (Shih and Been, 2002), and VS (Lilley, 2004) ribozymes are naturally involved in the replication process of RNA genomes in which they are contained. In particular they cleave the multimeric products of rolling circle replication of viroids, satellite RNAs or viral RNA genomes into single monomers (Table 1.1).

Despite the similarity of their chemical reactions, each of these four ribozymes also appears to utilize a distinct catalytic mechanism, reflecting the diversity of catalytic strategies available to ribozymes. Different approaches in performing the same reaction are very important from an evolutionary point of view. Moreover, the secondary and tertiary structures of these ribozymes are distinct, suggesting that they represent independent evolutionary solutions to the challenge of catalyzing site-specific RNA strand scission.

The *glmS* ribozyme cleaves the messenger RNA of the *glmS* gene in many Gram-positive bacteria (Winkler *et al.*, 2004). It is part of the 5'-UTR (5' untranslated region) of the mRNA that encodes GlcN6P (glucosamine-6-phosphate) synthetase and its self-cleavage activity is activated by binding to GlcN6P.

This ribozyme is of particular interest for the RNA World hypothesis, first of all because it is also a riboswitch involved in the regulation of gene expression and the production of GlcN6P (Winkler *et al.*, 2004). A riboswitch is part of a mRNA molecule that can directly bind a small target molecule, affecting the expression of its own gene. Thus, a mRNA that contains a riboswitch is directly involved in regulating its own expression, depending on the presence or absence of its target molecule. Moreover riboswitch molecules can be considered as the remaining representatives of an ancient metabolic system that was present in the early RNA world. The wide distribution of some classes of riboswitches among prokaryotes and the presence of conserved metabolite-binding RNA domains in eukaryotes (Vitreschak *et al.*, 2004) support this hypothesis. In fact the aptamer (oligonucleic acid or peptide molecules that bind a specific molecular target) domains of

riboswitches carry some of the most highly conserved natural elements in all living cells (Gesteland, 2006). For example, members of the guanine-binding class of riboswitches, as well as the TPP (thiamine pyrophosphate) and FMN (flavin mononucleotide) riboswitches, show a conserved sequence core. All these features suggest that in the ancient RNA world there could have existed ribozymes also able to act as riboswitches, thus regulating their own activity. Over time, some molecules might have lost their catalytic function, evolving towards riboswitches, whereas others could have lost the riboswitch function, thus acting only as ribozymes.

The second characteristic that makes the *glmS* ribozyme interesting is that it catalyzes a reaction using a small molecule (GlcN6P) as cofactor, as many protein enzymes do. Recent studies reveal that, unlike all other examples of riboswitches, GlcN6P does not induce a conformational change in the *glmS* ribozyme-riboswitch, but instead functions as a catalytic cofactor for the reaction (Cochrane *et al.*, 2007). This proves that RNA, as do protein enzymes, can employ the chemical diversity of small molecules to promote catalytic activity. The use of these specifically bound cofactors broadens the chemical repertoire accessible to an evolving RNA world.

Even thought *glmS* is, to date, the only example of a natural cofactor-dependent ribozyme, various other RNAs are able to bind and harness the chemical potential of cofactors. These cofactor-dependent ribozymes still exist in modern genomes and may represent relics of an ancient RNA world.

Hammerhead ribozyme

This is the best described ribozyme, since that it was the first to be discovered (Buzayan *et al.*, 1986; Hutchins *et al.*, 1986) and the first one to be crystallized (Pley *et al.*, 1994; Scott *et al.*, 1995). It is the smallest of the naturally occurring ribozymes (about 40 nt), and it is found in several circular viroid RNAs that infect the plants, where it acts in the processing of single stranded RNA transcripts arising from rolling circle replication (Buzayan *et al.*, 1986; Forster and Symons, 1987; Haseloff and Gerlach, 1988; Hutchins *et al.*, 1986; Prody *et al.*, 1986; Symons *et al.*, 1997) (Table 1.1).

Despite hammerhead and hairpin ribozymes catalyse identical chemical reactions, there are some differences: other than the structure they have some different biochemical features, like the difference metal-cation dependencies and

different proficiencies for catalysing RNA ligation (Fedor, 2000). However, in a recent study, (Canny *et al.*, 2007) showed that the *Schistosoma mansoni* hammerhead ribozyme is both an efficient nuclease and ligase in *vitro*.

The minimal hammerhead motif that support catalytic activity, definited by deletion essay, contains three base-paired helices (I, II and III) around a core of 15 conserved nucleotides. They fold in a way that resembles, in the secondary structure, the shape of a hammer head. Mutation of most of the core residues results in a substantial loss of cleavage activity (Ruffner *et al.*, 1990).

The minimal hammerhead ribozyme structure was the first to be elucidated (Fig. 1.2) (Pley *et al.*, 1994; Scott *et al.*, 1995).

More recently, the characterization of a more extensive hammerhead RNA (De la Pena *et al.*, 2003; Khvorova *et al.*, 2003), has evidenced also the importance of motif outside the catalytic core; in particular loop-loop tertiary interactions between helices I and II.

Despite of the hammerhead ribozyme was the much better studied, for many years there were many disagreements between the minimal hammerhead structure and the biochemical data on the cleavage properties of chemically modified hammerhead (Blount and Uhlenbeck, 2005; Nelson and Uhlenbeck, 2006). In fact, this paradox was recently resolved with the identification of the crystal structure of a natural, full-length hammerhead ribozyme (Martick and Scott, 2006), Fig. 1.3).

Role of Mg^{2+}, and of metal ions in general, has been exhaustively studied for the hammerhead ribozyme. Previous studies on the minimal hammerhead ribozyme indicate that divalent metal ions are primarily involved in stabilizing the catalytically active structure and play only a small role in the chemistry of the cleavage/ligation reaction of the ribozyme (Curtis and Bartel, 2001; Murray *et al.*, 1998; O'Rear *et al.*, 2001). It was earlier hypothesized that all catalytic RNAs were metalloenzymes (Pyle, 1993; Yarus, 1993), which required metal ions both in the folding of the hammerhead structure and in the chemistry.

Successive studies on the "extended" *Schistosoma* hammerhead ribozyme have shown that the cleavage and the global folding occurs at much lower Mg^{2+} (physiological) concentrations compared to the minimal hammerhead ribozyme, thanks to tertiary interaction, that may stabilize the ribozyme in a catalytically active conformation (Heckman *et al.*, 2005; Khvorova *et al.*, 2003; Kim *et al.*, 2005; Kisseleva *et al.*, 2005; Penedo *et al.*, 2004). Nevertheless, divalent metal ions are

required for efficient cleavage and the observed rate of cleavage of the *Schistosoma* hammerhead ribozyme is proportional to Mg^{2+} over a wide range (100 μM to 10 mM) (Canny *et al.*, 2004). However, the global folding into the Y-shaped conformation occurs at much lower Mg^{2+} concentration than is required for maximum catalysis. These data demonstrate that there are at least two Mg^{2+} involved in the hammerhead: a tightly associating Mg^{2+} involved in folding into the Y-shape, and a weaker associating Mg^{2+} required for activity. This weaker associating Mg2+ plays a structural and/or catalytic role. Additional data are required to determine the number of Mg^{2+} ions involved and whether Mg^{2+} association is in the catalytic core or the loop-loop motif (Canny *et al.*, 2004).

Divalent metal ions are proposed to stabilize the formation of the loop-loop tertiary interaction (Boots *et al.*, 2008).

Recent studies also showed a crucial role of the metal cations cofactors directly in hammerhead general acid catalysis (Thomas and Perrin, 2009).

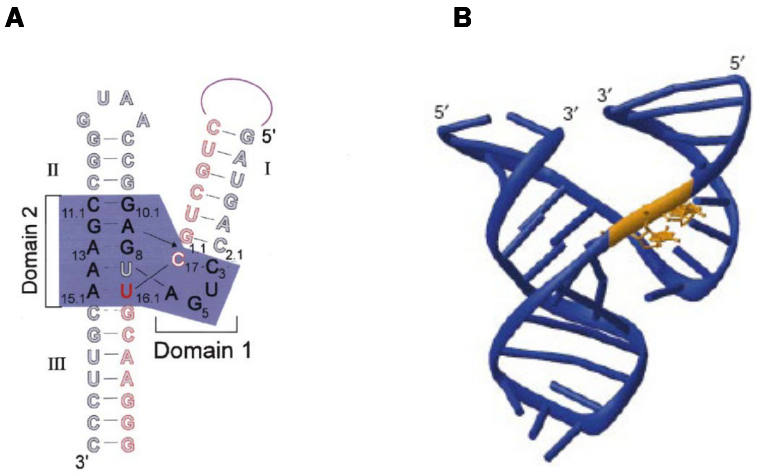

Fig. 1.2. The hammerhead ribozyme.
a) Secondary structural representation of a classical minimalist bimolecular hammerhead ribozyme. The substrate strand is shown in red with a black arrow indicating the cleavage site. Nucleotides whose sequence is essential are shown as filled letters. The shaded area indicates the core structural domains 1 and 2, from which helices I, II, and III radiate.
b) Crystal structure of the hammerhead ribozyme. Coordinates are from (Pley *et al.*, 1994). The nucleotides flanking the scissile bond are shown in gold.

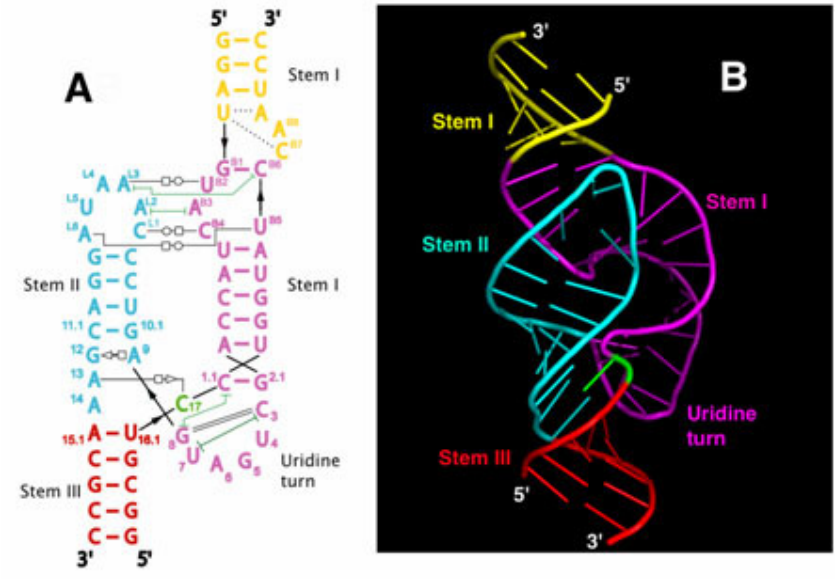

Fig. 1.3. Schematic (A) and ribbon (B) diagrams depicting the crystal structure of the full-length hammerhead ribozyme. The sequence and secondary structure in Figure A is color-coded to match the structural features shown in Figure B. The cleavage site nucleotide, C-17, is shown in green, and various helical stems and loops are denoted using several other colors. Tertiary hydrogen bonding contacts are denoted as thin black lines, and tertiary stacking interactions as thin green lines.

1.2.1.2. Self-splicing ribozymes

The group of self-splicing ribozymes includes self-splicing introns (groups I and II), the Group I-like cleavage ribozyme (GIR1 branching ribozyme (Pyle, 2005) and RNase P.

Self-splicing introns (groups I and II) and the GIR1 ribozyme catalyze their own splicing from a pre-mRNA and at the same time covalently join the flanking exonic sequences (Fig. 1.4 a and b).

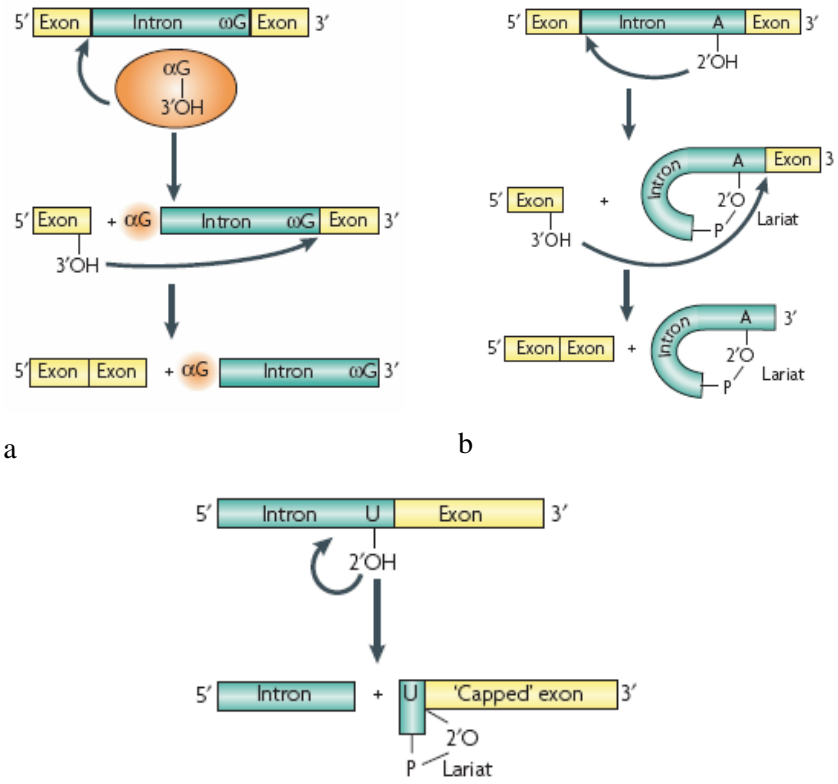

Fig. 1.4. Self-splicing by group I and II introns and GIR1 ribozyme.
The mechanism of splicing of group I and II introns proceeds through two sequential transesterification reactions.
a) Group I: the reaction is initiated by nucleophilic attack by the 3'-OH of external guanosine (αG) at the 5′ splice site. This results in covalent linkage of αG to the 5′ end of the intron and release of the 3′-OH of the 5′ exon. In the second step, the 3′-OH attacks the 3′ splice site located immediately after the conserved guanosine (ωG), resulting in excision of the intron with αG at the 5′ end and release of the ligated exons.
b) Group II: self-splicing of group II introns by a branching reaction. In the first step, the 5′ splice site is attacked by the 2′-OH of a conserved unpaired adenosine, resulting in the formation of a 2′, 5′-phosphodiester linkage. In the next step, the free 3′-OH group of the 5′ exon attacks the 3′ splice site, liberating the circular intron lariat and ligated exons.
c) GIR1 ribozyme: the 'capping' reaction of the GIR1 ribozyme is similar to the first step of the branching reaction of group II introns. The reaction joins nucleotides by a 2′, 5′-phosphodiester linkage, thereby forming a 3-nucleotide lariat that might be a protective 5′ cap of the mRNA.

The discovery of a self-splicing group I intron in the large ribosomal RNA (rRNA) subunit of *Tetrahymena thermophila* (Cech *et al.*, 1981), and the presence of these elements in the genes of a wide variety of organisms, led to the idea that RNA catalysts continue to guide part of protein synthesis and RNA splicing in modern cells.

The common secondary structure and splicing pathway (for recent reviews see (Gesteland, 2006; Strobel and Cochrane, 2007), and the conserved core (Michel *et al.*, 1982), shared by all group I introns, provide an additional support for the ancient and common origin of these molecules. The same considerations could be made for the group II introns because of their highly conserved secondary structure, and for the RNase P RNAs because they share a conserved core (Hartmann and Hartmann, 2003).

The two-metal ion mechanism of splicing of group I introns (Stahley and Strobel, 2005) suggests that the active site of the introns is mechanistically equivalent to a large number of protein-based phosphoryl transferases, including all known DNA and RNA polymerases. Moreover, this group of introns is also able to perform 3', 5' RNA ligation, like protein polymerases and engineered ribozymes (Vicens and Cech, 2009). The similarity with protein polymerases is a further evidence that primitive replication could have been catalyzed by ribozymes related to group I introns. In particular, the analogy between the active site of group I introns and polymerases could be an example of convergent evolution, suggesting an intrinsic chemical capacity of the two-metal-ion catalytic architecture for phosphoryl transfer. It is possible that this was a mechanism used by the ancient RNA polymerase that continues to be used by other RNA splicing systems.

Group II introns possibly left the most conspicuous imprint of the RNA World on modern genomes. Indeed, it is generally believed that the eukaryotic spliceosomal introns (introns not able to perform their own splicing, but that are spliced by the spliceosome), as well as snRNAs (small nuclear RNAs), evolved from this group (Michel and Ferat, 1995). Moreover, the ability of group II introns to act as autonomous mobile elements strongly suggests that they are the predecessors of modern non-LTR (long terminal repeat) retrotransposons (Lambowitz and Zimmerly, 2004; Robart and Zimmerly, 2005). In addition, the mechanistic and structural similarities between self-splicing group II introns and spliceosomal RNAs strongly

suggest that the latter are the catalytic components of spliceosomes (Valadkhan, 2007). The spliceosome is the multi-megadalton molecular machine that performs splicing and it consists of over 200 different proteins and five snRNAs.

The GIR1 ribozyme catalyzes cleavage of the 5' end of the I-*Dir*I (*Didymium iridis*) mRNA (Johansen and Vogt, 1994). It was recently demonstrated (Nielsen *et al.*, 2005) that this cleavage occurs by transesterification resulting in the formation of a 2',5' phosphodiester bond between the first and the third nucleotide of the 3'-cleavage product. The downstream cleavage product is thereby capped with a lariat containing 3 nt in the loop. The mechanism is similar to the first step of the branching reaction of group II introns (Fig. 1.4 b and c). These evidences render the GIR1 ribozyme particularly interesting in an evolutionary context. In particular, the lariat cap resulting from splicing seems to contribute by increasing the half-life of the HE (homing endonuclease) mRNA (Nielsen *et al.*, 2005; Vader *et al.*, 1999), thus conferring an evolutionary advantage to the HE.

The discovery that a group I–like ribozyme can catalyze a branching reaction (Fig. 1.4 c) could suggest that branching ribozymes evolved independently on numerous occasions (Pyle, 2005).

Most reports of branching reactions in natural systems involve viral RNAs that must persist for a long time in the cell to carry out their biological function. This indicates that lariat formation provides protection (for instance against cellular nucleases) and stability to the RNA, the same kind of protection that could have been important for small genomes in the primordial RNA world (Nielsen and Johansen, 2007). Moreover, lariat formation enables the RNA to conserve bonding energy that allows the molecules to react in a reverse reaction. Since the evolution of a RNA molecule relies at least on i) the protection against degrading agents, such as those probably existing in primeval habitats (strong UV, high temperatures), and ii) the ability to interact with surrounding molecules so as to recombine and evolve towards more complex systems able to perform new and more complex functions, the lariat features might have been useful for the evolution of ancient RNA molecules. Another interesting feature of GIR1 is that the sequence and secondary structure are very similar to that of the bacterial IC3 introns (small group I ribozymes from *Azoarcus* and *Synechococcus*) at the second step of splicing. This suggests an evolutionary relationship between GIR1 and this specific subgroup of splicing

ribozymes (Johansen *et al.*, 2002), supporting the hypothesis of a common RNA ancestor.

RNase P, the last representative of this group, is distinct from other ribonucleases in that it is also a ribozyme. It is an essential enzyme required for the maturation of all tRNAs.

It was among the first ribozymes discovered (Guerrier-Takada *et al.*, 1983), and it is the only ubiquitously occurring ribozyme besides the ribosome.

The fact that this ribonucleoprotein contains both RNA and protein subunits and that it occurs in archaea, bacteria and eukaryotes, makes RNase P an intriguing natural system to study principles of RNA evolution and mechanism of conversion from self-sufficient ribozymes to protein-dependent RNA enzymes (Evans *et al.*, 2006).

While the RNA subunit of bacterial RNase P (and of some archaea) are efficient catalysts *in vitro* in the absence of the single protein cofactor (Guerrier-Takada *et al.*, 1983), those from eukaryotes and most archaea require protein subunits for their activity. A hypothesis could be that RNase P RNAs from eukaryotes, organelles and most archaea followed a different evolutionary course from bacterial RNase P RNAs, during which they acquired more RNA-protein and protein-protein interactions (Evans *et al.*, 2006), almost entirely losing their RNA-alone activity. Nevertheless a very low but specific precursor tRNA processing activity of eukaryotic RNase P RNA was recently detected in the absence of any protein cofactor (Kikovska *et al.*, 2007).

1.2.1.3. Mammalian ribozymes

In spite of the great number of naturally occurring ribozymes, only few ribozymes are found associated with mammals: the CoTC-motif containing ribozyme, the CPEB3 and HDV.

The discovery that the co-transcriptional cleavage (CoTC) process in the human β-globin gene involves an RNA self-cleaving activity (Teixeira *et al.*, 2004) demonstrates that another important mechanism in the present-day transcriptional machinery is controlled by a ribozyme.

The functional similarities found between this ribozyme and those of the myxomycetes *Didymium iridis* (Vader *et al.*, 1999) and *Physarum polycephalum*

(Rocheleau and Woodson, 1994), suggest an evolutionary conservation of this molecular process.

Additional evidence is provided by the finding in the 3' flanking regions of the β-globin genes of several primates, of sequences homologous to the full-length human CoTC element. The most highly conserved region corresponds exactly to the catalytic core (Teixeira *et al.*, 2004). This sequence similarity is especially significant because the sequences in the 3' flanking regions are normally highly divergent. The CoTC motif is the only known self-cleaving human ribozyme, with orthologs in other primates. Moreover, the stem structure of the core CoTC also seems to be highly conserved.

Another ribozyme found in all mammalian species including opossum (a marsupial) is the CPEB3 ribozyme (Salehi-Ashtiani *et al.*, 2006). The CPEB3 ribozyme sequence (as also the CPEB3 gene itself) occurs as a single copy in the genome. It is found only in mammals where it is highly conserved, suggesting a mammalian origin for this sequence and a recent appearance, less than 200 million years ago. Moreover, the high conservation of the ribozyme sequence among mammals indicates that the sequence is functionally important.

The rare occurrence of self-cleaving motifs in mammals could indicate that this class of catalytic RNAs was lost during evolution or alternatively, that they escaped detection. Nevertheless, the possibility also exists that further studies will reveal other mammalian ribozymes.

1.2.1.4. The ribosome

Among the naturally occurring ribozymes, the discovery that the ribosome is a ribozyme (Bashan and Yonath, 2008; Hansen *et al.*, 2002), is perhaps the foremost contribution in favour of the RNA world hypothesis. The fact that the peptidyl-transferase reaction in the ribosome is catalyzed by a ribozyme strongly suggests that this might have been the functional mode of the primordial translation system. Moreover, although the chemistry of amide-bond formation is distinct from phosphate-group transfer reactions catalyzed by other ribozymes, the catalytic requirements for transition-state stabilization are quite similar. This could suggest that the ribosome derives from ancient ribozymes, and that it evolved from smaller functional units capable of carrying out the different translation steps (Gesteland, 2006). These small functional RNAs could have assembled to form a larger structure.

Finally the influence of the peptides produced by a primitive ribosome on its own structure could have played an early role in shaping the extant form and function of the ribosome.

In contrast to other catalytic RNAs, RNase P RNA and the ribosome are true enzymes in the sense that they turnover i.e. they naturally conduct multiple catalytic cycles.

They might be remnants of some protobiological RNA world that must have been retained because of the unique qualities of RNA – qualities that remain indispensable to life.

1.2.2. Unnatural ribozymes and *in vitro* selected ribozymes

Starting from the assumption that the RNA world preceded the advent of translation and the evolution of modern cells, it seems likely that the RNA world contained a large number of pathways and catalysts that would have mimicked those in modern metabolism. It is possible to experimentally reconstruct the process whereby ancient catalysts may have arisen, by means of combinatorial chemistry approaches such as *in vitro* selection and evolution (Joyce, 2004).

To date, many artificial ribozymes able to catalyze various reactions have been obtained, but most studies aimed to select ribozymes capable of self-replication, ribozymes adopting cofactors to assist catalysis, and ribozymes creating activated chemical intermediates that could participate in entirely new pathways such as translation (Chen *et al.*, 2007). In each of these fields, progresses were made in selecting ribozymes that mimic the mechanisms of modern protein enzymes, in order to find an RNA system able to auto-sustain, such as the one supposed to have existed in the primordial RNA world (Gilbert, 1986).

1.2.2.1. Self-replication

One of the first, essential reactions that would have arisen in a putative RNA world was the ability of a primordial nucleic acid enzyme to reproduce itself from simpler components.

In the scenario proposed by Levry and Ellington (Levy and Ellington, 2001) primordial oligonucleotides would have served as the basis for template-directed

ligation and amplification. Such primitive replication cycles would have provided the starting point to obtain longer oligonucleotides, which in turn could have been the basis for selecting more complex catalysts, capable of more efficient self-replication. For example, other than accelerating catalysis via simple templating, ligase ribozymes could have greatly accelerated the catalysis of phosphodiester bond formation. A number of different ligase ribozymes have now been selected *in vitro*. The first one was selected by Bartel and Szostak (Bartel and Szostak, 1993). This ribozyme RNA ligase utilizes an RNA with a 5'-triphosphate as substrate and forms a 3'-5' phosphodiester bond at the ligation junction. This reaction is analogous to the reaction carried out by an RNA-dependent RNA polymerase. In spite of the fact that the ligase selected by Bartel and Szostak exhibits limited polymerization activity using nucleoside triphosphates (Ekland and Bartel, 1996), apparently excellent for adaptation to polymerization reactions, it seems unlikely that such a catalyst could have been an early self-replicator. This ligase ribozyme acts as polymerase I does, on a substrate annealed to itself. Consequently it could not have readily changed the position of the active site without unwinding itself. Therefore, the group of Bartel selected a variant of the original ribozyme operating entirely in *trans* (Johnston *et al.*, 2001). This ribozyme was capable of extending the primer by up to 14 nt, i.e., more than a complete turn of an RNA helix, in a 24 h incubation reaction, with higher fidelity than the first ligase selected.

Since the shortest version of this ribozyme RNA polymerase was 165 nts, it is likely that early nucleic acid replicases utilized oligonucleotides rather than mononucleotides as substrates. Oligonucleotide ligases could have supported an early self-replicator.

Much shorter ribozyme ligases have been selected from random sequence pools, such as the "R3C" RNA enzyme (Rogers and Joyce, 2001). Using oligonucleotide substrates, some of these ligase ribozymes have satisfactorily been shown to self-replicate (Kim and Joyce, 2004; Paul and Joyce, 2002).

A self-replicating system can be defined as autocatalytic when the newly formed product is also able to direct the assembly of product molecules.

Paul and Joyce (Paul and Joyce, 2002) developed a self-oligomerization system, starting from the R3C ligase. The ribozyme was designed so that it would direct the ligation of two substrates to generate an exact copy of itself, which then would behave in a similar way. The substrates were in fact constructed in such a way

that the product of their ligation catalyzed by the ribozyme, would be identical to the template (Fig. 1.5). At each ligation event new template catalyst molecules are thus generated: through an RNA catalyzed RNA ligation reaction, the ribozyme could catalyze the assembly of additional copies of itself.

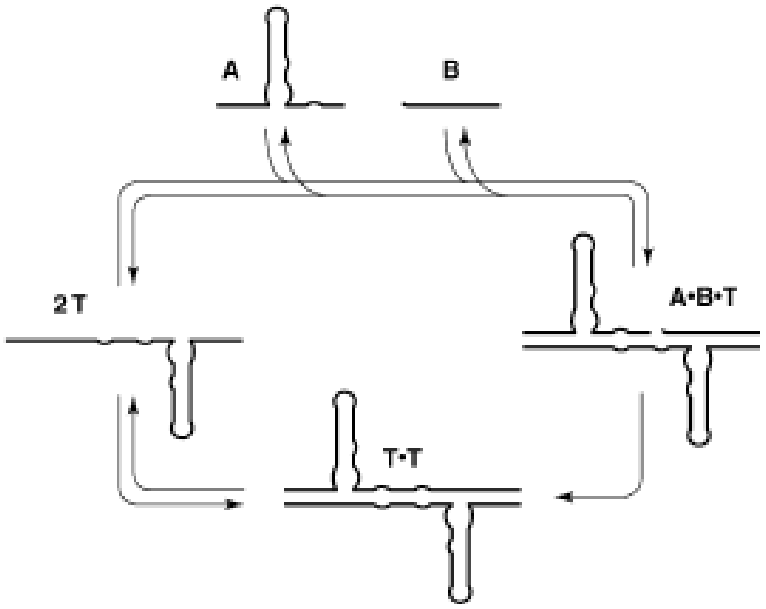

Fig. 1.5
Replication cycle of the R3C ligase ribozyme.
A and B are the substrate, T is the template and the product of the catalytic reaction

Although a linear dependence between the initial rate of formation of new copies and the starting concentration of ribozyme was observed, exponential growth was limited because of the formation of non-productive complexes.

The possibility of cross-catalytic ligation of oligonucleotides has also been demonstrated (Kim and Joyce, 2004): a selected ribozyme ligase was broken into two pieces, and engineered so that one ribozyme could act on the complementary junction of another, leading to its activation. The mixture of the ribozyme substrates led to the formation of new catalysts. Nevertheless their accumulation was sub-exponential: the autocatalytic cycle was partially inhibited by product binding and by the formation of alternative products through side reactions.

A similar demonstration was carried out by Hayden and Lehman (Hayden and Lehman, 2006), based on dividing the group I self-splicing intron into four pieces and then catalyzing reassembly of the pieces by ribozyme-mediated ligation.

Recently (Zaher and Unrau, 2007) an RNA polymerase ribozyme (B6.61), exhibiting more extension and fidelity relative to its progenitor, the Round-18 polymerase, was selected.

Lincoln and Joyce (Lincoln and Joyce, 2009) improved the cross-replicating RNA enzyme found by Kim and Joyce (Kim and Joyce, 2004), such that exponential growth could be continued indefinitely. They also constructed variants of the cross-replicating RNA enzyme necessary to support their amplification. Thus the problem of self replication in an RNA world seems very close to being resolved.

1.2.2.2. Cofactors in a RNA world

Many studies have turned to the selection of ribozymes that use cofactors, whose importance in present-day biology is well established. In modern cells more than half of the protein enzymes require cofactors to facilitate and further diversify their catalytic activities (White, 1982). Moreover, many cofactors used by protein enzymes (ATP, NAD, FAD) are RNA-like, prompting the RNA world hypothesis itself. Therefore it is likely that cofactors would have been necessary also in the primitive RNA world. Ribozymes of the RNA world may have used amino acids and other small organic cofactors to expand their otherwise limited catalytic potential (Kun, 2006; Roth and Breaker, 1998; Szathmary, 1993; Szathmary, 1999).

Cofactors are considered the oldest metabolic fossils (White, 1975). This idea relies on the fact that many different biochemical reactions may require the same cofactor and in a specific conformation. If this cofactor should change its conformation, cellular metabolism would cease. Therefore the structure of this cofactor is essential for cell life. If this hypothesis is true, we can assume that the structures of cofactors are ‘stuck’ in evolutionary time in a manner far more stringent than biochemical reactions or the catalysts that support them. If most cofactors are old and based on nucleotides, it is likely that RNA cofactors may have been available and essential even in an early RNA world.

For these reasons many *in vitro* synthesized ribozymes using a cofactor have been selected (Breaker and Joyce, 1995; Huang and Yarus, 1997; Lorsch and Szostak, 1994; Meli *et al.*, 2003; Paul and Joyce, 2002).

Examples are selected ribozymes that utilized ATP-γ S as substrate and could phosphorylate themselves (Lorsch and Szostak, 1994). Different classes of present-day kinases catalyze the transfer of the gamma-thiophosphate of ATP-γ S to the 5'-

hydroxyl or to internal 2'-hydroxyls. The selected ribozyme is able to transfer thiophosphate from ATP-γ S to the 5'-hydroxyl of an exogenous oligoribonucleotide substrate with multiple turnover, thus acting as a true enzyme.

Redox ribozymes that utilize NAD^+ as cofactor have also been selected [55], or ribozymes that require adenine as catalytic cofactor for their reversible self-cleavage (Meli *et al.*, 2003).

1.2.2.3. Translation

One of the central problems in evolutionary biology is the origin of the translation machinery. The problem is that high translation fidelity can hardly be achieved without a complex, highly evolved set of RNAs and proteins, but that an elaborate protein machinery can not exist without an accurate translation system.

It has been proposed that the evolutionary process that led to the emergence of translation started with the selection of ribozymes initially binding abiogenic amino acids that stimulated ribozyme-catalyzed reactions, and subsequently with the synthesis of increasingly versatile peptides. Several aspects of this scenario are amenable to experimental testing.

A recent study (Chen *et al.*, 2007) focuses on *in vitro* selected ribozymes that catalyze reactions involved in the origin of translation. It is likely that many of the steps in this process are at least chemically similar today to those that would have been present initially.

All the three elementary reactions required for translation (amino acid activation, (t)RNA aminoacylation, and transpeptidation) have been successfully reproduced with ribozymes (Coleman and Huang, 2002; Illangasekare *et al.*, 1995; Li and Huang, 2005; Nielsen and Johansen, 2007).

1.3. Viroids

Viroids are small (246–401 nt), single-stranded, circular, non-encapsidated RNAs with the ability to infect certain plants, and to replicate autonomously in susceptible hosts (Diener, 2003; Flores *et al.*, 2005; Tabler and Tsagris, 2004) (Fig. 1.6). A first peculiar characteristic of these vegetal pathogens is that, in contrast to viruses, they are able to complete their infectious cycle without encoding any protein and without resorting to a helper virus (Diener, 2001). This means that all the pathogenic action is exclusively due to their structural proprieties, by means of which they can interact with host plant proteins, modifying normal metabolic functions (Flores *et al.*, 2004). Viroids, acquiring a well-defined secondary structure are able to manipulate many of the cellular functions in their own benefit. The shape of these RNAs is in fact one of the most important properties of viroids and sometimes is considered their only phenotype.

The second peculiar feature is that some viroids (*Avsunviroidae* family, see below) are catalytic RNAs with ribozyme self cleavage activity, that resides in their capacity to form hammerhead ribozyme (Flores *et al.*, 2000; Flores *et al.*, 2001; Forster and Symons, 1987; Hutchins *et al.*, 1986; Prody *et al.*, 1986). The hammerhead structure mediates self-cleavage of the multimeric RNA intermediates of both polarities generated in the replication of members of this family (Fadda *et al.*, 2003b; Flores *et al.*, 2000). Even in this case, it is necessary to point out the fundamental importance of the structure of the RNA, that is at the base of the enzymatic activity of the ribozymes.

All the features over mentioned support the idea that viroids have an evolutionary origin very old and independent from that of viruses. For these reasons viroids are considered molecular fossil of the precellular RNA world (Diener, 1989; Diener, 2003).

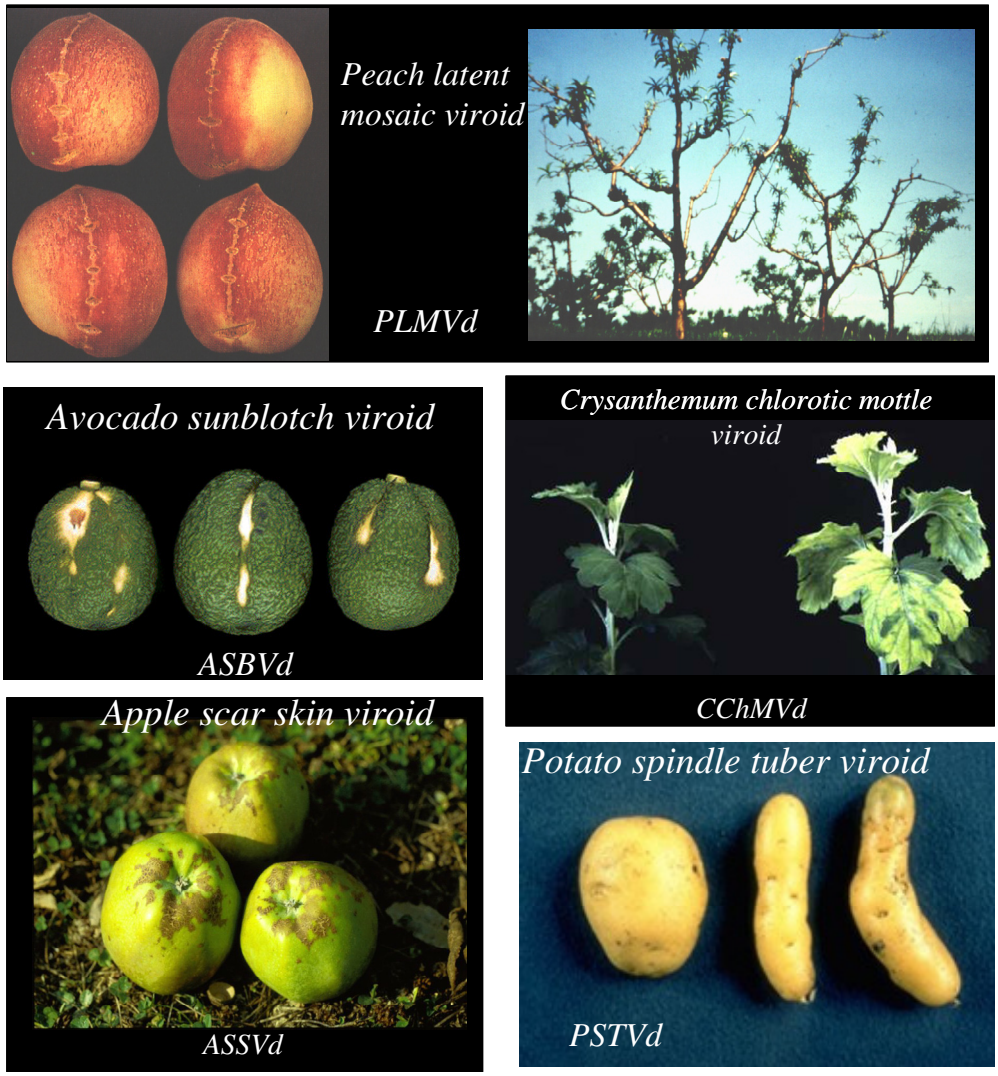

Fig. 1.6. Effect of some viroids

1.3.1. Classification

Approximately 30 species of viroids and many of their variants currently are known. A recent compilation of viroid species and their classifications (Ding, 2009b; Flores *et al.*, 2005; Gora-Sochacka, 2004) and the Subviral RNA Database (Rocheleau and Pelchat, 2006) present an updated taxonomy as well as sequence and structural analyses. Viroids are classified into two families: *Pospiviroidae* and *Avsunviroidae*. The salient features that distinguish the two families are listed in Table 1.2. The type member of the former is Potato spindle tuber viroid (PSTVd), and that of the latter is Avocado sunblotch viroid (ASBVd). The members of *Pospiviroidae* have highly conserved regions in their rod-shaped secondary structure,

replicate in the nucleus, and generally are considered to lack ribozyme activity. Five broad structural domains are defined in the secondary structure of viroids in *Pospiviroidae*. These include the left-terminal domain, pathogenicity domain, central domain that contains a central conserved region (CCR), variable domain, and right-terminal domain (Keese and Symons, 1985) (Fig. 1.7). Their hosts are mostly herbaceous species.

The members of *Avsunviroidae* have limited sequence conservation and most of them have highly branched secondary structures (Fig. 1.7). All of them have ribozyme activities and replicate in the chloroplasts. Their hosts are mostly woody species.

In recent years there are evidences for host range expansion for some viroids (Matousek *et al.*, 2007a), indicating that there is always the potential for a viroid to invade new plant species if conditions permit it.

	Family	
Features	*Pospiviroidae*	*Avsunviroidae*
Secondary structure	Rod-shaped	Branched for most members
Replicate site	Nucleus	Chloroplast
Rolling circle	Asymmetric	Symmetric
Ribozyme activity	Uncertain	Yes for all current members
Hosts	Mostly herbaceous species	Mostly woody species

Table 1.2. The salient features that distinguish the two families of *Pospiviroidae* and *Avsunviroidae*.

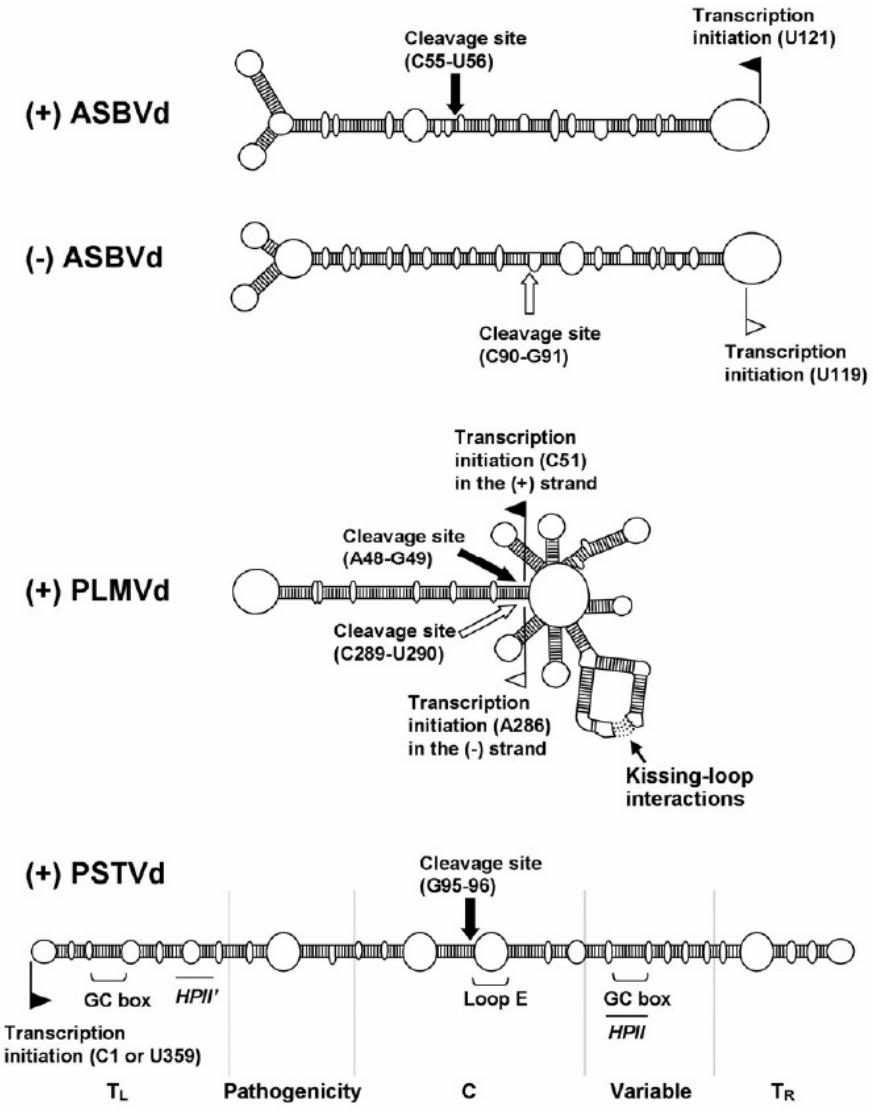

Fig. 1.7. Secondary structures of representative viroids from the two viroid families, Avsunviroidae: Avocado sunblotch viroid (ASBVd) and Peach latent mosaic viroid (PLMVd), and Pospiviroidae: Potato spindle tuber viroid (PSTVd). The transcription initiation sites on the viroid genomic RNAs are indicated. Note that for ASBVd and PSTVd, these sites are mapped to terminal loops. The transcription initiation site for the (–)-PSTVd RNA template remains to be determined. For PLMVd, the dashed lines indicate kissing-loop interactions. For PSTVd, the five structural domains (Keese and Symons, 1985) are indicated. TL = left-terminal domain, C = central domain, and TR = right-terminal domain. HPII′ and HPII indicate nucleotide sequences that base pair to form the metastable hairpin II structure.

1.3.2. Mechanism of infection and replication

The establishment of systemic infection by both families of viroids involves the following steps: i) import into specific subcellular organelles (the nucleus for *Pospiviroidae* and chloroplast for *Avsunviroidae*); ii) replication; iii) export out of the organelles; iv) cell-to-cell trafficking; v) entry into the vascular tissue, vi) long-distance trafficking within the vascular tissue; and vii) exit from the phloem to invade nonvascular cells and repeat the replication and trafficking cycle (Fig. 1.8) (Ding, 2009a; Ding and Itaya, 2007). Accomplishment of each step likely involves direct interactions between specific viroid motifs and cellular factors. It is crucial that viroid RNAs are protected against cellular degradation at each step. Viroid replication follows a rolling circle mechanism. For the two families different variants of the mechanism have been proposed (Fig. 1.9).

The members of *Pospiviroidae* replicate via an asymmetric rolling circle mechanism (Branch and Robertson, 1984) (Fig. 1.9 A). The incoming (+) circular RNA initially is transcribed into concatemeric linear (–) strand RNA, which then serves as the replication intermediate for the synthesis of concatemeric, linear (+) strand RNA. This (+) strand RNA subsequently is cleaved into unit-length monomers that are ligated into circles. In contrast, the members of *Avsunviroidae* adopt a symmetric rolling circle replication mechanism (Branch and Robertson, 1984; Daros *et al.*, 1994; Flores *et al.*, 2000; Navarro *et al.*, 1999) (Fig. 1.9 B). The circular (+) RNA is transcribed into linear, concatemeric (–) strand RNA. The concatemeric (–) strand RNA is cleaved into unit-length molecules followed by circularization. The circular (–) RNA then serves as the template for the synthesis of linear, concatemeric (+) strand RNA, which subsequently is cleaved into unit-length monomers and circularized. Thus, this mechanism involves two rolling circles.

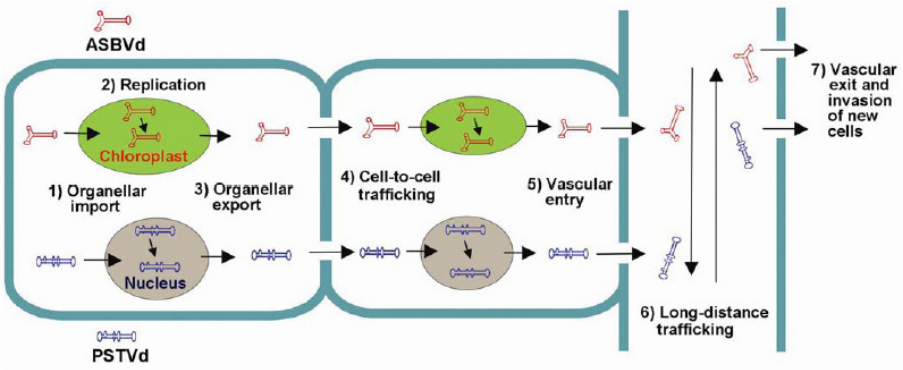

Fig. 1.8. Schema of distinct steps of systemic infection of Avocado sunblotch viroid (ASBVd) and Potato spindle tuber viroid (PSTVd), type members of the two viroid families.

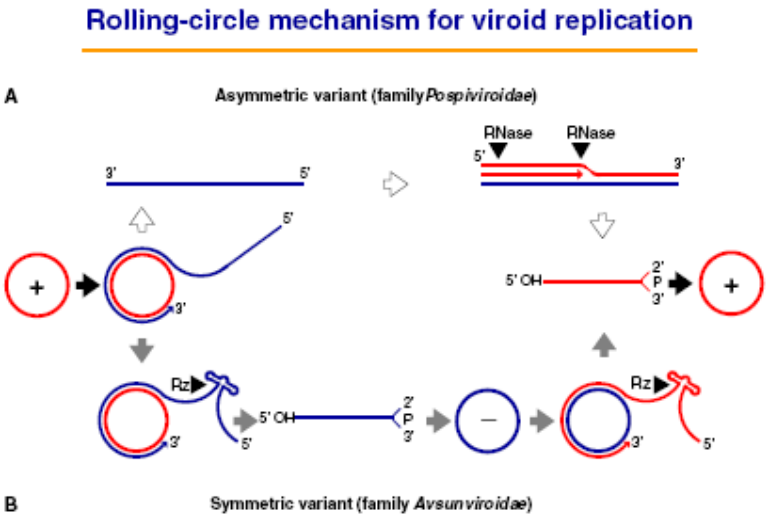

Fig. 1.9. Replication of viroids through a rolling-circle mechanism. (A,B) Asymmetric and symmetric pathways with one and two rolling circles proposed to operate in members of the families Pospiviroidae and Avsunviroidae, respectively. White and gray arrows indicate the asymmetric and symmetric pathways, respectively (the first and the last step, indicated with black arrows, are common to both pathways). Red and blue lines represent plus (+) and minus (-) polarities, respectively, and cleavage sites are marked by arrowheads.

1.3.2.1. The enzyme machinery for transcription

The DNA-dependent RNA polymerase II (Pol II) is generally accepted to be involved in the transcription of members of *Pospiviroidae*. Many are the observations supporting this hypothesis. (Fels *et al.*, 2001; Flores, 1989; Kolonko *et al.*, 2006; Rackwitz *et al.*, 1981; Schindler, 1992; Warrilow and Symons, 1999).

For the transcription of *Avsunviroidae*, two types of DNA-dependent RNA polymerases in the chloroplast need to be considered: the nuclear-encoded and phage-like single-unit polymerase (NEP), and the plastid-encoded bacterial-like multi-unit RNA polymerase (PEP) (Stern, 1997).

In vitro transcription assays with chloroplasts isolated from infected avocado leaves suggest that the NEP is involved in ASBVd transcription (Navarro *et al.*, 2000). A recent study suggests that NEP is more likely involved also in the transcription of PLMVd *in vivo* (Delgado *et al.*, 2005).

Transcription initiation sites have been mapped for two members of *Avsunviroidae* (ASBVd, (Navarro and Flores, 2000) and PLMVd, (Motard *et al.*, 2008) and for one member of *Pospiviroidae* (PSTVd, (Kolonko *et al.*, 2006) (Fig. 1.7).

1.3.2.2. RNA motifs and protein factors for cleavage and ligation

Concerning *Pospiviroidae*, it was showed that the CCR contains all the necessary elements for cleavage and ligation (Schrader *et al.*, 2003). It generally thought that a cellular RNase, which remains to be identified, catalyzes the cleavage of concatemeric RNAs (Tsagris *et al.*, 1987a; Tsagris *et al.*, 1987b). However, self-cleavage similar to that of the *Avsunviroidae* was demonstrated for some members of *Pospiviroidae* (Amari *et al.*, 2001). Ligation of PSTVd RNAs occurs with low efficiency autocatalytically, but with high efficiency enzymatically (Baumstark *et al.*, 1997).

The members of *Avsunviroidae* form hammerhead ribozymes in both the (+) and (–) strands of RNAs to catalyze self-cleavage *in vitro* (Beaudry *et al.*, 1995; Fadda *et al.*, 2003a; Flores *et al.*, 2000; Forster *et al.*, 1988; Hernandez and Flores, 1992; Hutchins *et al.*, 1986; Navarro and Flores, 1997).

Analyses of *Chrysanthemum* chlorotic mosaic viroid (CChMVd) showed that RNA sequences peripheral to the ribozyme structure can greatly enhance self-

cleavage activities (De la Pena *et al.*, 2003; Khvorova *et al.*, 2003), a finding that has broadened our understanding of ribozyme structure and functions. Flores and co-worker (Daros and Flores, 2002) identified a chloroplast protein, PARBP33, that has a RNA-binding motif, interacts with ASBVd *in vivo*, and accelerates self-cleavage of concatemeric ASBVd RNAs *in vitro*. Its *in vivo* role remains to be studied. How the self-cleaved RNAs are ligated remains unclear. Self intra- and inter-molecular ligation has been demonstrated for PLMVd *in vitro* (Lafontaine *et al.*, 1995). The self-ligation produces a 2′,5′-phosphodiester bond *in vitro* that may protect the circular RNAs from cleavage by cellular enzymes (Cote and Perreault, 1997). Côté and associates (Cote *et al.*, 2001) demonstrated the presence of the 2′,5′-phosphodiester bond at the ligation site of the circular PLMVd RNAs isolated from infected peach plants. Thus, this evolutionarily primitive phosphodiester linkage still occurs in nature, making PLMVd an excellent model to further investigate the evolution and modern significance of this linkage.

1.3.2.3. Intra and inter-cellular trafficking

In order for replication to take place, viroid RNAs must be localized to the correct subcellular sites to gain access to the cellular machineries that recognize, transcribe, and process the RNAs. In contrast to the mechanisms involved in replication, the mechanisms responsible for intracellular localization have been much less studies.

Results so far obtained, (Young-Min *et al.*, 1999; Zhao *et al.*, 2001) suggest that PSTVd has a nuclear import signal which remains to be identified. The cellular machinery that recognizes and imports the viroid RNA is not known. How the viroid RNAs exit the nucleus also remains to be investigated.

Even for *Avsunviroidae* the mechanism that directs them into chloroplast is poorly understood. One possibility is that these RNAs elicit abnormal changes in the permeability of the chloroplast envelope, so that they enter the organelle via a unique mechanism. Alternatively, these RNAs have evolved a motif that is recognized by a machinery for normal RNA import into the chloroplast that is yet to be discovered.

To establish a systemic infection, viroid RNAs must traffic from initially infected cells into neighboring cells and distant organs. For a recent review on the viroid intercellular trafficking see (Takeda and Ding, 2009).

Viroid intercellular cell-to-cell trafficking does not occur via plasma membrane-mediated transport, but rather occurs via plasmodesmata (Ding *et al.*, 1997). In the case of long-distance spread between different plant organs, a viroid utilizes the phloem, as shown by the similar movement patterns in a whole plant between PSTVd and photoassimilates (Palukaitis, 1987) and by direct *in situ* localization of PSTVd to the phloem (Zhu *et al.*, 2001).

Given that viroids do not codify for any protein, they must rely on direct interactions with cellular factors to traffic within a plant.

Recent studies based on genome-wide mutational analysis successfully identified a range of structural motifs in the PSTVd genome that play a critical role in trafficking. Furthermore, detailed studies of some motifs indicate their requirement for trafficking between specific cell types (Zhong *et al.*, 2008). This work shows that most loops in PSTVd play a role in trafficking.

These advances start to shed light on the viroid structural elements critical for trafficking and build a basis for further discoveries in this direction. Detailed genetic, structural and cellular studies determined that loop 7 has a defined tertiary structure and it enables PSTVd to enter the phloem (Zhong *et al.*, 2007). Has been demonstrated that a bipartite motif is required for trafficking from bundle sheath to mesophyll (Qi *et al.*, 2004).

Proved that viroid intercellular trafficking is mediated by specific structural motifs, a simple model would predict interactions between these motifs with cellular factors. However, no cellular factors that function in viroid trafficking have been conclusively identified. Recently a phloem-mobile ribonucleoprotein complex from pumpkin for the selective trafficking of some cellular RNAs has been identified (Ham *et al.*, 2009). It could be interesting to test whether this complex, or some component(s) of this complex, plays a role in viroid trafficking.

Most progress on viroid trafficking motifs has been made with analyses of PSTVd. For the members of family *Avsunviroidae* it remains a major knowledge gap. Recently has been reported the first trafficking analysis of PLMVd (Rodio *et al.*, 2007). Results contrast with some data obtained for PSTVd (Zhu *et al.*, 2002), suggesting the existence of some fundamentally different mechanisms for the trafficking of viroids in the two families.

1.3.3. Viroid pathogenicity

Despite the non-coding nature of their small RNA genomes, the visible symptoms of viroid infection resemble those associated with many plant virus diseases. For a recent review see (Owens and Hammond, 2009).

Many studies have been carried out to identify structural motif modulating viroid pathogenicity.

It was shown that nucleotides within in the P domain play an important role in PSTVd symptom induction (Dickson *et al.*, 1979; Visvader, 1985). For several naturally-occurring isolates of PSTVd, thermodynamic calculations indicate that virulence is correlated with the instability of a single structural motif within the P domain, called the "virulence modulating region". These findings induced to suppose that symptom expression might be regulated by the ability of this region to interact with unspecified host components (Schnolzer *et al.*, 1985).

Further successive studies suggested that the molecular mechanism underlying viroid pathogenicity might be more complicated (Sano *et al.*, 1992; Visvader, 1985). These studies identified three discrete regions of sequence and/or structural variability that may correspond to pathogenicity determinants.

Characterization of naturally-occurring variants of several other viroids, like Hop stunt viroid (HSVd) (Reanwarakorn and Semancik, 1998; Reanwarakorn and Semancik, 1999), Coconut cadang-cadang viroid (CCCVd) (Rodriguez and Randles, 1993), ASBVd (Semancik and Szychowski, 1994), CChMVd, and PLMVd (Schnell, 2002) has identified still more pathogenicity determinants.

The rod-like secondary structure of ASBVd does not contain the five structural/functional domains found in PSTVd and related viroids. Characterization of ASBVd variants associated with bleached, variegated, or symptomless leaf tissue suggests a transition in sunblotch disease from a severe acute to a persistent mild form of infection (Semancik and Szychowski, 1994). During this transition, sequence changes, accumulating in the right terminal loop, may lead to a more open structure of this portion of the molecule, potentially altering its ability to bind RNA polymerase.

The branched secondary structures of PLMVd and CChMVd differ from the overall rod-like structure of ASBVd. It has been shown that the sequence changes in a single hairpin loop are sufficient to convert a symptomatic strain to an asymptomatic one (De la Pena and Flores, 2002; de la Pena *et al.*, 1999).

How these proposed pathogenicity determinants could influence the disease process remains to be determined.

Several earlier studies (Itaya *et al.*, 2001; Markarian *et al.*, 2004; Martinez de Alba *et al.*, 2002; Matousek *et al.*, 2007b; Papaefthimiou *et al.*, 2001) had shown that viroid-infected plants contain small RNAs derived from the invading viroid genome. Thus, attention has shifted from RNA-protein interactions to RNA silencing as the primary mediator of viroid pathogenicity.

In fact it is possible that viroids could be inducers (and targets) of post transcriptional gene silencing (PTGS), and that phenomena of this kind could mediate viroid pathogenesis.

RNA-mediated gene silencing is a powerful antiviral mechanism in plants and animals (Ding, 2004; Dunoyer and Voinnet, 2005; Li and Ding, 2005; Schutz and Sarnow, 2006; Voinnet, 2005) and plays crucial roles in regulating a wide range of developmental and growth processes (Brodersen and Voinnet, 2006; Carthew and Sontheimer, 2009; Ding and Voinnet, 2007; Jones-Rhoades *et al.*, 2006; Ruiz-Ferrer and Voinnet, 2009; Wassenegger *et al.*, 1994). RNA silencing involves several classes of 21- to 24-nt small RNAs as key mediators. These include microRNAs (miRNAs) and short interfering RNAs (siRNAs), which are produced by cleavage of structured precursor RNAs or cleavage of double-stranded RNAs (dsRNAs), respectively. RNase III dicer or dicer-like proteins (DCLs) and their associated proteins carry out the cleavage. The cleavage yields duplex miRNAs or siRNAs. One strand of the duplex is incorporated into the RNA-induced silencing complex (RISC) to guide degradation or translation inhibition of a target RNA, or into a RNA-induced initiator of transcriptional silencing complex (RITS) to guide DNA methylation-based chromatin modifications (Baulcombe, 2004; Chan, 2004; Ekwall, 2004; Jones-Rhoades *et al.*, 2006; Matzke and Birchler, 2005). As a counter-defense strategy, many viruses encode one or more proteins that function as silencing suppressors (Roth *et al.*, 2004).

The first evidence that RNA silencing might play a key role in modulating viroid-host interaction appeared in 1994 when a study (Wassenegger *et al.*, 1994) reported that certain PSTVd cDNAs became specifically methylated following introduction into the tobacco genome via *Agrobacterium*-mediated leaf-disc transformation. The involvement of small RNAs in this process was not yet apparent,

but one eventual link to RNA silencing was clear: methylation was dependent upon viroid replication, and non-infectious PSTVd cDNAs remained unmethylated.

Several recent studies reported the presence of small, viroid-related RNAs in plants infected by a number of viroids from both the families *Pospiviroidae* and *Avsunviroidae*.

These results suggest that viroid RNAs can trigger RNA silencing. In a recent review the findings that evidence the major role of this mechanism in viroid pathogenesis and evolution are summarized (Gomez *et al.*, 2009). In this work a model that links synthesis of trans-acting small interfering RNA (ta-siRNA) with viroid replication and pathogenesis is also proposed.

How the viroid small RNAs are produced is not well understood. Interesting is that there is no consistent relationship between (viroid)siRNA concentration and symptom severity; however it was shown that development of visible symptoms in PSTVd infected plants is accompanied by a shift from 21-22 to larger 24-nt siRNAs (Machida *et al.*, 2007). Several evidences suggest that a significant proportion of (PSTVd)siRNA is derived from structured regions of viroid genomic RNAs.

It is also not very clear how (viroid)siRNAs can induce disease in susceptible hosts. Some studies suggest that (PSTVd)siRNAs can directly target host mRNAs for RISC-mediated degradation (Itaya *et al.*, 2007; Vogt *et al.*, 2004). A very recent study suggests that viroid RNAs may interact with host enzymes involved in the RNA-directed DNA methylation pathway. This indicates more complex scenarios than previously thought for both (viroid)sRNAs genesis and possible interference with host gene expression (Navarro *et al.*, 2009). Moreover they showed that different DCLs target viroid RNAs, preferentially accessing to the same viroid domains.

Viroid siRNAs might also act indirectly by altering levels of host siRNA metabolism. In fact certain symptoms such as epinasty and rugosity commonly associated with viroid infection reflect changes in leaf developmental patterns.

A recent study (Gomez *et al.*, 2008) shows that symptom development in transgenic *Nicotiana benthamiana* plants, that express a dimeric form of HSVd, is dependent upon expression of RNA-dependent RNA polymerase 6 (RDR6). Moreover, symptom development can be suppressed by growth at low temperatures (14°C), at which RNA silencing is also reduced (Qu *et al.*, 2005).

As discussed in several reviews (Boller and He, 2009; Wise *et al.*, 2007), virus infection has been shown to i) induce a variety of plant defense and stress responses and ii) down-regulate other genes with potential roles in plant growth and development. Similarities in the visible symptoms induced by viruses and viroids suggest that plants respond to the presence of these infecting agents in a very similar fashion, but this hypothesis has yet to be critically tested.

A fascinating question is how an alien, noncoding, and non-encapsidated viroid RNA can achieve the remarkable feat of surviving the cellular RNA surveillance and degradation systems. However, the specific mechanisms plants may have evolved to defend themselves against viroid infection and the counter-measures a viroid may have evolved to survive, remain open questions.

Probably the key is in their structure. The secondary structure of a viroid RNA may have evolved to be the optimal compromise between the necessity to survive cellular degradation by RNA silencing or nucleases and the necessity to interact with cellular factors for replication and trafficking (Carbonell *et al.*, 2008; Itaya *et al.*, 2007; Wang *et al.*, 2004). Thus, the secondary structure of a viroid is very likely to be important for survival. Other possible ways to further enhance viroid survivability include nuclear or chloroplastic localization, binding to specific cellular proteins, and rates of replication that exceed rates of degradation.

1.4. Problems related with the RNA world

Naturally occurring ribozymes and viroids, thanks to their characteristic proprieties, are the major proves that a RNA world could be existed. These elements are considered “relics” of an ancient RNA world that still continues to exist in present-day cells.

The demonstrations and results provided by SELEX experiments suggest, also, that ribozymes are potentially able to perform almost all the essential reactions that could be necessary in a primordial environment and that they have a greater catalytic potential than previously suspected, supporting their proposed role as pervasive catalysts during early evolution and in the postulated RNA world.

However, there are some obstacles concerning this theory. Does a unitary and simple physical-chemical frame exist in which nucleic bases may form and evolve to their open or closed nucleoside forms, and in which nucleosides may be

phosphorylated, oligomerize and possibly ligate to yield larger oligonucleotide fragments? How the self-replicating systems, once formed, could be protected by degrading agents?

Scientists are looking for the answers and some of these problems seem now on the way to be solved.

1.4.1. Nucleoside formation

The problem of β-nucleoside formation under prebiotic conditions represents one of the most significant challenges to the "RNA world" hypothesis. Orgel and co-workers demonstrated that adenine and hypoxanthine form glycosidic bonds with D-ribose when dried and heated together (Fuller *et al.*, 1972). However, this simple approach proved to be less promising with the other bases: neither cytosine nor uracil, nor guanine (probably due to the low solubility of the free guanine base) give rise to nucleosides under these conditions (Zubay and Mui, 2001). The lack of a mechanism for the prebiotic synthesis for the pyrimidine bases has been considered a crucial problem for most contemporary theories concerning the origin of life.

A stepwise synthesis of the base cytosine on a preformed sugar was first accomplished by Sanchez and Orgel (Sanchez and Orgel, 1970) and more recently explored in greater detail by the Sutherland laboratory (Ingar *et al.*, 2003). This approach has proven to be regioselective, yielding very little β-cytidine. Improvements in β-cytidine formation by this approach were made very recently (Powner *et al.*, 2009; Powner *et al.*, 2007). The problem is that none of these approaches is able to produce all four nucleosides, or even one purine and one pyrimidine. Some scientists hypothesized that the original bases differed from the canonical AUCG (Gesteland, 2006; Kolb *et al.*, 1994; Mittapalli *et al.*, 2007), and the possibility that some of these bases might have formed glycosides more easily than the current bases under prebiotic conditions.

Recently was reported the first successful synthesis of a pyrimidine nucleoside from a free base (2-pyrimidinone) and a nonactivated sugar (D-ribose) in a plausible prebiotic reaction (Bean *et al.*, 2007). The same group presented a detailed computational study of glycosidic bond formation during a pyrimidine nucleoside formation reaction (Sheng *et al.*, 2009). Results obtained showed that the reaction between ribose and free 2-pyrimidinone would not likely take place in water at neutral pH due to the high activation energy. Moreover, the study of the reaction

between ribose and protonated 2-pyrimidinone, which models an acidic experimental condition, showed that acid does catalyze glycosidic bond formation. Another important conclusion was that the formation of the β-ribofuranosyl nucleoside product is greatly facilitated by the presence of Mg^{2+} ions in the acidic solution.

1.4.2. Prebiotic synthesis of nucleotides

The fact that the most appropriate compound, i.e. phosphate, is the one that is currently present in extant nucleic acids, prompted scientists to investigate the possible existence of a spontaneous and prebiotically plausible reaction allowing phosphorylation of nucleosides. The low efficiency and limitations of methods for phosphorylation of nucleosides have been reviewed (Joyce, 2004; Orgel, 2004).

Formamide is considered an important building block in the origin of life (Saladino *et al.*, 2009). Di Mauro group showed that when nucleosides were treated with formamide in the presence of a source of phosphate as provided by soluble phosphates or by one of several phosphate minerals (Costanzo *et al.*, 2007), nucleotides were actively formed.

Recently the same group observed monophosphorylation of adenosine in water in the presence of a phosphate source at 90 °C. The reaction yielded to the formation of 2'AMP (adenosine monophosphate), 3'AMP, 5'AMP and the cyclic forms 2',3'-cAMP and 3',5'-cAMP (adenosine 2',3'-cyclic monophosphate and adenosine 3',5'-cyclic monophosphate). The same reaction was faster and more efficient in formamide (Costanzo *et al.*, 2007; Saladino *et al.*, 2006). Moreover, in this condition the products were more stable.

However, the very important fact is that nucleoside phosphorylation may take place in water in non-enzymatic abiotic conditions. This observation is relevant for an understanding of the spontaneous origin of (pre)genetic polymers.

Another recent study (Powner *et al.*, 2009) showed that activated pyrimidine ribonucleotides can be formed in a short sequence that bypasses free ribose and the nucleobases, proceeding through arabinose amino-oxazoline and anhydronucleoside intermediates. The starting materials for the synthesis-cyanamide, cyanoacetylene, glycolaldehyde, glyceraldehyde and inorganic phosphate are plausible prebiotic feedstock molecules (Bryant and Kee, 2006; Pasek and Lauretta, 2005; Thaddeus, 2006), and the conditions of the synthesis are consistent with potential early-Earth geochemical models.

1.4.3. Oligomerization

A key step missing in the reconstruction of the origin of living systems is an abiotically synthesis of RNA oligomers.

Recently the capacity of the 5 differently phosphorylated forms to undergo spontaneous polymerization was analyzed (Costanzo *et al.*, 2009). They showed an unprecedented result: polymerization takes place in water at temperatures between 40 and 90°C. Data obtained showed that both 2',3'-cAMP and 3',5'-cAMP underwent polymerization events, while no oligomerization was observed for 2'AMP and 3'AMP, with only trace amounts of short oligomers formed from 5'AMP. Thus, the polymerization spontaneously occurs in water without needing template, catalysts and dry-chemistry conditions.

Moreover, evidences for physical polymerization following liquid crystallization of RNA oligomers have been recently reported (Zanchetta *et al.*, 2008), pointing to the relevance of self-assembly processes in favoring RNA chain growth. Non-enzymatic RNA ligation in water at moderate temperature has also been recently described (Pino *et al.*, 2008).

During the last decades the catalytic role of minerals (Bernal, 1951) and metal ions in the abiotic synthesis of biopolymers has been thoroughly investigated (Ferris, 2006; Monnard, 2005). In particular were studied the catalytic properties of montmorillonite, an abundant phyllosilicate believed to have formed large deposits on the early Earth (Ferris, 2006; Joshi *et al.*, 2007). It catalyzes the formation of single stranded RNA oligomers from activated ribonucleotides (Ferris, 2002; Ferris and Ertem, 1993; Huang and Ferris, 2006), the polymerization of up to 50 mers of poly(A) and poly(U) (Ferris, 2002), the formation of 30 to 40 mer RNA homopolymers in the absence of a primer (Huang and Ferris, 2003), the reaction of methyladenine-activated monomers of the four ribonucleotides, yielding RNA oligomers of up to 20 nt long (Huang and Ferris, 2006).

Moreover, montmorillonite can also catalyze the formation of vesicles from simple fatty acids supplied as micelles (Hanczyc and Szostak, 2004; Hanczyc *et al.*, 2003). Clay particles, with RNA molecules adsorbed on them, can be encapsulated within vesicles, which provide compartmented environments for further biochemical reactions: a sort of protocell-like compartment. It was shown that vesicle membranes composed of simple amphiphilic molecules are enough permeability to nucleotides to

allow nucleic acid elongation inside the protocell (Mansy *et al.*, 2008). On the bases of these observations two possible scenarious were proposed for the molecular evolution of RNA: on mineral surfaces in contact with a bulk aqueous medium, or inside vesicles that could also encapsulate mineral particles (Briones *et al.*, 2009).

1.4.4. Protection of RNA self-catalytic system

Another problem in the putative RNA world is the protection of RNA catalytic molecules against degrading agents, which were probably present on early Earth. In particular strong UV, X-ray radiations and high temperatures could have represented a big obstacle to the formation and evolution of the first genetic biomolecules.

Based on Bernal's observation and on the experimental data over mentioned, a protection role of biomolecules by mineral surfaces was hypothesized. In fact clays could have served as a "primitive membrane", thanks to their ability to supply compartimentalized microenvironment (Parsons *et al.*, 1998; Smith, 1998).

Protection by clays of genetic molecules (DNA, RNA) against biotic (i.e. nucleases) and abiotic (UV, X-ray radiation) degrading agents was demonstrated. Moreover, nucleic acid molecules adsorbed on clays maintained their biological activities, such as the ability to transform competent bacterial cells, to transmit the genetic information and to interact with molecules present in the environment (Franchi and Gallori, 2005; Gallori *et al.*, 2006; Gallori *et al.*, 1994; Scappini *et al.*, 2004; Stotzky, 1996; Vettori *et al.*, 1996).

More recently the same results were obtained on catalytic RNA molecules: montmorillonite are able to protect an *in vitro* selected hairpin ribozyme from UV damages (Biondi *et al.*, 2007a) and the ASBVd against aspecific degradation (Biondi *et al.*, 2007b). Moreover, it was shown that the monomeric form of the ASBVd is still active when it is tightly bound on the clay surface, and the rate of self cleavage enhances when the reaction is performed in the presence of montmorillonite.

These observations suggest that mineral surfaces could have played a crucial role in the formation and preservation of genetic material on the early Earth.

Of course, other possible scenarious could be suggested.

2. Aim of the work

There are many theories on the nature of ancestral biological systems, but the most widely accepted one is the "RNA World" hypothesis (Gilbert, 1986), indicating RNA as the first informative polymer. According to this hypothesis, the RNA world contained "only RNA molecules, which served to catalyze the synthesis of themselves". The idea that an RNA world preceded the DNA/RNA/PROTEIN world was largely supported by the discovery of ribozymes, RNA molecules with catalytic activity (Cech *et al.*, 1981; Guerrier-Takada *et al.*, 1983). The fact that RNA has the ability both to transfer genetic information (performed by DNA in present day cells) and to carry out catalytic activity (performed by proteins) makes it an extraordinary molecule. The discovery of a vast repertory of naturally occurring ribozymes in contemporary cells, and the crucial importance of their reactions, strongly suggest not only that an RNA world could have existed but also that it still lurks within modern living forms. The foremost contribution to acceptance of the RNA world hypothesis was the discovery that the ribosome is a ribozyme (Steitz and Moore, 2003).

The best known ribozyme is the hammerhead, which is capable of self-cleavage in the presence of divalent metal cations (Mg^{2+}). Metal cations play a fundamental role in both the folding into the characteristic "Y-shape" and ribozymatic activity of RNA (structural and/or catalytic role). In nature, these ribozymes are found in small, circular, non-coding RNA molecules called viroids, the smallest RNA plant pathogens known (Diener, 1989; Diener, 2003). Thanks to their catalytic activity and other peculiarities, viroids are considered molecular "living fossils of a precellular RNA world" (Diener, 1989). Most interestingly, viroids are non-protein-encoding RNAs, which implies that all the information (genetic and catalytic) lies within their structure. In fact, the catalytic activity of viroids, a necessary condition for primitive RNA molecules, is exclusively due to the attainment of a certain structure. Therefore, the passage from an inactive to an active structure could have been a fundamental step in the evolution of self-replicating RNA molecules in the primitive RNA world, making the study of viroid structure of pivotal importance.

Nevertheless, the hypothesis of a primeval RNA world is strongly affected by the hostile environmental conditions likely present on early Earth. In particular, strong UV, X-ray radiations and high temperatures could have been major obstacles to the formation and evolution of the first genetic biomolecules.

Therefore, in addition to attaining the proper folding necessary for their catalytic activity, RNA molecules would have had to be protected against degrading agents. Indeed, these requirements would have been the necessary conditions allowing primitive molecules to undergo molecular evolution.

The present thesis deals with the study of the structure, activity and protection of primordial catalytic RNA molecules, with the aim of understanding how they could have evolved in the supposed primitive RNA world.

The first part of the work investigates the *in vitro* activity of the Avocado Sunblotch viroid, and its structural organization in different environmental conditions, obtained by varying the temperature and Mg^{2+} concentrations. In particular, the research focused on the viroid structural changes induced by Mg^{2+} in order to identify its active form. The second part explores the possibility that a dipeptide (Lys-Lys) could have played a protective role for an ancient RNA molecule in a hot primordial environment. We examine the effect of high temperatures on the activity of a trans-acting ribozyme in the presence/absence of Lys-Lys, simulating a scenario in which both RNA molecules and primordial amino acids or short polypeptides could have been present at the same time.

3. Results

3.1. Structural and functional characterization of the Avocado Sunblotch viroid in different environmental conditions

The catalytic activity of some viroids (*Avsunviroidae* family), together with the small size, the circular structure, the fact that they are non-protein-encoding RNAs and that all the information is contained within their structure, support the idea that viroids have an evolutionary origin that is very ancient and independent from that of viruses. For these reasons viroids are considered molecular fossil of the precellular RNA world (Diener, 1989; Diener, 2003). Thus, the study of their behaviour and the characterization of their mechanism of cleavage, replication, infection in the present-day cell system could help our understanding of the behaviour of ancient RNA molecules in the putative RNA world.

Furthermore, the catalytic activity of viroids, which was a necessary condition for primitive RNA molecules, is exclusively due to the reaching of a certain structure. In particular, it has been shown that the so called hammerhead structure plays a key role in the cleavage reaction. The passage from an inactive to an active conformation could have been therefore a fundamental step in the evolution of self-replicating RNA molecules in the primitive RNA world, making the study of the viroid structure of pivotal importance.

With this aim, this work is based on the study of the *in vitro* activity of the Avocado Sunblotch Viroid (ASBVd, *Avsunviroidae* family), and the characterization of its structural organization in different environmental conditions.

In particular, the monomeric and linear forms of the ASBVd were studied under three different conditions, obtained by varying the temperature and the Mg^{2+} concentrations:

1) *Physiological conditions*; to simulate the intercellular compartment referred to as chloroplast in which the viroid replication takes place.

2) *Different cleavage conditions*; in order to characterize the structural changes of the viroid promoting a cleavage reaction (inactive and active structures), interactions with different cations including Mg^{2+}.
3) *Extreme conditions*; such as high temperatures, to simulate a primordial environment.

For these investigations we used different techniques: the activity of the viroid was analyzed by performing *in vitro* self-cleavage kinetics, while its structural organisation was assessed through Circular Dichroism and Raman spectroscopy.

3.1.1. Sequence and theoretical structure analysis of plus and minus mASBVd RNA

Monomeric and linear form of plus (+) and minus (-) strands of ASBVd were obtained by *in vitro* transcription as described in Material and Methods (section 5.1).

Both the (+) and (-) RNAs of the 247 nt mASBVd carry a hammerhead ribozyme in their sequences; the formation of the hammerhead structure catalyzes the self-cleavage reaction (Hutchins *et al.*, 1986). Fig. 3.1 shows the hammerhead structures of the self-cleaving RNAs of (+) (A) and (-) (B) ASBVd. This reaction occurs *in vitro* in the absence of proteins and requires only the presence of a divalent cation, such as Mg^{2+}, and around neutral pH conditions to yield 5'-hydroxyl and 2', 3'-cyclic phosphate termini.

The primary sequences of the (-) and (+) mASBVd RNA are shown in Fig. 3.2. The sequences are complementary to each other, but the cleavage site occurs in two different positions. Thus, after the cleavage (-) and (+) strands (247 nucleotides) will give two different fragments with different length of 84nt/163nt and 98nt/149nt respectively.

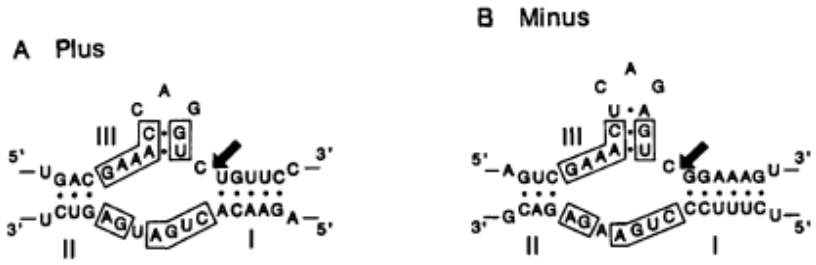

Fig. 3.1. Hammerhead structures of the self-cleaving RNAs of (+) (A) and (-) (B) ASBVd (Forster *et al.*, 1988). Base-paired stems are numbered I to III according to Forster and Symons (Forster and Symons, 1987), sites of cleavage are indicated by arrows and nucleotides conserved between all self-cleaving RNAs (Bruening, 1989; Forster and Symons, 1987; Symons, 1989) are boxed.

AAGAGAUUGA	AGACGAGUGA	ACUAAUUUUU	UUAAUAAAAG	UUCACCACGA	CUCCUCCUUC
UUCUCUAACU	UCUGCUCACU	UGAUUAAAAA	AAUUAUUUUC	AAGUGGUGCU	GAGGAGGAAG
UCUCACAAGU	CGAAACUCAG	AGUCGGAAAG	UCGGAACAGA	CCUGGUUUCG	UCAAACAAAG
AGAGUGUUCA	GCUUUGAGUC	UCAGCCUUUC	AGCCUUGUCU	GGACCAAAGC	AGUUUGUUUC
UUUAAUCAUA	UCCUCACUUC	UUGUUCUAAU	AAACAAGAUU	UUGUAAAAAA	ACAAUGAAGA
AAAUUAGUAU	AGGAGUGAAG	AACAAGAUUA	UUUGUUCUAA	AACAUUUUUU	UGUUACUUCU
UAGAGGAAUA	AACCUUGCGA	GACUCAUCAG	UGUUCUUCCC	AUCUUUCCCU	GAAGAGACGA
AUCUCCUUAU	UUGGAACGCU	CUGAGUAGUC	ACAAGAAGGG	UAGAAAGGGA	CUUCUCUGCU
AGUGAUC					
UCACUAG					

Fig. 3.2. Sequences (-) and (+) of mASBVd are shown in black and blue, respectively. The conserved sequences of hammerhead ribozyme are highlighted in red, whereas the yellow mark refers to the cleavage site.

The linear and monomeric secondary structures of (+) and (-) mASBVd transcripts were checked at 25°C, subjecting the primary sequence to Mfold software (Mathews *et al.*, 1999; Zuker, 2003) (Fig. 3.3 and Fig. 3.4). Both were very similar to the circular and monomeric predicted secondary structures of the (+) and (-) ASBVd (Ding and Itaya, 2007).

The more stable structures of both (+) and (-) strands (dG = -99.36 and -78.80 kcal/mol respectively) present numerous double stranded regions because of the high self-complementarity level of the nucleotide sequence of the molecule. Moreover, we did not observe any hammerhead structure formation, because the conserved

hammerhead nucleotides are trapped inside base-pairs with other nucleotides that probably give more stability to the molecule. Thus, the catalytically active conformation with hammerhead is not the most stable for mASBVd, and the molecules preferentially adopt alternative inactive structures.

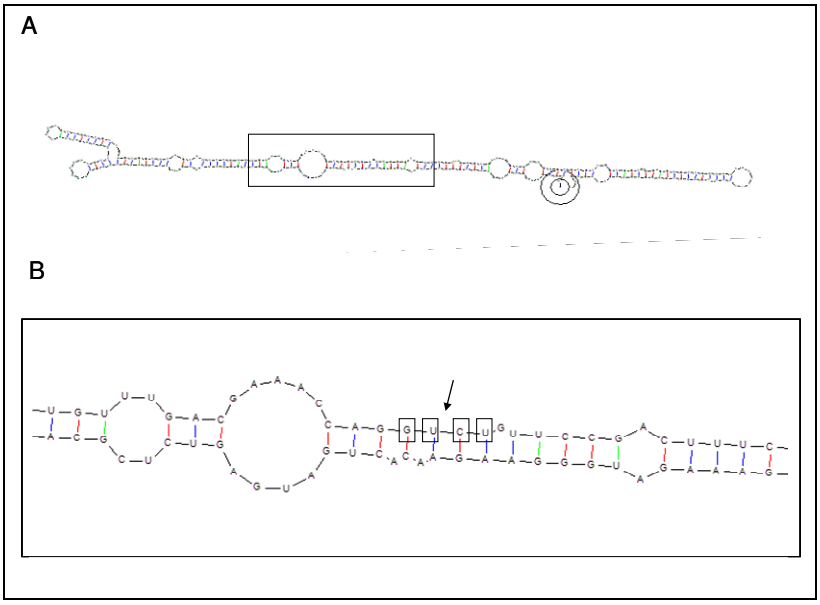

Fig. 3.3. A: Secondary structure of (+) mASBVd calculated with Mfold software at 25°C. The box enlarged in B contains the part corresponding to the hammerhead ribozyme. The conserved nucleotides around the cleavage site (indicated by the arrow) are boxed.

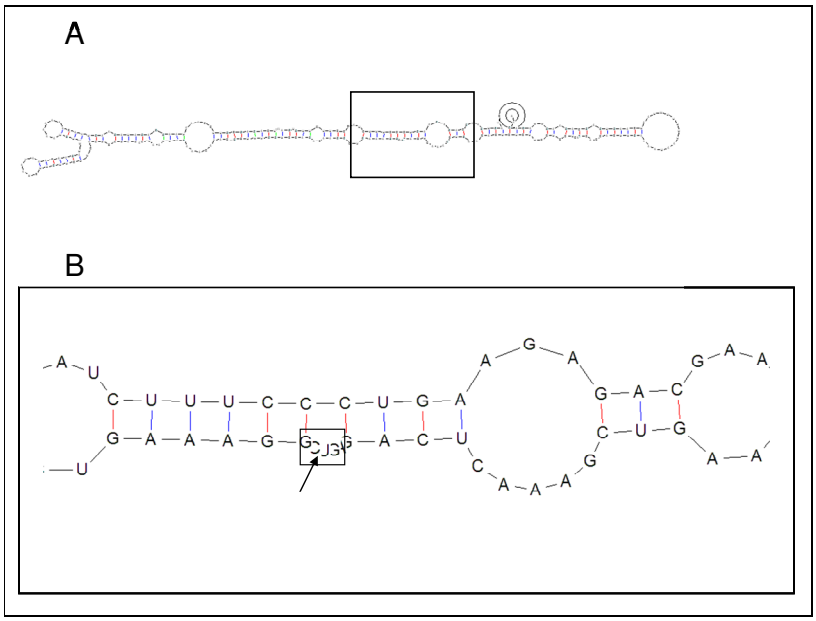

Fig. 3.4 A: Secondary structure of (-) mASBVd calculated with Mfold software at 25°C. The box enlarged in B contains the part corresponding to the hammerhead ribozyme. The conserved nucleotides around the cleavage site (indicated by the arrow) are boxed.

3.1.2. Analysis of the activity of (+) and (-) mASBVd strands

The activity of the linear and monomeric form of (+) and (–) strands of the ASBVd has been initially determined.

mASBVd self-cleavage reaction can be outlined according to the equation (1)

$$C_I \rightleftharpoons C_A \longrightarrow 5'F + 3'F$$

where C_I and C_A are the inactive and active conformations of the various monomers, respectively; 5'F and 3'F are the self-cleavage product fragments carrying 5' and 3' termini of the molecule (Sheldon and Symons, 1989).

The first step of the pathway represents a chemical equilibrium between the various inactive forms and the catalytically active structures of the monomer, while the second part represents the self-cleavage process. In order to have self-cleavage, the inactive structures must undergo a conformational change to an active hammerhead structure. Once the active structure has formed, the self-cleavage step is very fast. The pathway and extent of the self-cleavage reaction has not been considered as a result of the rate of the second step (always very fast), but rather it is determined by the relative stabilities of the inactive and active structures. Therefore, the formation of the active structures is the rate-limiting step of the self-cleavage reaction. The fraction of RNA that does not cleave presumably is folded into stable inactive structures.

To test the catalytic activity of (+) and (-) mASBVd, kinetic self-cleavage reactions were performed by varying several experimental parameters, such as Mg^{2+} concentration and temperatures (see section 5.2.1. of Material and Methods), which could influence the first step's shift towards C_A.

3.1.2.1. Studies at different Mg^{2+} concentrations

The role of Mg^{2+}, and of metal ions in general, has been exhaustively studied both for minimal (Curtis and Bartel, 2001; Murray *et al.*, 1998; O'Rear *et al.*, 2001; Pyle, 1993; Yarus, 1993) and "extended" *Schistosoma* (Boots *et al.*, 2008; Canny *et al.*, 2004; Khvorova *et al.*, 2003; Kim *et al.*, 2005; Kisseleva *et al.*, 2005; Lee *et al.*,

2009; Penedo *et al.*, 2004; Thomas and Perrin, 2009) hammerhead ribozyme. These data show that metal cations are required for efficient cleavage and that they are of fundamental importance for both the folding into the characteristic "Y-shape" and ribozymatic activity of RNA (structural and/or catalytic role).

Despite many studies focused on the role of metal cations in the hammerhead ribozyme, little is known about their role on the entire viroid. Nevertheless, there are no evidences in literature on the *in vitro* activity of viroids without Mg^{2+}, indicating that the presence of this cation is essential, at least *in vitro*, for the self-cleavage of the entire viroid. Probably it promotes the correct folding of the hammerhead ribozyme contained in the viroid sequence. "Presumably, in the presence of a divalent cation such as Mg^{2+}, the hammerhead secondary structure forms an active tertiary complex that lowers the activation energy sufficiently and specifically at the internucleotide bond of the cleavage site to allow the phosphoryl transfer of the self-cleavage reaction" (Davies *et al.*, 1991).

Given that hammerhead ribozymes seem to be cation-dependent for both the stabilization of the active structure and the catalytic reaction itself, Mg^{2+} concentration in equation (1) influences both the first and the second step of the reaction.

Kinetics at several different Mg^{2+} concentrations (10, 20, 50, 100 mM), 37°C and pH 7.5, were performed for both strands of mASBVd (Fig. 3.5).

The percentage of the cleavage, calculated 5 hours after adding Mg^{2+} (Table 3.1 and Fig. 3.6), shows an increase in the activity with the increase of Mg^{2+} for both strands. It is also evident that the (-) strand is more active than the (+) strand: at 10 mM of Mg^{2+} after 5 hours the (-) strand reached about the 26 % of the cleavage, while the (+) strand only the 2%. Moreover, at this temperature (37°C) the percentage of the (-) strand cleavage apparently reached a plateau at 20 mM of Mg^{2+}.

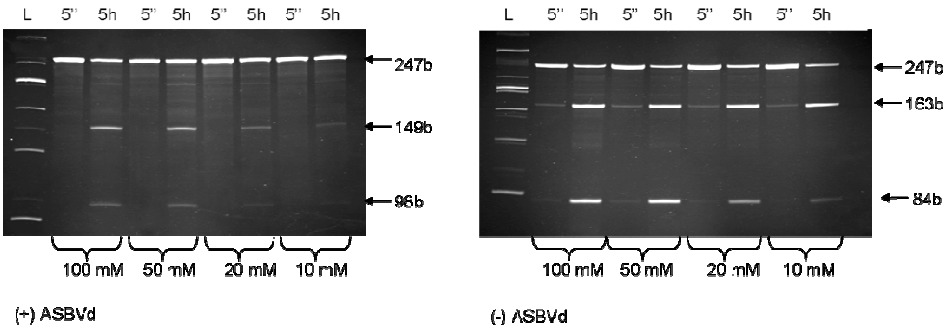

Fig. 3.5. 10% urea-PAGE of (+) (left hand) and (-) (right hand) mASBVd self-cleavage kinetic reactions at 37°C with 100, 50, 20 and 10 mM of Mg^{2+}. Numbers at the top are the time at which kinetics were stopped, the ones on the right are the lengths of the entire and cleavage fragments.

[Mg^{2+}] mM	% Cleav after 5h (+) ASBVd	% Cleav after 5h (–) ASBVd
10mM	2.04 % ± 0.42	25.61 % ± 0.98
20mM	5.23 % ± 1.30	70.18 % ± 1.72
50mM	13 % ± 1.45	71.98 % ± 1.25
100mM	22.37 % ± 0.83	74.07 % ± 1.03

Table 3.1. Percentages of cleavage calculated after 5h at 37°C at different Mg^{2+} concentrations for (+) and (-) strand of mASBVd.

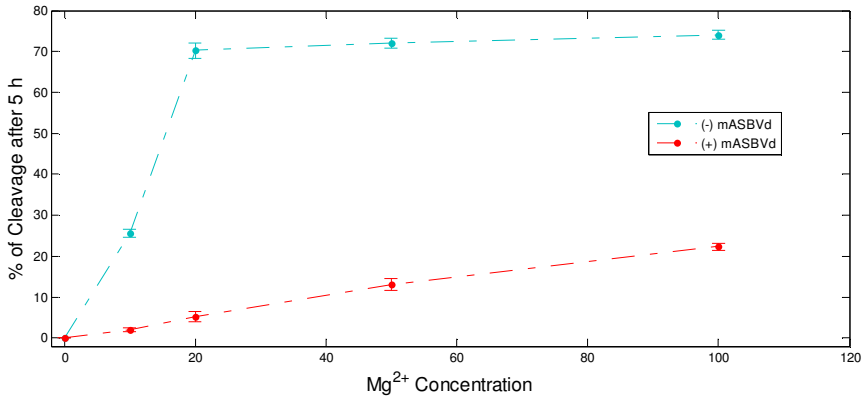

Fig. 3.6. Percentages of cleavage calculated after 5h at 37°C at different Mg^{2+} concentrations (0, 10, 20, 50 and 100 mM) for (+) and (-) strand of mASBVd, plotted versus Mg^{2+} concentrations.

3.1.2.2. Studies at different temperatures

The temperature is another factor that influences the cleavage reaction. Indeed, the increase in temperature provides a larger amount of energy to the system and the molecules have a higher chance to reach the active conformation. Thus, higher temperature helps the Mg^{2+} in its structural roles. However a too high temperature could have an opposite effect because it promotes the degradation of the RNA molecules.

Three several different temperatures (25, 37, 45°C) were tested for both strands of mASBVd (Fig. 3.7). On the basis of previous results, we checked two different Mg^{2+} concentrations for each temperature: 100 mM and 50 mM for the (+) strand, and 50 mM and 10 mM for the (-) strand. The pH was maintained at 7.5 for all the experiments. Also in this case, the percentage of cleavage, estimated after 5 hours since the beginning of the reaction, shows an increase in the activity with the increase of temperature for both strands (Table 3.2 and Fig. 3.8).

These results confirmed that the (-) strand is more active than the (+) strand and that is more resistant to degradation at higher temperatures. For these reasons, further experiments were mostly performed using the (-) strand.

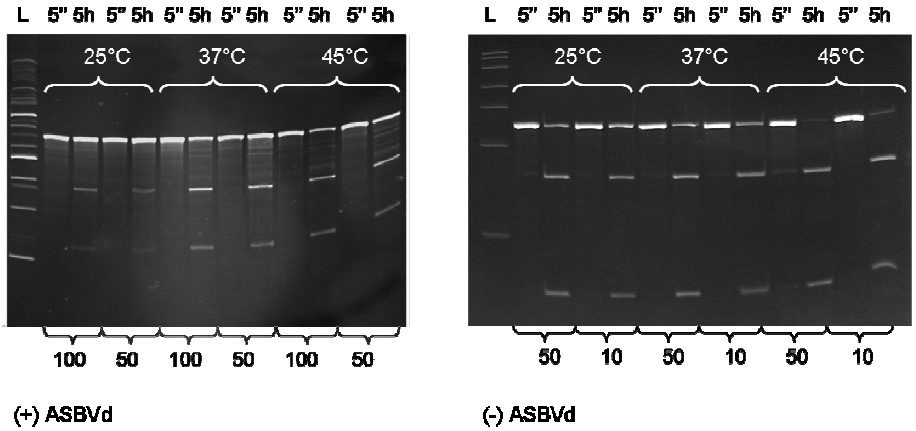

Fig. 3.7. 10% urea-PAGE of (+) (left hand) and (–) (right hand) mASBVd self-cleavage kinetics at several different temperatures (25, 37, 45°C) and Mg^{2+} concentration (100 and 50 mM for (+) strand and 50 and 10 mM for (-) strand). Numbers at the top are the time points at which the kinetics were stopped and at the bottom the respective Mg^{2+} concentrations tested. Bands on gel represent (from the top to the bottom) entire (247 nt) and cleavage fragments (149 and 98 nt for (+) strand, 163 and 84 nt for (-) strand) of viroid.

Temp, °C	[Mg2+], mM (+)ASBVd	% Cleavage after 5h (+)ASBVd	[Mg2+], mM (-)ASBVd	% Cleavage after 5h (-)ASBVd
25°C	100mM	6.73 % ± 0.91	10mM	5.36 % ± 0.7
25°C	50mM	4.6 % ± 0.64	50mM	20.73 % ± 1.29
37°C	100mM	22.28 % ± 1.26	10mM	25.37 % ± 1.03
37°C	50mM	11.01 % ± 1.03	50mM	72.35 % ± 1.16
45°C	100mM	39.87 % ± 1.53	10mM	57.75 % ± 1.02
45°C	50mM	23.11% ± 0.96	50mM	94.15 % ± 0.98

Table 3.2. Percentages of cleavage calculated after 5h at different temperatures (25, 37, 45 °C) and Mg^{2+} concentration (100 and 50 mM for (+) strand and 50 and 10 mM for (-) strand).

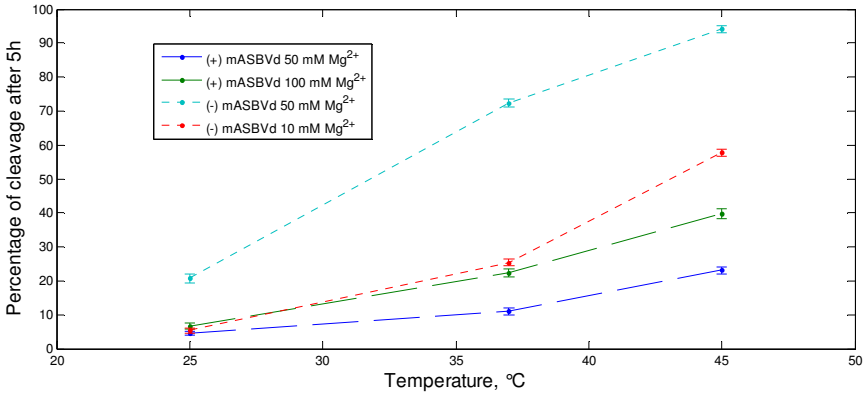

Fig. 3.8. Percentage of cleavage calculated after 5h at different temperatures (25, 37, 45 °C) and Mg^{2+} concentration (100 and 50 mM for (+) strand and 50 and 10 mM for (-) strand) plotted versus temperature.

3.1.3. Study of the *in vitro* self-cleavage activity of (–) mASBVd

In order to characterize the behaviour of the viroid in physiological conditions, we initially performed experiments reproducing some of the conditions of the chloroplast, the cellular compartment in which the ASBVd replicates (Navarro *et al.*, 1999). For this purpose, kinetics were made at 25°C, pH 7.5, 2 mM of Mg^{2+} and 150 mM of K^{+} (Demmig and Gimmler, 1983; Igamberdiev and Kleczkowski, 2001; Portis, 1981) (see section 5.2.2 of Material and Methods).

Fig. 3.9 shows that under these *in vitro* conditions the viroid is not active, probably because the concentration of Mg^{2+} and/or the temperature are too low and not sufficient to shift the chemical equilibrium between C_I and C_A towards C_A (see eq. 1 in section 3.1.2). In fact any cleavage is observed after 24 h.

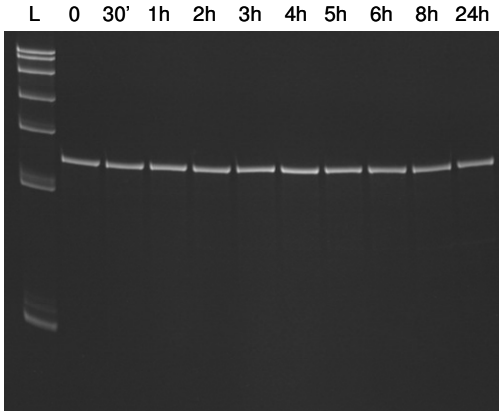

Fig. 3.9. Kinetic performed in physiological conditions: 25°C, pH 7.5, 2mM of Mg^{2+}, 150mM of K^+.

Given that the viroid is inactive under physiological conditions, we carried out different kinetics changing Mg^{2+} concentration and temperatures (same pH and K^+ concentration), in order to find good conditions allowing the cleavage. Kinetics were performed at

- 25°C with 10, 50, 100 mM of Mg^{2+}
- 35°C with 10, 20, 50 mM of Mg^{2+}
- 45°C with 2, 10, 50 mM Mg^{2+}
- 55°C with 2, 10, 50 mM of Mg^{2+}

For each kinetic the percentage of cleavage was calculated as reported in Material and Methods (section 5.2). Data were plotted and fitted with the equation $F_t = F_0 + F_\infty(1\text{-}e^{-k_{obs}t})$, where F_t, F_0 and F_∞ are the fractions of products cleaved at time t, at time 0 and at the plateau, respectively, and k_{obs} is the observed kinetic constant of the reaction (Fig. 3.10, Fig. 3.11, Fig. 3.12, Fig. 3.13).

The K_{obs} (Table 3.3) and the F_∞ (Table 3.4) observed at each temperature were plotted versus the Mg^{2+} concentration (Fig. 3.14 and Fig. 3.15). The K_{obs} value increases by increasing both Mg^{2+} concentration and temperature (Fig. 3.14), while

the F_∞ value increases with the temperature reaching a plateau at about 10 mM of Mg^{2+} (Fig. 3.15).

On the basis of these experiments we can conclude that the best temperature and Mg^{2+} concentration for the cleavage of (-) mASBVd are 55°C and 50 mM, respectively.

We also made two negative controls for each temperature to test the effect of the K^+ and of the cacodylate buffer: neither the kinetic with cacodylate pH 7.5 and 150 mM of K^+ (Fig. 3.16 A), nor the one without K^+ (same temperature, same pH, Fig. 3.16 B) show the cleavage. The same results are obtained at any temperature analyzed. In Fig. 3.16 only the negative controls performed at 55°C are reported. These results represent a further evidence that viroid self-cleavage requires the presence of Mg^{2+}.

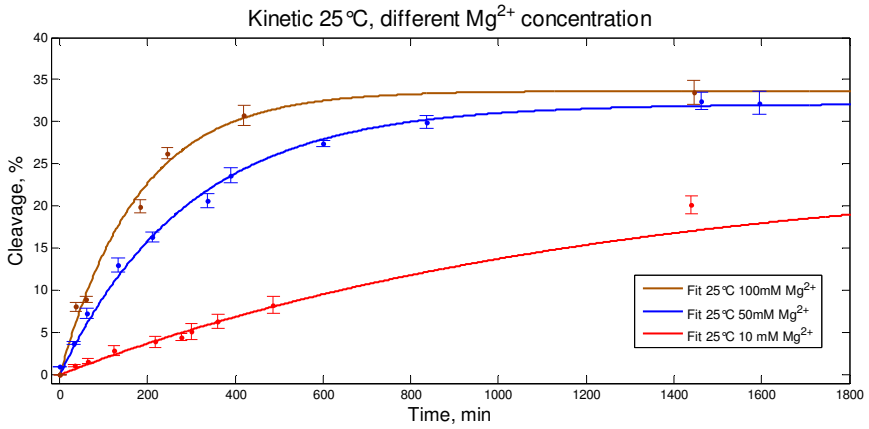

Fig. 3.10. Kinetics at 25°C, different Mg^{2+} concentrations (10, 50, 100 mM), 150 mM K^+, pH 7.5.

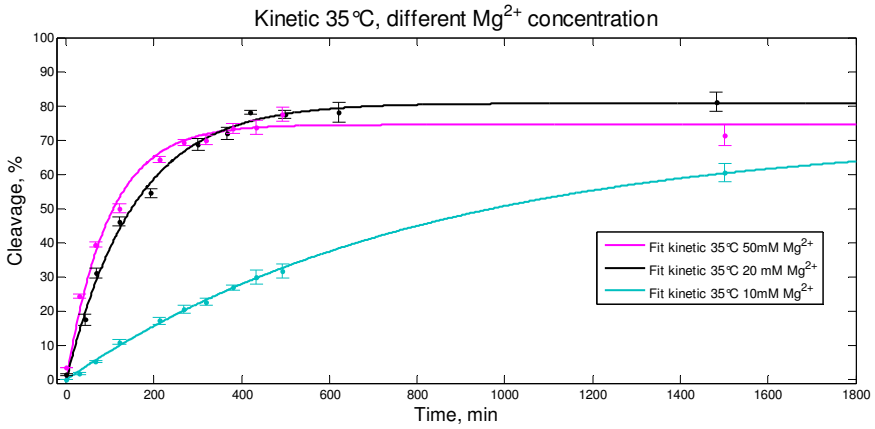

Fig. 3.11. Kinetics 35°C, different Mg^{2+} concentrations (10, 20, 50 mM), 150mM K^+, pH 7.5

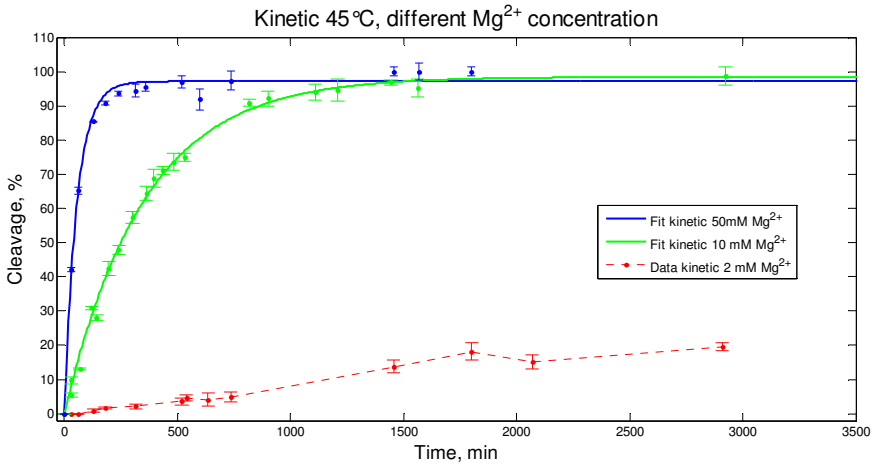

Fig. 3.12. Kinetics at 45°C, different Mg^{2+} concentrations (2, 10, 50 mM), 150 mM K^+, pH 7.5. The self-cleavage kinetic at 2 mM of Mg^{2+} (red dotted line) was impossible to fit because the reaction not arrives at plateau.

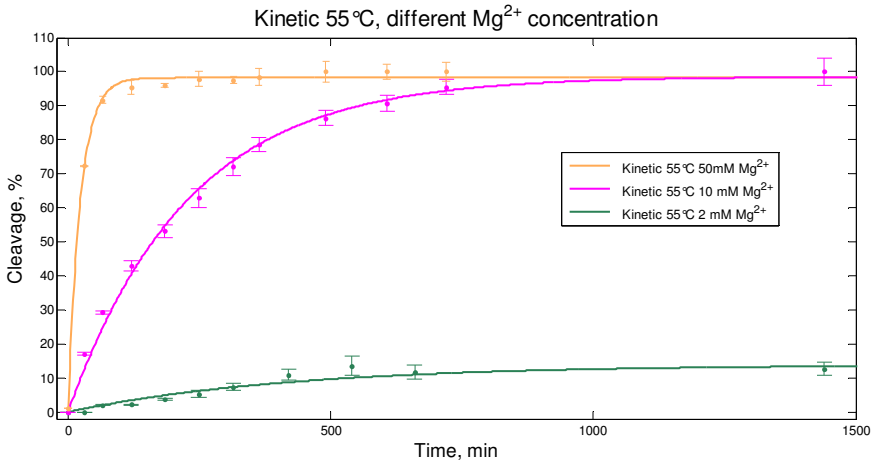

Fig. 3.13. Kinetics 55°C, different Mg^{2+} concentrations (2, 10, 50 mM), 150 mM K^+, pH 7.5

	2mM Mg^{2+}	10mM Mg^{2+}	20mM Mg^{2+}	50mM Mg^{2+}	100mM Mg^{2+}
25°C	Inactive	0.000812 ± $1.8*10^{-4}$		0.003404 ± $4*10^{-4}$	0.004322 ± $1.3*10^{-3}$
35°C	Inactive	0.001239 ± $9.5*10^{-5}$	0.006494 ± $1.1*10^{-3}$	0.01035 ± $2*10^{-3}$	
45°C	imp to fit	0.002846 ± $1.68*10^{-4}$		0.0179 ± $1.8*10^{-3}$	
55°C	0.002365 ± $1*10^{-3}$	0.004393 ± $5*10^{-4}$		0.04239 ± $2.1*10^{-3}$	

Table 3.3. K_{obs} calculated for each kinetic performed

	2mM Mg^{2+}	10mM Mg^{2+}	20mM Mg^{2+}	50mM Mg^{2+}	100mM Mg^{2+}
25°C	Inactive	24.72±2.10		32.1±1.29	33.65±2.92
35°C		71.45±3.35	80.77±4.95	74.5±3.71	
45°C	Imp to fit	98.48±2.07		97.12±1.67	
55°C	13.92±3.1	98.58±4		98.23±1.22	

Table 3.4. F_{∞} calculated for each kinetic performed

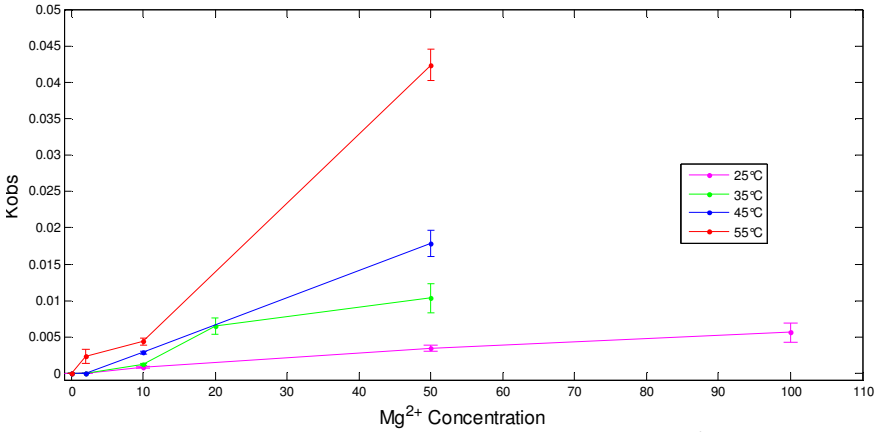

Fig. 3.14. K_{obs} obtained at each temperature plotted versus Mg^{2+} concentration

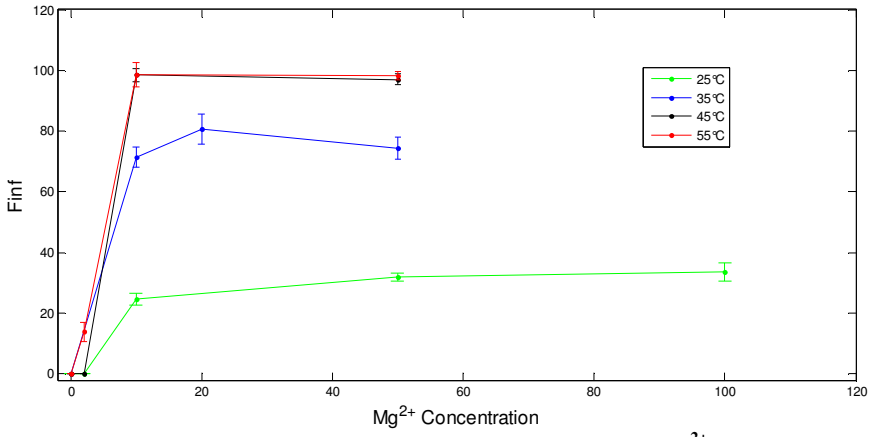

Fig. 3.15. F_∞ calculated at each temperature plotted versus Mg^{2+} concentration

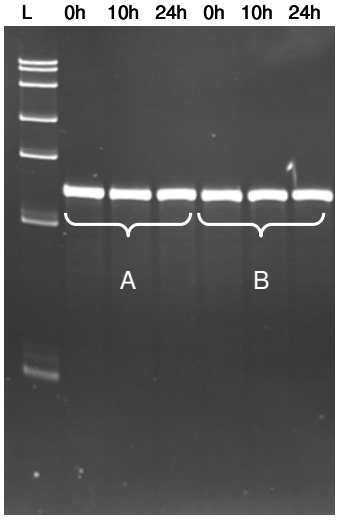

Fig. 3.16. Negative control kinetics performed without Mg^{2+} at 55°C and pH 7.5. A: 10 mM buffer cacodylate pH 7.5 and 150 mM K^+. B: the same without K^+.

3.1.4. Studies on the structural changes of (-) mASBVd by Circular Dichroism (CD) and Raman spectroscopy

These studies were performed with the aim to evaluate which were the structural changes leading to an inactive or an active structure, and to understand if there was a correlation between the cleavage efficiency and the structural changes of viroid.

For these purposes different self-cleavage reactions of the (-) mASBVd were followed by CD and Raman spectroscopy. On the basis of previous experiments we chose three different conditions:

- physiological conditions, in which the viroid was inactive:
  25°C, 2 mM Mg^{2+}, 150 mM K^{+}, pH 7.5
- Two different cleavage conditions:
  a) 25°C 100 mM Mg^{2+}, 150 mM K^{+}, pH 7.5 (K_{obs}=0.004322 min^{-1}, F_{∞}=33.65)
  b) 35°C 20 mM Mg^{2+}, 150 mM K^{+}, pH 7.5 (K_{obs}= 0.006494 min-1, F_{∞}=80.77)

The cleavage condition "a" was chosen to be compared with the physiological condition; in fact, the Mg^{2+} concentration is the only parameter that changes. These experiments allowed us to compare a condition where the viroid undergoes self-cleavage activity with another one where it is inactive.

The cleavage condition "b" was chosen to have higher viroid activity than "a" with less concentration of Mg^{2+}, that necessarily implies a higher temperature. For this reason both Mg^{2+} concentration and temperature change. These experiments allowed us to compare two different conditions of cleavage.

Structural changes of the viroid were also investigated with CD at different concentration of Mg^{2+} and different temperatures.

3.1.4.1. Circular Dichroism

Circular dichroism (CD) is a phenomenon originating from interactions of chiral molecules with circularly polarized electromagnetic rays (Woody, 1995). For more details on the phenomenon and the applications of CD spectroscopy in biochemistry see section 5.3 of Material and Methods. With the discovery of ribozymes the CD spectroscopy has been used to characterize the RNA structure and

secondary and tertiary RNA folding transitions (Pan and Sosnick, 1997; Sosnick, 2001; Sosnick *et al.*, 2000).

All CD experiments were performed with the same method used in the *in vitro* self-cleavage kinetics (see section 5.3.3 of Material and Methods for details). After RNA heating (95°C x 30sec) and slow cooling (3°C/min) up to the temperature of interest, the spectrum of the RNA in water was measured. Then cacodylate buffer (pH 7.5) and K^+ (150 mM), and finally the Mg^{2+} (2, 20 or 100 mM) were mixed to RNA in water. The spectrum of the RNA was measured after adding each component. When Mg^{2+} came in contact with RNA the reaction started and the first spectrum was called "Time 0" of the reaction. Spectra were monitored at different time points after Mg^{2+} was added, to assess any possible change in the viroid structure during the reaction, both in the case of inactivity and activity. Moreover, before each measure, we took aliquots of the solution at different time points, and stopped the reaction in order to verify the results of the cleavage kinetics by denaturant polyacrylamide gel electrophoresis (PAGE).

All the spectra were measured between 210 and 310 nm. RNA strongly absorbs in the far UV and measurements below 200 nm are difficult, due to high absorbance. In the region above 200 nm the maximal absorbance is due to the nucleotide bases, which have a broad maximum in the region around 260 nm (Sosnick, 2001).

CD spectrum of the viroid in water

The CD spectrum of viroid in water (Fig. 3.17, black line) is associated with the A-conformation of a polynucleotide helix, characterized by a dominant positive band at about 265 nm and a negative band at about 210 nm (Williams *et al.*, 1986). The A-form is the predominant shape that double-helix RNAs adopt. This is very similar to the A-helix type assumed by dehydrated DNA.

Effects of buffer-K^+ and Mg^{2+}

As observed in Fig. 3.17, the addition of cacodylate buffer-K^+ (green line) to the viroid in water induces a change in the CD spectrum represented by a blue shift and an increase in the band located at 265-270 nm. In contrast, the change induced by Mg^{2+} on the CD spectrum of viroid in buffer-K^+ involves a slight red shift and an

increase of the same band (red line). The CD signal of this band mainly results from the coupling between the electronic transitions of the stacked bases in a chiral helical fashion. Changes in the intensity and position of this band reflect variations in the spatial relationship between the bases, hence in the structural organisation of bases. Therefore, on one hand the effect of buffer-K^+, on the other hand the effect of Mg^{2+}, result in different structural organizations in the base stacking of the viroid. However, the CD spectra of viroid are still typical of A-RNA form. An important consideration is that the viroid is inactive until the Mg^{2+} is added. In fact, previous experiments showed the inactivity of the viroid in K^+ (150 mM) and buffer cacodylate (pH 7.5, 10 mM) without Mg^{2+}.

Given that the Mg^{2+} is of fundamental importance to allow the *in vitro* self-cleavage reaction, we also analyzed the structural changes of (-) ASBVd at several different concentrations of Mg^{2+}. A gradual increase in Mg^{2+} concentration (0.5 mM each step, see section 5.3.5 of Material and Methods), from 0.5 to 10 mM, leads to an increase and a shift of the main peak at around 260 nm toward the red (Fig. 3.18). Moreover the CD signal at ~260 nm increases as Mg^{2+} concentration increases, without keeping any obvious isodichroic point (Fig. 3.18). For each spectrum, measured at each Mg^{2+} concentration, the maximum value of the main peak was detected and plotted versus the Mg^{2+} concentration (Fig. 3.19). The average curve shows the trend: there is a gradual increase in the main peak from 0.5 to 10 mM of Mg^{2+}, suggesting a gradual change in the structural organization of the bases. *In vitro* kinetics showed that the viroid is inactive with 0.5 mM of Mg^{2+} (Fig. 3.20 A), while it was active with 10 mM of Mg^{2+} (Fig. 3.20 B). Moreover, we know that the activity of the viroid depends on the Mg^{2+} concentration under the same conditions of temperature, pH and K^+.

These experiments lead to the same conclusion: the increase and the red-shift of the main peak at about 260 nm of the viroid spectrum is induced by Mg^{2+}. Mg^{2+} effect on the viroid spectral changes is enhanced by increasing Mg^{2+} concentrations which in turn results in an increased viroid activity. For this reason this kind of structural change could be related with the achievement of active conformation of the viroid.

In contrast, the change induced by cacodylate buffer and K^+, could be related with an inactive viroid conformation, since no cleavage is observed under these conditions.

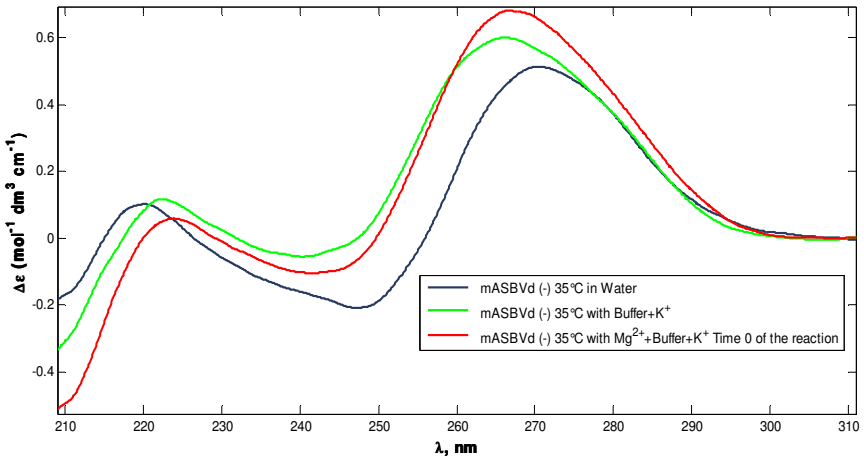

Fig. 3.17. Effects of buffer+K^+ (green line) and Mg^{2+} (red line) on the CD spectrum of viroid in water (black line).

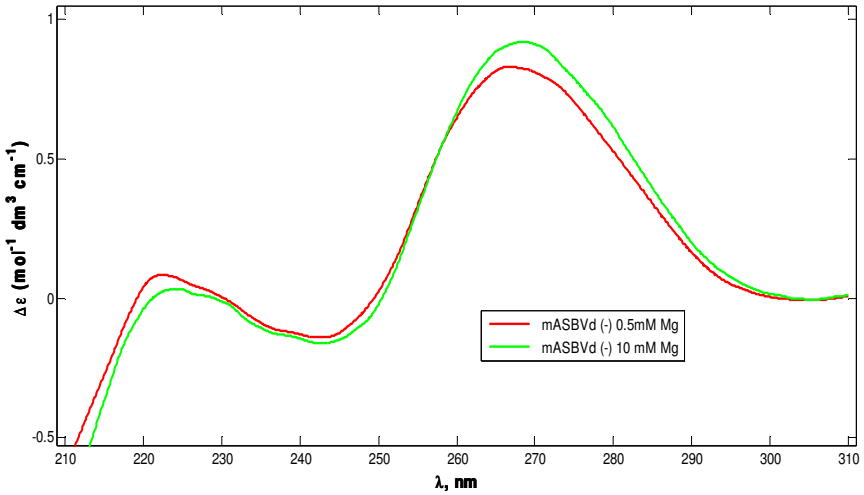

Fig. 3.18. Structural change in the RNA at different concentrations of Mg^{2+}. The concentration of Mg^{2+} was increased from 0.5 to 10 mM (0.5 mM each step). Here we show only the spectrum at the lower concentration (0.5 mM) and the one at the higher (10 mM). Red line: 0.5 mM of Mg^{2+}. Green line: 10 mM of Mg^{2+}.

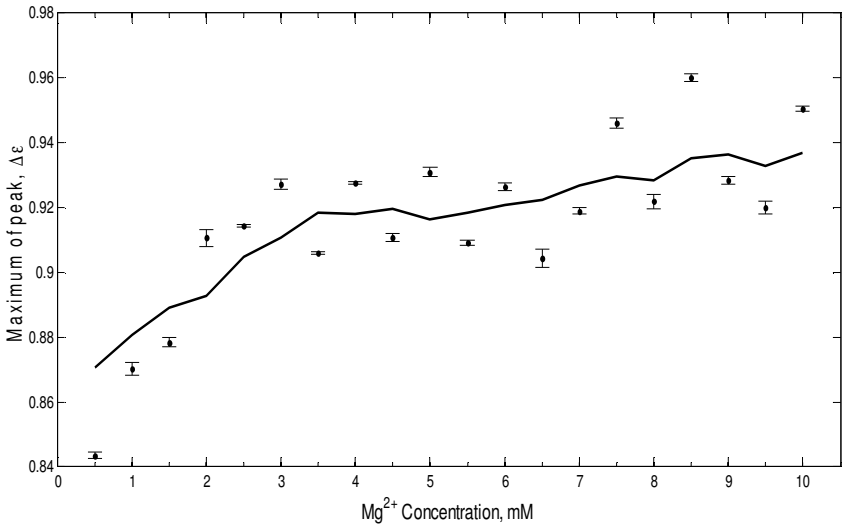

Fig. 3.19. Maximum value of the main CD peak obtained at different Mg^{2+} concentration. The average curve (solid line) shows the trend.

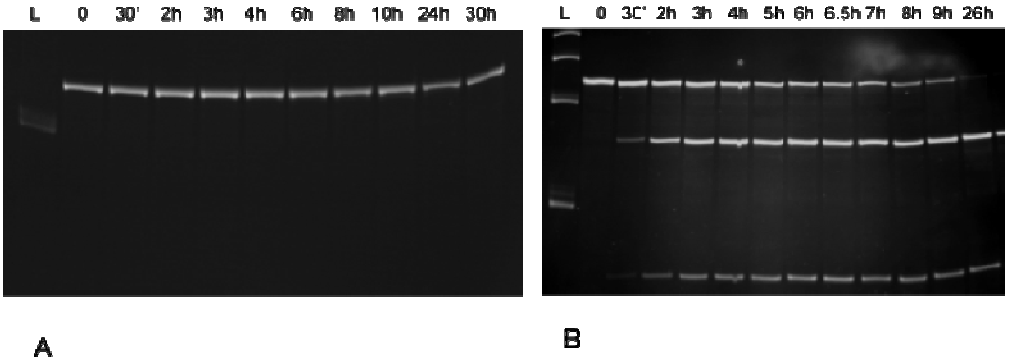

Fig. 3.20. 10% urea-PAGE of (-) mASBVd self-cleavage kinetic reaction at 0.5 mM Mg^{2+}, pH 7.5, 45°C (A) and at 10 mM Mg^{2+}, pH 7.5, 45°C (B). In the gel A only the band corresponding to the entire viroid (247 nt) is detected (viroid inactive). In the gel B we can see the three bands corresponding (from the top to the bottom) to the entire viroid (247 nt) and to the two cleavage fragments (163 nt and 84 nt) (self-cleavage). "L" indicates the RNA ladder and the time points at which the cleavage reaction was stopped are reported.

Time dependent analysis of viroid CD spectra during kinetics

The CD spectra were monitored at different time points after Mg^{2+} addition, to assess any possible change in the viroid structure during the kinetics.

The green line in Fig. 3.21 (physiological conditions) shows that the spectrum obtained after 6.5h since the beginning of the reaction is the same as at time 0, measured immediately after Mg^{2+} addition (black line). Results by PAGE show that in these conditions no cleavage is observed (Fig. 3.22); in fact, there is no variation in the spectra over time.

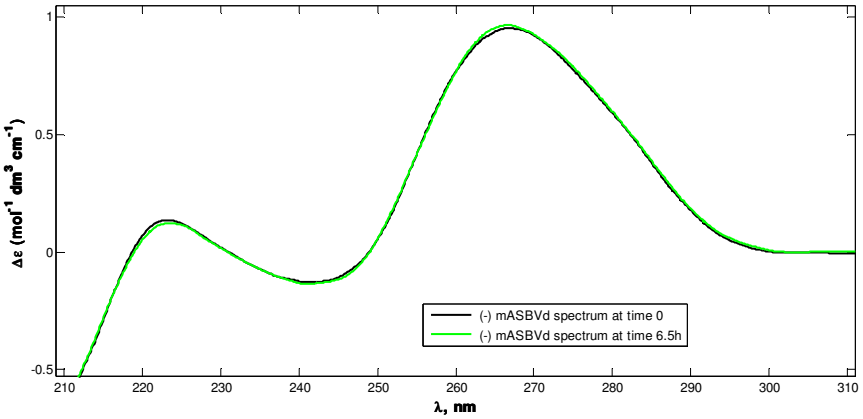

Fig. 3.21. (-) mASBVd CD spectra at different time points during the reaction in physiological conditions. Black line: viroid spectrum at the beginning of the reaction, 'time 0' (immediately after Mg^{2+} addition). Green line: viroid spectrum after 6.5h since the beginning of the reaction.

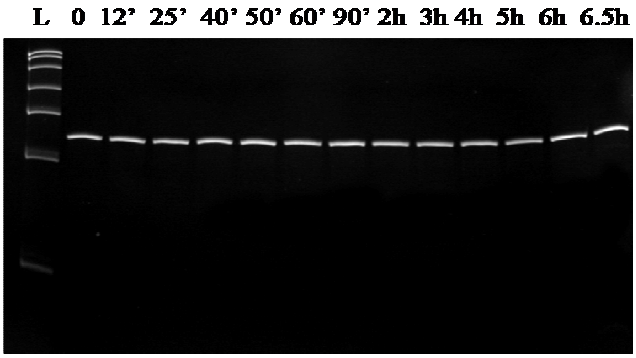

Fig. 3.22. 10% urea-PAGE of (-) mASBVd self-cleavage kinetic at physiological conditions during CD experiment. The band observed corresponds to the entire viroid (247 nt). Top: "L" indicates the RNA ladder, and the time points at which the reaction was stopped are reported.

However, the same CD result is obtained in cleavage conditions. In fact during the cleavage reaction we do not observe any changes in the spectra (Fig. 3.23), even after 2.5h since the beginning of the reaction, when the percentage of the cleavage is around 50% (Fig. 3.24).

We can conclude that the cleavage does not have any effect on the signal evidenced by CD.

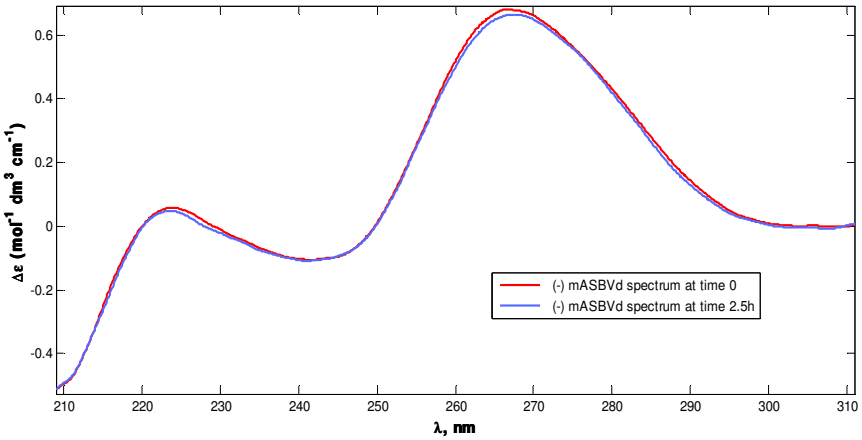

Fig. 3.23. (-) mASBVd CD spectra at different time points during the reaction in cleavage conditions "b". Red line: viroid spectrum at the beginning of the reaction 'time 0' (immediately after Mg^{2+} addition). Blue line: viroid spectrum after 2.5h since the beginning of the reaction.

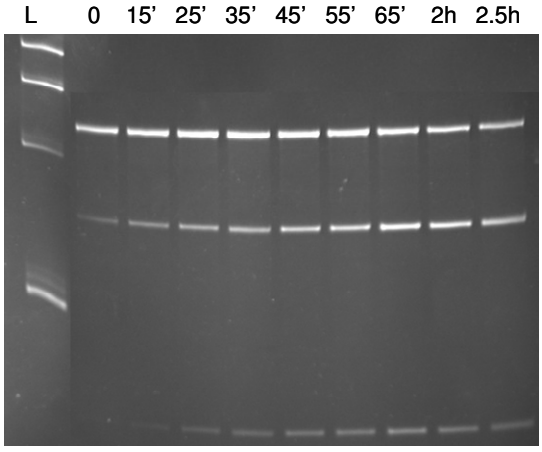

Fig. 3.24. 10% urea-PAGE of (-) mASBVd kinetic at cleavage condition "b" during CD experiments. After 2.5h the percentage of cleavage is 50%. Bands correspond (from the top to the bottom) to the entire viroid (247 nt) and to the two cleavage fragments (163 nt and 84 nt).

Studies of the effect of temperature on CD spectra of (-) mASBVd

The dependence on the temperature of the structural changes of (-) mASBVd were also analysed through CD spectroscopy (see section 5.3.6). After RNA was heated and slowly cooled up to 4°C, Mg^{2+} (10 mM) was added and the spectrum at 4°C measured. As a first step the temperature was varied from 4°C to 95°C (5°C/time). As a second step it was decreased from 95°C to 4°C (5°C/time).

As one can observe in Fig. 3.25 and Fig. 3.26 (blue line) the increase of the temperature from 4°C to 95°C involved a decrease in the intensity and a red-shift of the main peak of the spectra (at about 260 nm). It is known that the temperature causes a melting of the structure. In Fig. 3.26 the maximum value of the main peak of each spectrum, measured at each temperature, was plotted versus the temperature. We can observe that the decrease of the spectra peak intensity is smoother when the temperature is increased from 4 to 50°C and steeper when the change is between 50 and 75°C. From 75°C to 95°C the spectra almost do not change.

These results suggest that there are small variations in the coupling between bases up to 50°C, while the effect observed between 50 and 75°C could be associated with a melting of the structure and a decrease of the spatial constraints between the bases. Probably at 75°C the structure of the viroid is completely denatured and an increase of the temperature does not cause further changes.

These results are compared with the predicted secondary structures obtained at the tested temperatures with the software Mfold (Fig. 3.27). In fact small changes are observed between 4 and 50°C: some bulges change their positions, but the structure remains almost the same, with numerous double-stranded regions. Between 50 and 55°C the formation of a big bulge in the structure is observed. At the same time, we started to observe steeper jumps in the decrease of the main peak in the CD spectra (Fig. 3.26, blue line). Bulges go to increase and the structure goes to melt till 75°C. At this temperature all the structure is completely opened and no further modifications occur by increasing the temperature up to 95°C. Thus, the theoretical calculated structures are in agreement with the evolution observed in CD spectra by increasing the temperature.

Finally, we also tried to test the reversibility of the process by decreasing the temperature from 95°C to 4°C. If the process was reversible the molecules should refold and an increase and a blue shift of the peak at about 260 nm should be observed. As shown in Fig. 3.26 (pink line) and in Fig. 3.28 there was an increase

and a blue-shift of the main CD peak by decreasing temperature, but the spectra did not return to the same position initially. However, the spectrum measured at 4°C after decreasing the temperature (i.e., second step) was very similar to the spectrum at 4°C measured at the beginning of the experiment (i.e., before increasing the temperature, first step) (Fig. 3.26, pink line and Fig. 3.29).

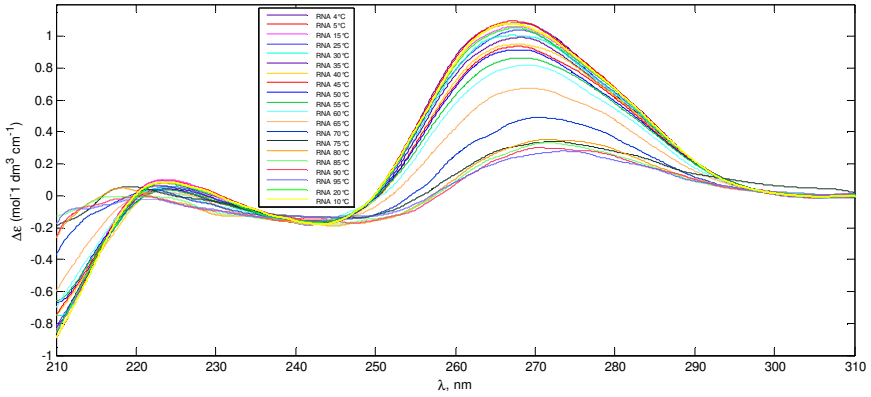

Fig. 3.25. Decreasing of the peak of the spectra with the increasing of temperatures.

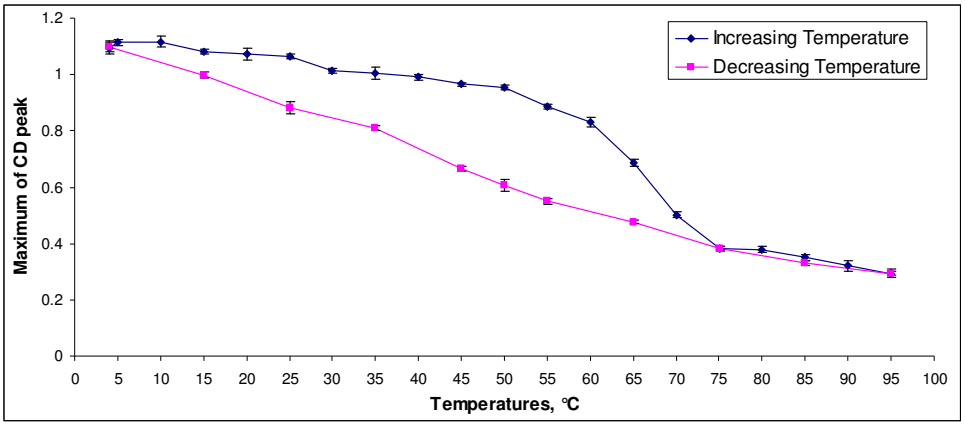

Fig. 3.26. Maximum of the main peak (Δε, range: 260-280 nm) measured for each spectrum in function of temperature. Blue line represents the first step (from 4°C to 95°C); pink line represents the second step (from 95°C to 4°C).

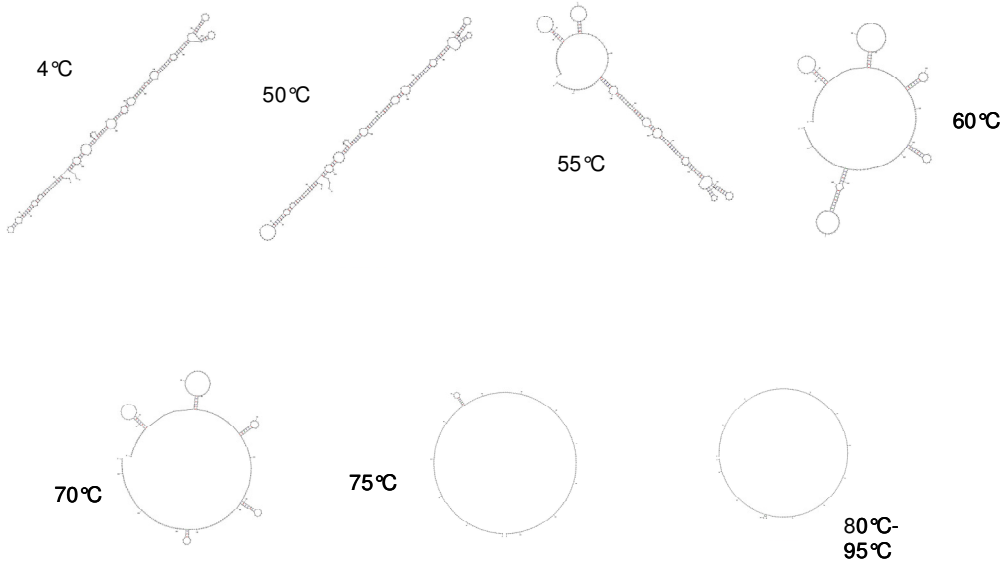

Fig. 3.27. Predicted secondary structures of (-) mASBVd calculated with the software Mfold.

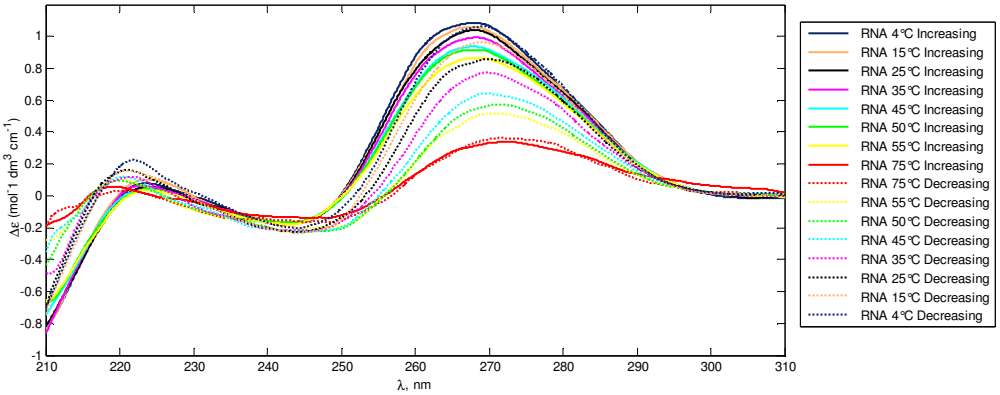

Fig. 3.28. CD spectra measured increasing and decreasing the temperature to test the reversibility of the system. Solid lines represent some of the spectra measured increasing the temperature from 4°C to 95°C. Dotted lines represent some of the spectra measured decreasing the temperature from 95°C to 4°C. The same colour represents the same temperature.

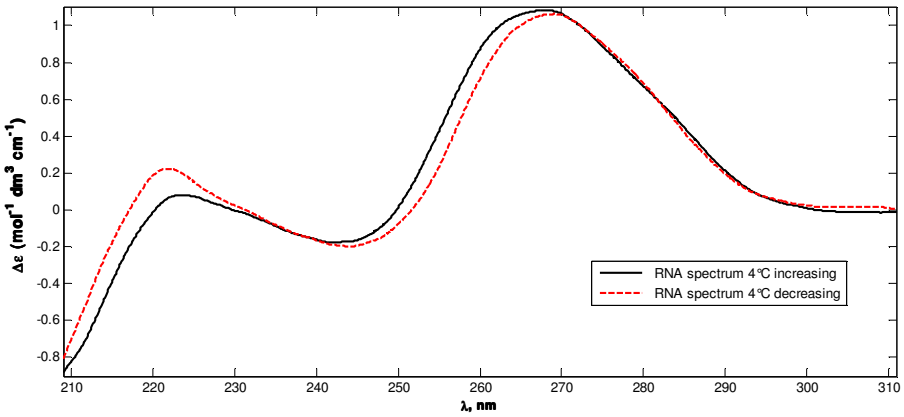

Fig. 3.29. CD spectra of (-) mASBVd at 4°C measured in the first step, by increasing the temperature from 4 to 95°C (black line), and in the second step, by decreasing temperature from 95 to 4°C (red line).

3.1.4.2. Structural analysis of (-) mASBVd with Raman spectroscopy

The structure of the (-) mASBVd RNA in several different conditions was analyzed with Raman spectroscopy as well. In order to interpret Raman spectra we considered published results concerning spectra of RNA (Benevides *et al.*, 1997). For more details on the Raman spectroscopy and its applications in biochemistry see section 5.4 of Material and Methods.

Our spectra were measured in the region between 680 cm^{-1} and 1800 cm^{-1}. In fact, bands below 600 cm^{-1} in Raman spectra of nucleic acids and other biomolecules typically have not been well characterized. Even if the whole spectrum of the viroid was analyzed, our attention was moreover focalized in the region 750-1100 cm^{-1}. In fact bands in this region are assigned to vibrations localized in the sugar phosphate backbone (Benevides *et al.*, 1997), giving us important informations on the backbone structure.

Raman experiments were performed by following the same protocol used for CD experiments. As previously done, the three different kinetic conditions of the (-) mASBVd (see sections 3.1.4 and 5.4.3) were investigated with Raman spectroscopy in order to analyse the viroid structure.

Raman spectrum of the viroid in water

The Raman spectrum of viroid in water (Fig. 3.30 red line) displays several peaks that can be assigned to known characteristic vibrational bands (Table 3.5). In RNA, diagnostic bands are expected for guanine at 668 cm^{-1} (Abdelkafi *et al.*, 1998), for adenine at 724 cm^{-1} (Benevides *et al.*, 1997; Hanus, 1999) and for both cytosine and uracil at 785 cm^{-1} (Baumruk *et al.*, 2001; Hanus, 1999). All these bands are found in our viroid spectra.

Bands from the ribose-phosphate backbone (approximately) 813, 930, 970, 1100 cm^{-1} are identified with bands from oligonucleotides (Benevides *et al.*, 1984; Reipa *et al.*, 2007; Vachousek J., 2008)**.**

In particular, the band at 813 cm^{-1} is characteristic of the symmetric stretching vibrations of -O-P-O- group and is considered a marker of organized A-RNA backbone (Abdelkafi *et al.*, 1998; Benevides *et al.*, 1997; Leulliot *et al.*, 1999). The band at 1100 cm^{-1} is characteristic of symmetric stretching vibrations of the PO_2^- group (Baumruk *et al.*, 2001; Benevides *et al.*, 1997). A quantitative estimate of the A-backbone content may be obtained by the ratio of intensities at 813 and 1100 cm^{-1}. I_{813}/I_{1100} is in fact diagnostic of the degree of ordered helical structures, i.e. of A-helix secondary structures (Lafleur *et al.*, 1972; Thomas and Hartman, 1973). The observed value is 1.1 and corresponds to partly organized A-RNA (i.e., ~ 70 %). The ratio expected for a pure A-helix is 1.6 (Benevides *et al.*, 1986; Erfurth *et al.*, 1972).

Approximate peak position wavenumbers (cm^{-1})	Assignment	Significance
670	rG	Hyperchromic? (Leulliot *et al.*, 1999)
710	backbone	A RNA marker (Leulliot *et al.*, 1999)
725	rA ring breathing	Hypochromic (Movileanu *et al.*, 2002)
783	rC, rU breathing	Hypochromic (Fish *et al.*, 1981)
813	O-P-O sym stretch	Ordered A RNA backbone (Benevides *et al.*, 1986)
860	A, U, G, C, backbone	(Leulliot *et al.*, 1999; Ueda *et al.*, 1993)
880	backbone	(Hobro *et al.*, 2007)
930-940	backbone	(Leulliot *et al.*, 1999)
970	backbone	(Leulliot *et al.*, 1999)
1000	backbone	(Leulliot *et al.*, 1999)
1045	backbone	(Leulliot *et al.*, 1999)
1097	PO^{2-}	A helix 1099 (Benevides and Thomas, 2005)
1175	A, U, G, C	(Hobro *et al.*, 2007)
1230	rU	Hypochromic (Leulliot *et al.*, 1999)
1245	rA, rC, rU	Hypochromic (Hobro *et al.*, 2007; Leulliot *et al.*, 1999)
1300	rA, rC	(Leulliot *et al.*, 1999)
1338	rA, rG, rU	(Hobro *et al.*, 2007; Leulliot *et al.*, 1999)
1375	rA, rG, rU	(Hobro *et al.*, 2007; Leulliot *et al.*, 1999)
1410	rC, rG	(Ueda *et al.*, 1993)
1420	backbone	1415 A RNA (Benevides *et al.*, 1986)
1460	A, C, U	(Hobro *et al.*, 2007; Ueda *et al.*, 1993)
1480	rA, rG	(Hobro *et al.*, 2007; Leulliot *et al.*, 1999)
1510	rA	(Hobro *et al.*, 2007; Leulliot *et al.*, 1999)
1530	rG, rC	(Ueda *et al.*, 1993)
1575	rA, rG	(Benevides *et al.*, 1997)
1600	rC	(Bell AF, 1997)
1615	rC	(Bell AF, 1997; Ueda *et al.*, 1993)
1680	base (U, G) C=O	(Benevides *et al.*, 1997)

Table 3.5. Interpretation of peaks resolvable in Raman spectrum of viroid in water

Effect of cacodylate buffer-K^+

Cacodylate buffer and K^+ affect the Raman spectrum of viroid in water. The difference spectrum resulting from the subtraction of the spectrum of viroid in cacodylate buffer-K^+ and the spectrum of viroid in water is presented in Fig. 3.30. Mainly, there is a decrease of spectral features at 784 (C, U), 1260 (C, U, A), 1330 (A, G, U), 1418 (A, G, C), ~1500 (A, G) cm^{-1}, probably reflecting a slight hypochromism increase. In the interval 1600-1700 cm^{-1} carbonyl groups are expected to contribute. The trough at 1680 cm^{-1} partly originates from carbonyls which are sensitive to base structural organization. Probably a partial base stacking becomes more effective. Troughs at ~830 and 1085 cm^{-1} and the bands at 880 and 960 cm^{-1} result from changes in the ribose phosphate backbone. The loss of intensity of the 830 cm^{-1} region means a weakening in the organized backbone, at least of the stem-A-form geometry (Vachousek J., 2008). Probably, the broad bands at 880 and 960 cm^{-1} are linked to a slackening of the structural constraints exerted on the backbone.

Globally, the buffer (cacodylate pH 7.5) and K^+ (150 mM) lead to a loss of the structural rigidity and to a widening in the structure distribution of the backbones. So there is a less homogeneous RNA population caused by the decrease of the ordered backbones. Moreover, the relaxation of conformational constraints on the backbone could allow a greater freedom for the stacking of bases (Stepanek *et al.*, 2007).

After the addition of cacodylate buffer and K^+, viroid spectra were measured for the following 30 minutes (every 5 min); after few minutes (about 10), the spectrum of viroid becomes stable (Fig. 3.31). Moreover, we do not observe any particular changes over time.

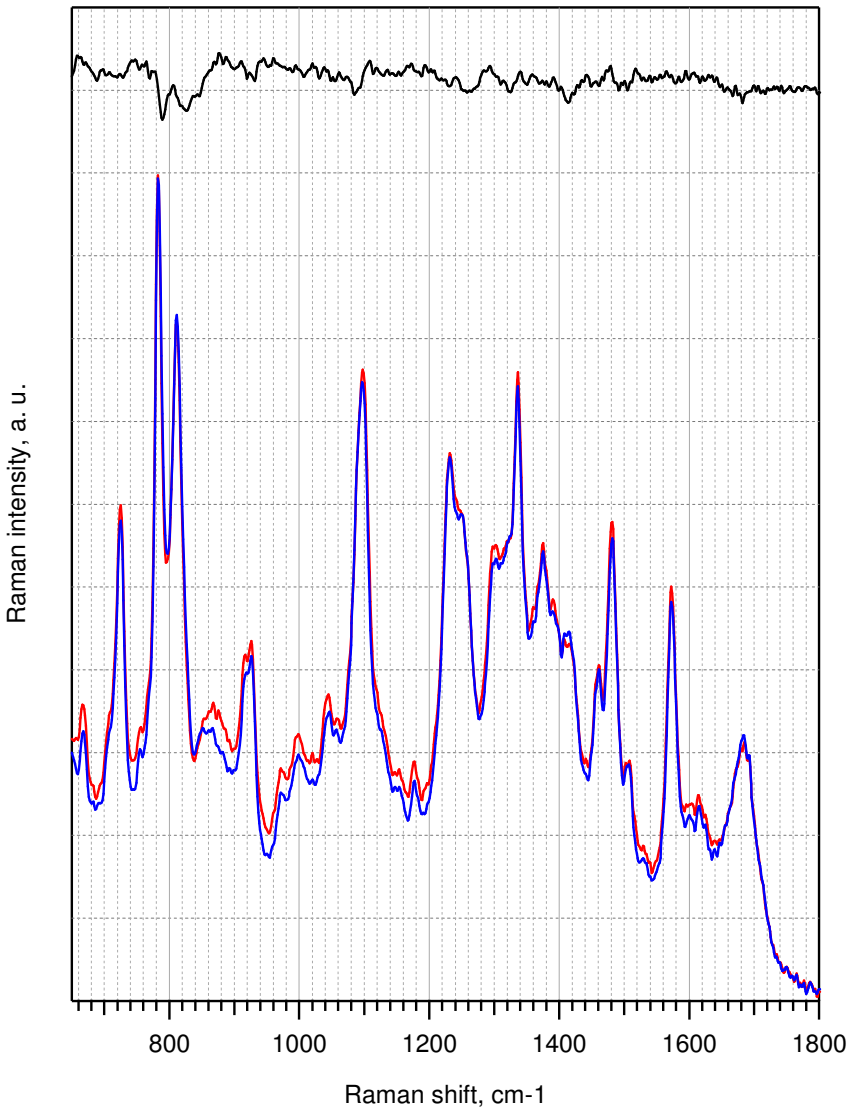

Fig. 3.30. Effect of buffer cacodylate + K^+ on the Raman spectrum of viroid. Bottom: spectrum of viroid in water (red line) and spectrum of viroid in buffer-K^+ (blue line). Top (black line): difference between spectrum in buffer-K^+ and spectrum in water.

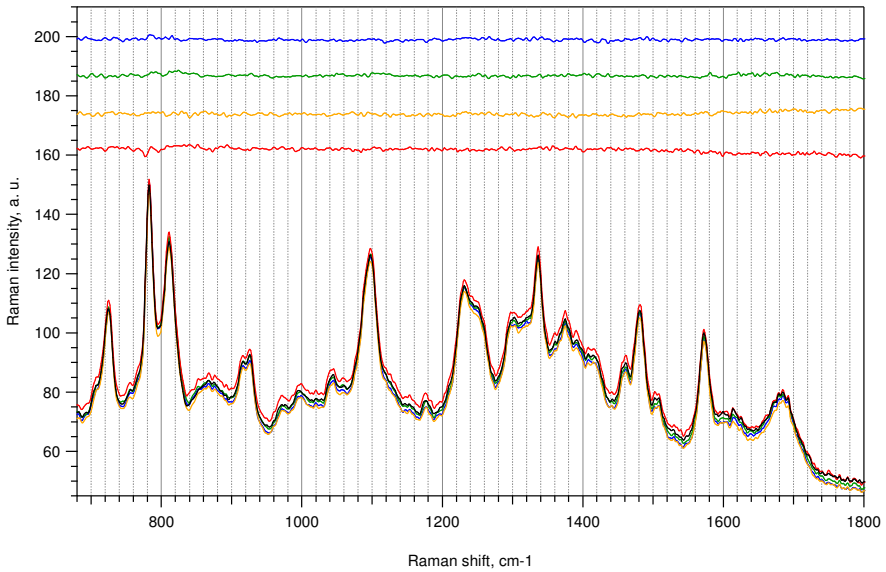

Fig. 3.31. Time evolution of spectra after buffer-K^+ addition. Bottom: several spectra measured at different time points after buffer-K^+ addition (5, 10, 15, 20 and 30 min) Top: differences between the viroid spectra measured at different time points after buffer-K^+ addition: 10 min-5 min (red line), 15 min-10 min (yellow line), 20 min-15 min (green line), 30 min-20 min (blue line).

Early effect of Mg^{2+}

We studied Mg^{2+} effect on the viroid conformation at three different concentrations: 2 mM Mg^{2+}, when the viroid is not able to cleave (physiological conditions), 20 and 100 mM Mg^{2+} when the viroid is active (cleavage conditions "b" and "a" respectively). In cleavage conditions "b" the viroid is more active that in cleavage conditions "a" (see section 3.1.4). Thus we are able two compare both one inactive conformation with an active one and two different active conformations.

Firstly we focused on early spectral changes of the viroid in presence of Mg^{2+}. Differently from CD, Raman signals involve time dependent multistep processes, with response times extending from 15 minutes to 24 hours. As discussed in detail below, the evolution of the Raman spectrum in presence of 20 mM Mg^{2+} is very fast. Probably there is a superimposition between the effect of Mg^{2+} and a fast evolution over time of the Raman signal. Instead the Raman evolution at 2 and 100 mM of Mg^{2+} is slower. For these reasons the early effect of Mg^{2+} was mostly evaluated in these two conditions.

The effects of 2 and 100 mM Mg^{2+} concentrations are similar. The difference spectra [(spectrum in Mg^{2+}) minus (spectrum in water)] reveal similar spectral features (Fig. 3.32 and Fig. 3.33). Mainly the same bands appear. However, at 2 mM the majority of the difference spectrum is negative, the bands are flushed with the baseline (Fig. 3.32), whereas, at 100 mM Mg^{2+} positive bands result from a higher background (Fig. 3.33).

The effect on backbone geometry is evident from the changes of the peaks in the region 750-1100 cm^{-1}. In particular the increase of the band at 813 cm^{-1}, correlated with a broad trough at 840 cm^{-1}, indicates a strengthening of the stem A-form geometry. This effect is given by an increase in the content and probably in the constraints of the A-helix organized backbones. At the same time there is a possible up-shift of the band at 1100 cm^{-1} (PO_2^-), which is consistent with an increase in the strength of the interactions of PO_2^-. The bands at 880 and ~ 930 cm^{-1}, which depend on the geometry of the backbone, are clearly defined. They are probably correlated with an increase of the structural constraints exerted on the backbone.

The effect on base stacking is also clear. The increase of the bands at 668 (G), 724 (A), 785 (C, U), 880 (A, U, G, C), 1240 (U, C), 1295 (C, A), 1340 (A, G, U), 1480 (A, G), 1577 (G, A) cm^{-1}, and the spectral features between 1600-1700 cm^{-1} (C=O) probably result from a partial base unstacking.

Therefore, Mg^{2+} leads RNA molecules to take an A-helix form and increases the structural rigidity of the ribose phosphate backbones. The increase of the organized A-RNAs means a more homogeneous viroid population distribution. Moreover, the conformational constraints of the backbone, enhanced by Mg^{2+}, could restrain the freedom of the bases, slightly impeding their stacking.

The effect of Mg^{2+} is different from the one induced by buffer-K^+, coherently with results from CD spectroscopy.

Changes in the structure of the viroid observed with 2 mM (Fig. 3.32) and 100 mM (Fig. 3.33) of Mg^{2+} are very similar. However, the effect at 100 mM is more evident: the increase of the bands is better definite. It seems that there is a correlation between the Mg^{2+} concentration and its effect.

As we have demonstrated, the presence of Mg^{2+} is essential for the *in vitro* cleavage of the viroid, and its activity enhances with Mg^{2+} concentration at the same temperature, pH and K^+ concentration. In fact the viroid is inactive without Mg^{2+}, even if in presence of 150 mM of K^+.

Therefore, we can come to the same conclusions of CD experiments: the structure induced by buffer-K^+ could be associated with an inactive viroid conformation, while the structure induced by Mg^{2+} could be associated with an active viroid conformation. However, Raman spectroscopy provides a supplementary information: an ordered and constrained A-helix form, induced by Mg^{2+}, is probably the type of structure that the viroid needs to assume for cleave itself. Probably, the higher is the number of molecules which assume such a conformation, the more is the cleavage efficiency.

Although the effect of the 20mM of Mg^{2+} at 35°C (cleavage conditions "b") is more difficult to be interpreted, the changes induced in the viroid spectra seem coherent with the afore mentioned ones. Fig. 3.34 shows the difference between spectra at 35°C with 20 mM Mg^{2+}, and the spectra at 35°C with buffer-K^+ (black line). The most important changes after Mg^{2+} addition are the increase of the band at 813 cm^{-1}. Thus, even in this case, we can correlate the effect of Mg^{2+} to a more homogeneous RNA population with an increase of the A-type structures.

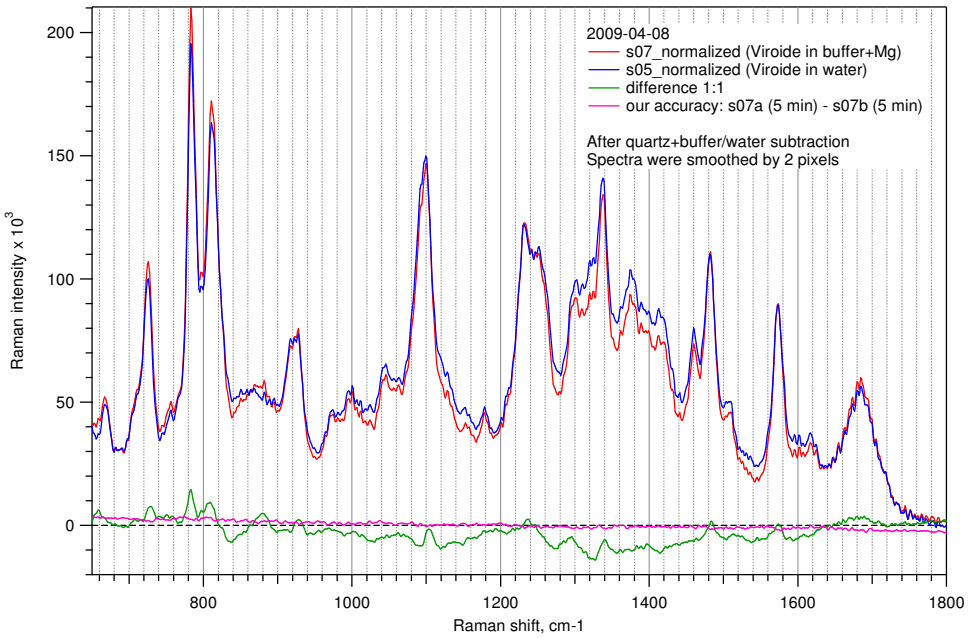

Fig. 3.32. Effect of 2 mM Mg^{2+} on the Raman spectrum of viroid at 25°C (Physiological conditions).
Green line: Spectrum of viroid in Mg^{2+} (red line) minus spectrum of viroid in water (blue line).

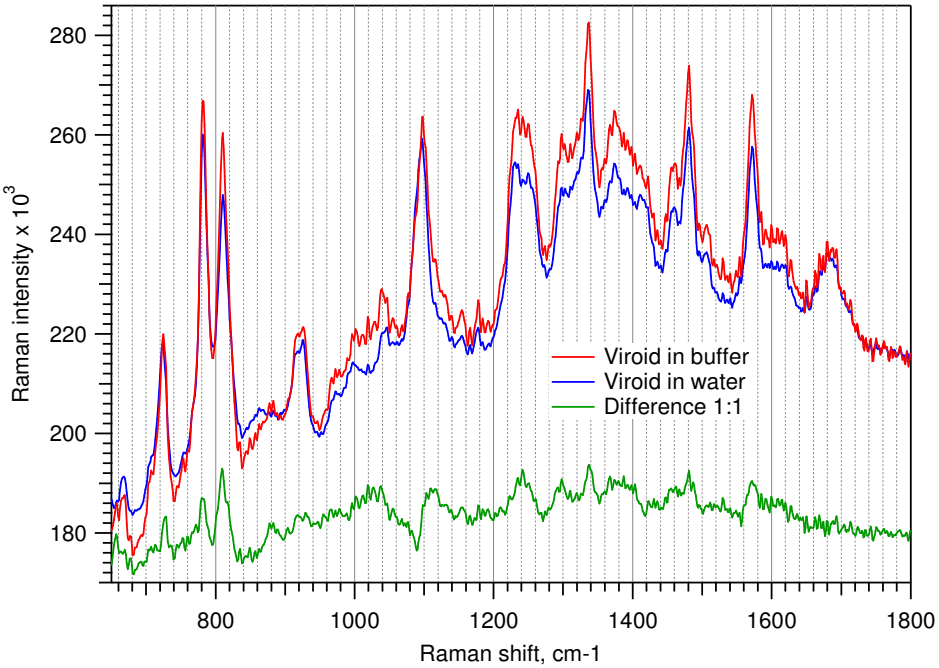

Fig. 3.33. Effect of 100 mM Mg^{2+} on the Raman spectrum of viroid at 25°C (Cleavage condition "a").
Green line: Spectrum of viroid in Mg^{2+} (red line) minus spectrum of viroid in water (blue line).

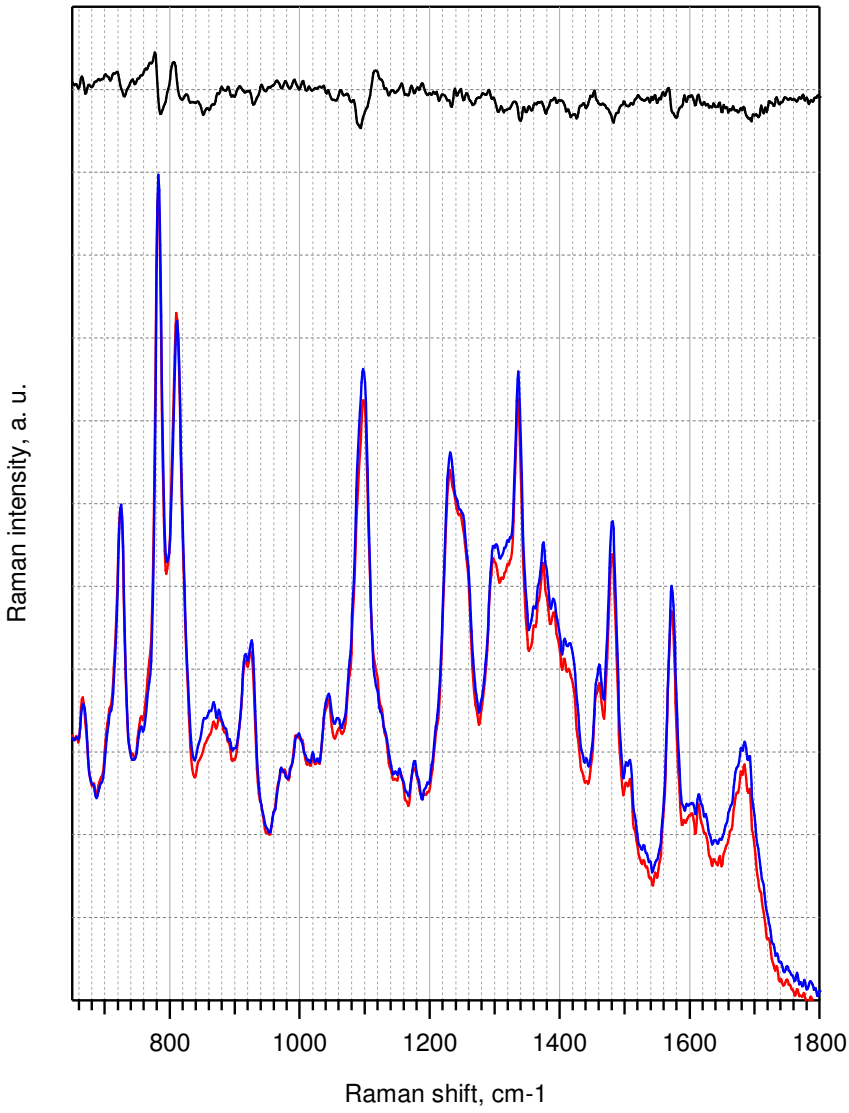

Fig. 3.34. Effect of 20 mM Mg^{2+} on the Raman spectrum of viroid at 35°C (Cleavage condition "b").
Black: Spectrum of viroid in buffer-K^+ + Mg^{2+} (red line) minus spectrum of viroid in Buffer-K^+ (blue line).

Time dependent analysis of viroid Raman spectra during kinetics

The evolution of Raman spectra over time was followed for the three experimental conditions taken into consideration. After Mg^{2+} addition the spectrum of the viroid was monitored at different time points to assess any possible change in the viroid structure during the reaction.

Differently from CD, the Raman signal involves time dependent multistep processes and the three different cleavage conditions have different time dependent windows.

In physiological conditions, even if the cleavage was not verified, we could observe two different changes on the Raman spectral features of the viroid (Fig. 3.35 and Fig. 3.36): a first one until 71 minute, and a second one is observable from 267 minutes until 24 hours (i.e., end of the monitoring period).

The first changes presented some similarities with the Raman signature given by cacodylate buffer-K^+ (Fig. 3.30). More specifically a decrease in the spectral features or troughs at ~800 (~785 + ~813), 1100, ~1400, ~ 1490, ~1570, 1600-1700 cm^{-1} and positive bands at ~880, 1460-1480, 1520 (1530) cm^{-1} were observed. The trough around 800 cm^{-1} most probably indicates a decrease of the band at 813 cm^{-1}, and so in the structural constrains exerted on the phosphate backbone and/or in the content of the A-helix organized backbones. However, in spite of the similarity with the observed buffer-K^+ dependent effect, the spectra showed some bands characteristic of the reaction in this condition, namely at 840, 1060, 1115, 1130, 1295 cm^{-1}.

After about 260 min, the spectral features of Raman spectra reversed and over time positive bands appeared at 720, 785, 813, 880, 920, 1040, 1100, 1460, 1575 cm^{-1}. These spectral features seem more similar with the Raman signature given by Mg^{2+} (Fig. 3.32 and Fig. 3.33).

The time dependent spectral features in cleavage conditions “a” (Fig. 3.37) and “b” (Fig. 3.38) presented some similarities with the first types of structural changes observed in physiological conditions. For instance, in conditions “b”, the evolution of the spectrum involved troughs at 785, 840, 960, 1265, 1420, 1480 and 1580 cm^{-1} (Fig. 3.38).

Results obtained suggest that there is no strict relationship between the kinetic of cleavage and the time dependent process disclosed by Raman spectroscopy. In fact, with 2 mM Mg^{2+} (25°C) (Fig. 3.36) changes in Raman spectra were observed over time although no cleavage occurred, and modifications were observed until 24 hours after Mg^{2+} addition. For 100 mM (25°C) (Fig. 3.37) and 20 mM of Mg^{2+} (35°C) (Fig. 3.38) the Raman temporal evolution was completed while cleavage kinetic was still proceeding.

Furthermore, the velocity of stabilization of the viroid structures (when no more changes are observed) is worth noticing. As already mentioned, spectra measured over time in physiological conditions, show that viroid spectral changes are observed until 24h (Fig. 3.35 and Fig. 3.36). This result indicates that in such conditions the viroid does not arrive to stabilization. In the Raman spectra followed at 100 mM of Mg^{2+} at 25°C we observed a faster stabilization with respect to the physiological conditions, anticipated by changes until 26 minutes, and further few changes until 1h (Fig. 3.37). By contrast, the cleavage kinetic was still running and, after 1h, only 9% of the cleavage was achieved (Fig. 3.39). In the case of the kinetic reaction followed at 20 mM of Mg^{2+} at 35°C (in which the viroid was more active than previously, see Fig. 3.39) we observed a much faster stabilization: some changes in Raman spectrum were observed in the first 10 minutes (Fig. 3.38), but no further modification occurred. In fact, the spectrum obtained after 16 minutes since the beginning of the self-cleavage reaction was identical to the one obtained after 10 minutes. Even in this case, the cleavage reaction was not at the plateau and after 16 minutes only the 8% of the molecules were cleaved (Fig. 3.39).

In summary, the viroid RNAs population, as observed in Raman spectra, reach a stabilization faster than the *in vitro* kinetic reaches the plateau. Moreover, once the stabilization is attained, no further spectral changes are observed, even if cleavage is still taking place. Thus, changes are no related with the cleavage itself and with the formation of 2'3' cyclic phosphate. In the light of what stated above, we can conclude that the cleavage reaction does not have any direct representation in the Raman spectra.

However, there is a relation between the velocity of stabilization of Raman spectra and the efficiency of cleavage: the more efficient the kinetic of cleavage is, the faster the time evolution of Raman signal and its stabilization are. No stabilization was observed for inactive conditions (physiological, 2 mM Mg^{2+} 25°C, Fig. 3.36), after about 1 hour for 100 mM of Mg^{2+} at 25°C (cleavage conditions "a", Fig. 3.37) (K_{obs} = 0.004 min^{-1}, F_∞=33.65, Fig. 3.39), and after 16 minutes for 20 mM of Mg^{2+} at 35°C (cleavage conditions "b", Fig. 3.38) (K_{obs} = 0.006 min^{-1}, F_∞= 80.77, Fig. 3.39).

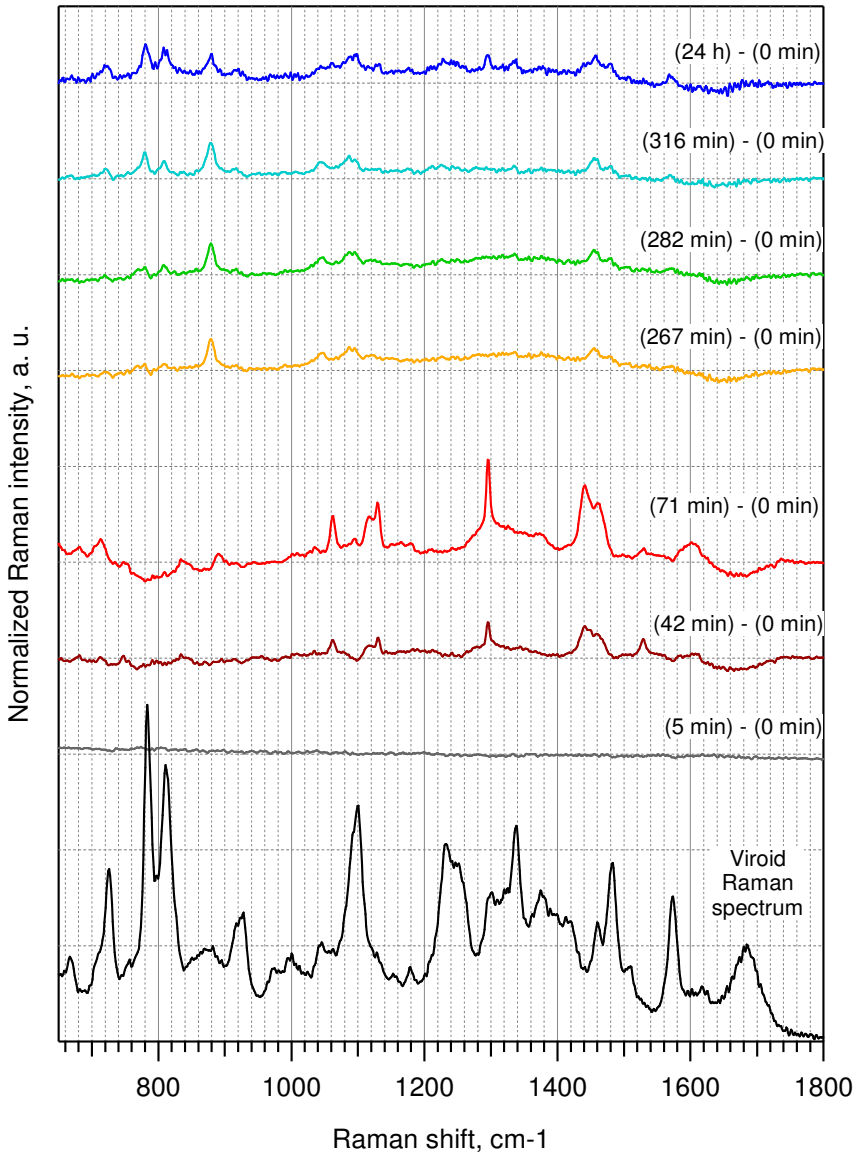

Fig. 3.35. Temporal evolution of the viroid Raman spectrum in physiological conditions. Bottom, black line: viroid Raman spectrum after 2 mM Mg^{2+} addition (conventionally called "time 0" of the reaction, measured in the first 5 minutes, because each spectrum is obtained with an accumulation time of 5 minutes). From bottom to top: differences between spectra measured at different time points (42, 71, 267, 282, 316 minutes, 24 hours) of the reaction (after Mg^{2+} adding) and the spectrum at "time 0".

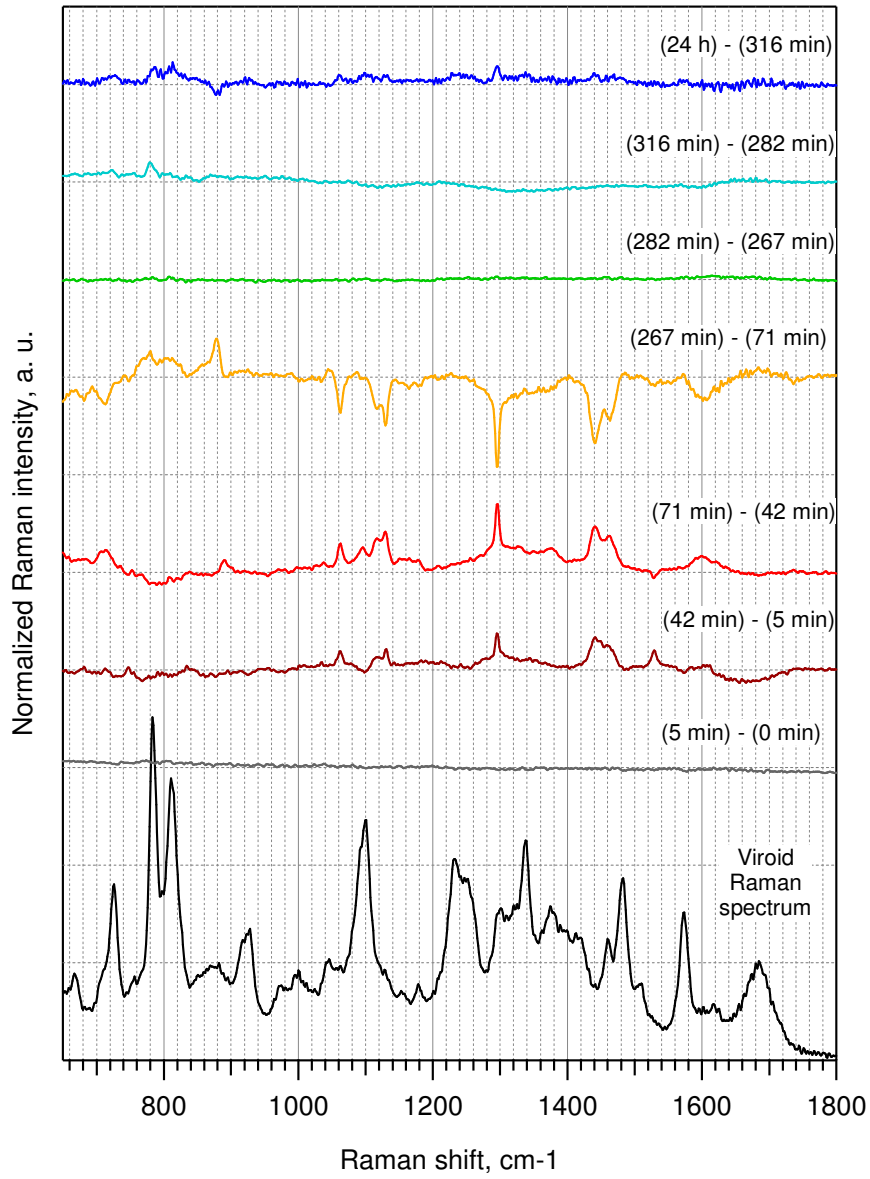

Fig. 3.36. Temporal evolution of viroid Raman spectrum in physiological conditions. Bottom, black line: viroid Raman spectrum after 2 mM Mg^{2+} addition (conventionally called "time 0" of the reaction, measured in the first 5 minutes, because each spectrum is obtained with an accumulation time of 5 minutes). From bottom to top: differences between spectra at different time of the reaction and the spectrum previous measured (42 minutes-time 0, 71 min-42 min, 267 min-71 min, 282 min-267 min, 316 min-282 min, 24 h-316 min).

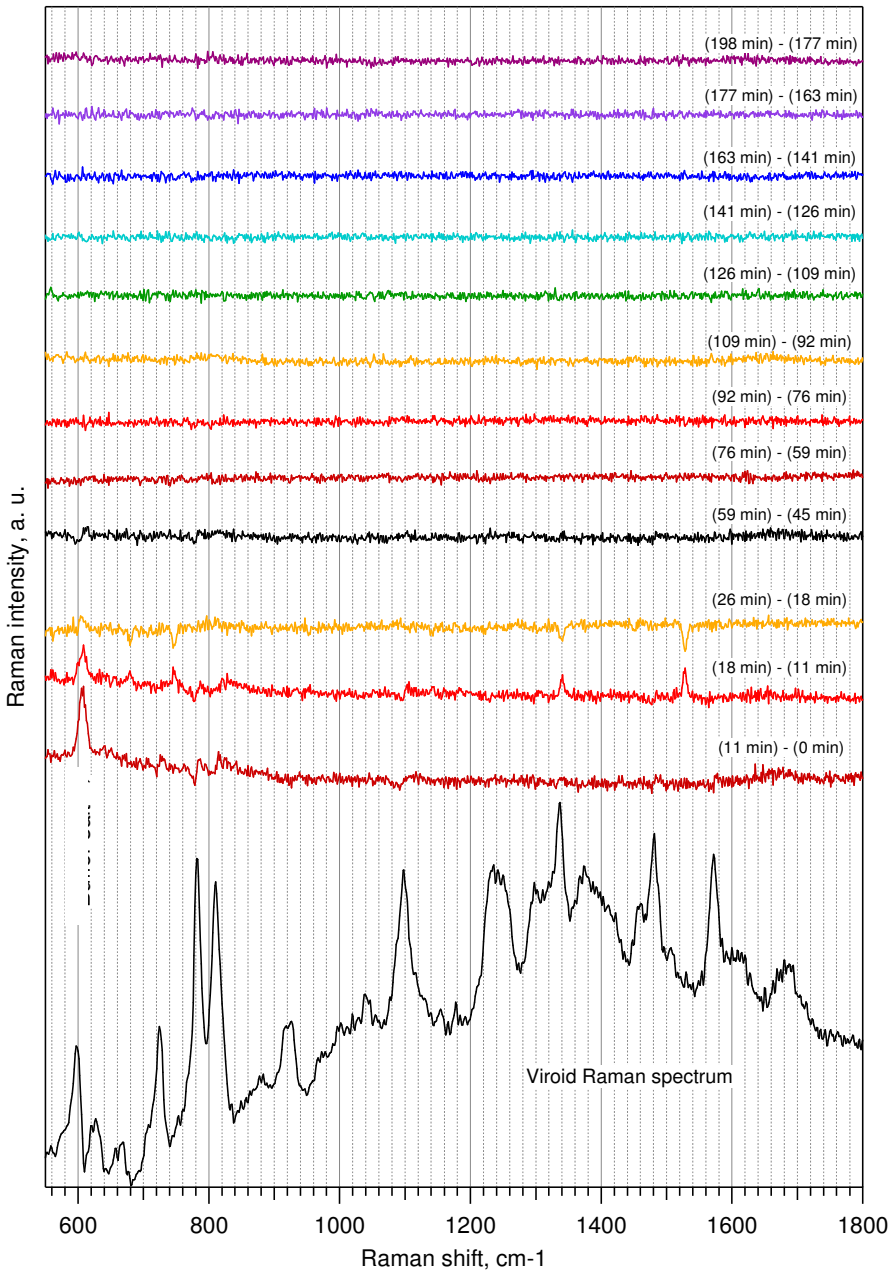

Fig. 3.37. Temporal evolution of viroid Raman spectrum in presence of 100 mM Mg^{2+} at 25°C (cleavage condition "a"). Bottom, black line: viroid Raman spectrum after 100 mM Mg^{2+} addition ("time 0" of the reaction, measured in the first 5 minutes). From bottom to top: differences between spectra at different time points of the reaction and the spectrum previous measured (11 min-time 0, 18 min-11 min, 26 min-18 min, 59 min-45 min, 76 min-59 min, 92 min-76 min, 109 min-92 min, 126 min-109 min, 141 min-126 min, 163 min-141 min, 177 min- 163 min, 198 min-177 min).

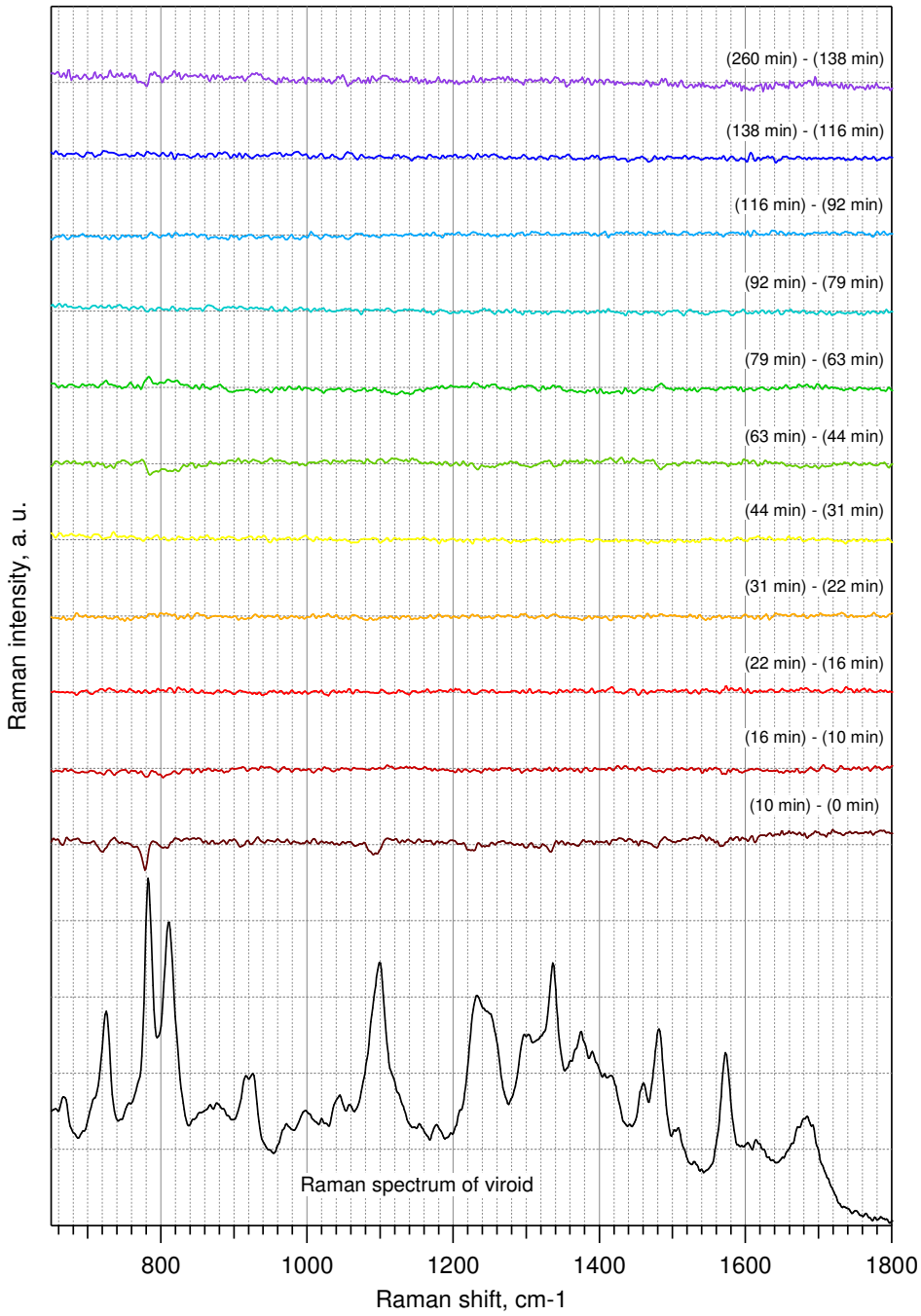

Fig. 3.38. Temporal evolution of viroid Raman spectrum in presence of 20 mM Mg^{2+} at 35°C (cleavage condition "b"). Bottom, black line: viroid Raman spectrum after 20 mM Mg^{2+} addition ("time 0" of the reaction). From bottom to top: differences between spectra at different time pints of the reaction and the spectrum previous measured (10 min-time 0, 16 min-10 min, 22 min-16 min, 31 min-22 min, 44 min-31 min, 63 min-44 min, 79 min-63 min, 92 min-79 min, 116 min-92 min, 138 min-116 min, 260 min- 138 min).

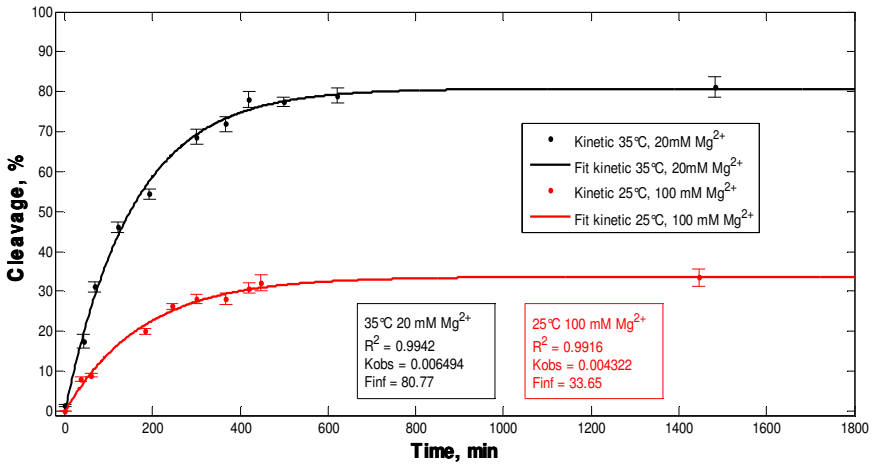

Fig. 3.39. Time course of the *in vitro* self-cleavage reactions of mASBVd in two different conditions: 25°C 100 mM of Mg^{2+} (red line) and 35°C and 20 mM of Mg^{2+} (black line).
Data from the two kinetic experiments are plotted and fitted with the equation $F_t = F_\infty (1\text{-}e^{-Kobs*t})$ where F_t is the percentage of cleaved molecules at time t, F_∞ is the percentage of cleaved molecules at the end point, and K_{obs} is the observed kinetic rate constant. In the black and red boxes are indicated the kinetic parameters of the two self-cleavage reactions.

3.2. Studies of a trans-acting ribozyme in hot primordial environments

The hypothesis of a primeval RNA world is strongly affected by the hostile environmental conditions, which were probably present on early Earth. In particular strong UV, X-ray radiations and high temperatures could have represented a big obstacle to the formation and evolution of the first genetic biomolecules.

With the aim of evaluating the possibility that a RNA world could have evolved in similar conditions, we studied the effect of one of these degrading agents, high temperatures, on the activity of a catalytic RNA molecule in two different environmental conditions:

1) Water solution, to simulate the primordial broth (Haldane, 1929; Oparin, 1924).
2) Presence of a dipeptyde, Lys-Lys, to simulate a situation where both RNA-like molecules and aminoacids or short polypeptides could have been present at the same time in the same environment.

It is well known that in the present day cells the DNA is associated with alkaline proteins (histons) which package and order the DNA into structural units called nucleosomes. Also the RNA is often found associated with proteins in the complexes called ribonucleoproteins (RNP). Examples are the ribosome, the enzyme telomerase and the small nuclear RNPs. Both histones and the RNA binding motif in RNPs are rich of basic amino acid residues (moreover Lysine and Arginine) that, thanks to their positive portion, are able to interact with the negatively charged phosphates of nucleic acids. Usually the proteins associated with nucleic acids have a structural and scaffolding role, but they could have also a protection role, for instance against nuclease.

One can imagine that primitive proteins (like amino acids or dipeptide) could have interacted with ribozymes in the ancient RNA world, with a consequent evolutionary advantage. In fact, it is hypothesized that "ribozymes of the RNA world may have used amino acids and other small organic cofactors to expand their otherwise limited catalytic potential" (Roth and Breaker, 1998; Szathmary, 1993; Szathmary, 1999). For these reasons, many *in vitro* synthesized ribozymes using a cofactor have been selected (Breaker and Joyce, 1995; Huang and Yarus, 1997; Lorsch and Szostak, 1994; Meli *et al.*, 2003; Paul and Joyce, 2002).

We hypothesized that such primordial amino acids, or short polypeptides, could have had a role in the protection of the ancient RNAs.

In order to corroborate our hypothesis, we constructed a hammerhead trans-acting ribozyme in which ribozyme and substrate were physically separated, thus able to take the hammerhead form and to perform the trans-cleavage reaction only when both were present at the same time in solution. We investigated the functionality of the catalytic system in water and in presence of the Lys-Lys dipeptyde, and we estimated the protection of the system supplied by Lys-Lys at high temperatures (80°C).

Lys-Lys was chosen since the lysine is one of the most important amino acid in both histones and the RNA binding motif in RNPs.

3.2.1. Construction of hammerhead "trans-acting" ribozyme

Firstly we constructed a "trans-acting" ribozyme starting with the sequence of the hammerhead ribozyme of the Peach Latent Mosaic Viroid (PLMVd).

In nature the PLMVd is a circular RNA molecule of 337 nucleotides, which presents a secondary "branched" structure (Fig. 3.40). Both the (+) and (-) RNAs of the PLMVd carry a hammerhead ribozyme in their sequences; the formation of the hammerhead structure catalyzes the *in vitro* (and probably also *in vivo*) self-cleavage reaction (Ambros *et al.*, 1998; Hernandez and Flores, 1992). In Fig. 3.41 the hammerhead structure of the (+) PLMVd self-cleaving RNA, from which we started to construct the trans-acting ribozyme, is shown.

In this sequence we indentified a catalytic subunit (CAT) and a substrate subunit (SUB). These were separately synthesized, so that the trans-cleavage reaction could exclusively verify when both the subunits interacted each other and formed the right hammerhead structure (Fig. 3.42).

We chose the sequences of CAT and SUB in order to:

- Maintain the conserved nucleotides in the catalytic core (Hernandez and Flores, 1992);
- Maintain tertiary interactions between internal loops I and II, that were recently found to increase the catalytic activity of a hammerhead ribozyme, compared with the minimal ribozyme that lack of these interactions (Heckman *et al.*, 2005; Khvorova *et al.*, 2003; Kim *et al.*, 2005; Kisseleva *et al.*, 2005; Penedo *et al.*, 2004). The same has been demonstrated also for trans-cleaving PLMVd ribozyme (Weinberg and Rossi, 2005);
- Indentify all the bands on gel, (i.e., the ones corresponding to the entire CAT and SUB, and to the cleavage fragments), appropriately choosing the lengths of the subunits.

In Fig. 3.43 the primary sequences of the two subunits, together with the lengths of the entire and cleaved fragments, are reported. Moreover, Fig. 3.44 shows a diagram of the secondary structure of the constructed ribozyme.

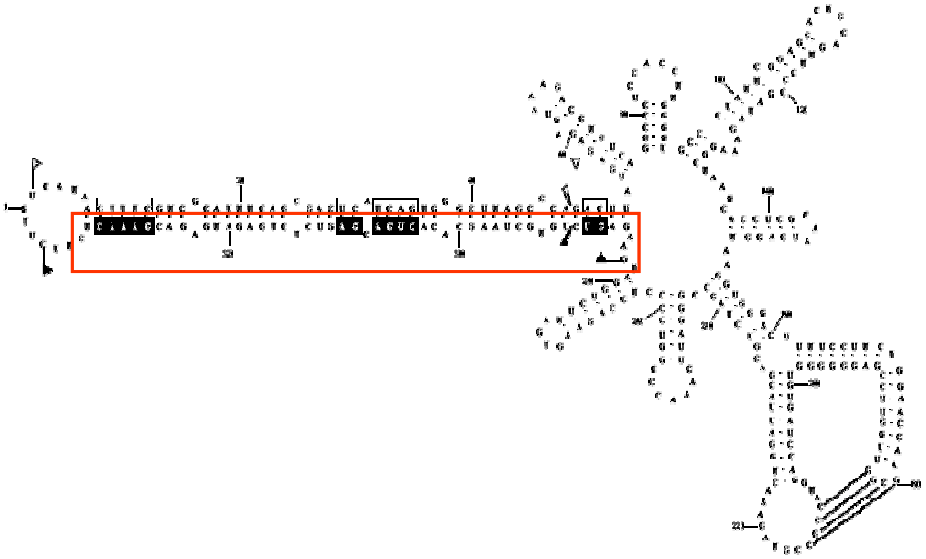

Fig. 3.40. Primary and predicted secondary structure of lowest free energy of the reference variant of PLMVd RNA (Ambros *et al.*, 1998; Hernandez and Flores, 1992). Plus and minus self-cleaving domains are delimited by flags, residues conserved in most natural hammerhead structures are indicated by bars, and the self-cleavage sites are indicated by arrows. Solid and open symbols refer to plus and minus polarities, respectively. The red box indicates the ribozimatic part in plus polarity.

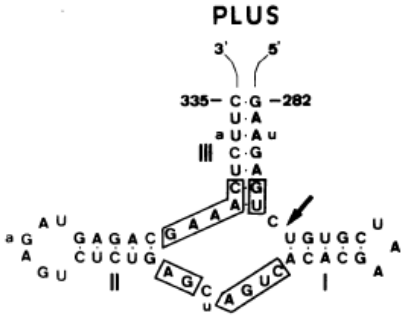

Fig. 3.41. Hammerhead structures of plus PLMVd RNA with arrows indicating the predicted self-cleavage sites. Residues boxed by solid lines are the conserved sequences present in all hammerhead structures in similar positions. I, II, III are the stems.

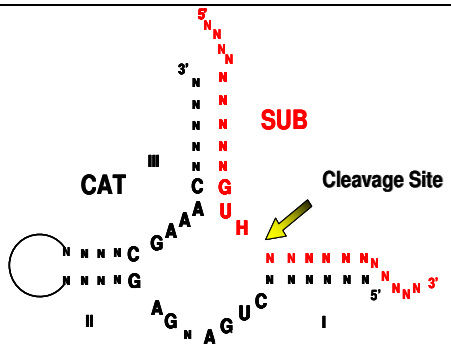

Fig. 3.42. PLMVd hammerhead trans-acting ribozyme. The catalitic subunit (black) is separated from the substrate (red). Only the conserved nucleotides are shown.

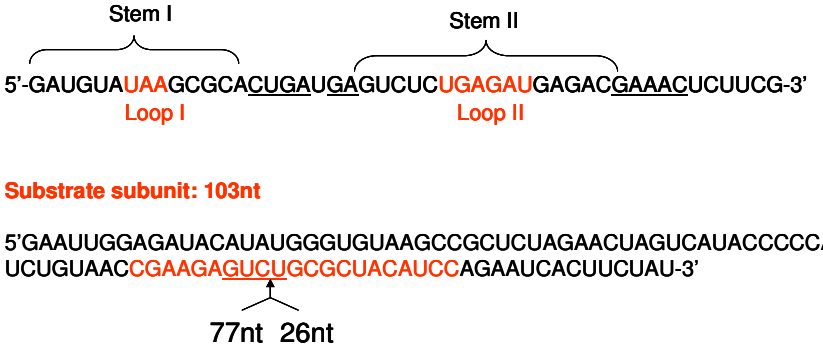

Fig. 3.43. Primary sequences of catalytic and substrate subunits of the trans-acting PLMVd hammerhead ribozyme. In CAT (48 nt) are signed the stems and the loops I and II (red) that go to make tertiary interactions (Fig. 3.44). Underlined bases are the conserved nucleotides in the core. SUB is 103 nt in its entire length. The cleavage (arrow) produces two fragments of 77 and 26 nt. In red is signed the SUB part represented in Fig. 3.44. The conserved core nucleotides are underlined.

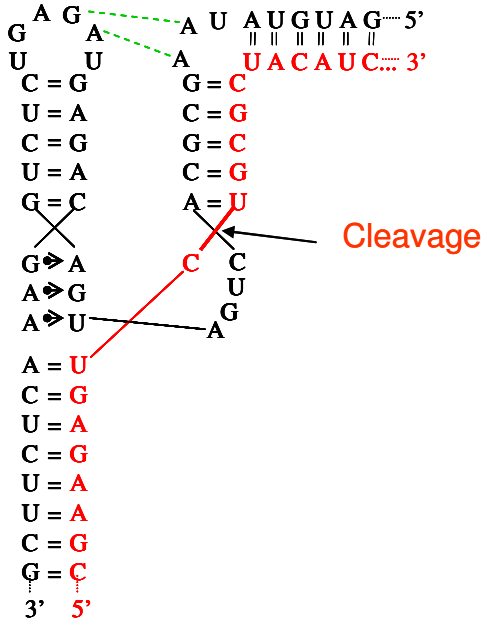

Fig. 3.44. Secondary structure diagram of the trans-acting ribozyme of PLMVd. The catalytic subunit is represented in black and part of the substrate in red. The green dotted line represents the tertiary loop interactions (Weinberg and Rossi, 2005).

3.2.2. *In vitro* cleavage reaction of the hammerhead trans-acting ribozyme

The two RNA subunits were synthesized by *in vitro* transcription starting with the two respective cDNA sequences preceded by the T7 RNA polymerase promoter sequence (see section 5.5 for details).

To test the activity of the trans-acting ribozyme we used one of the protocols commonly used in the literature (Sioud, 2004; Stage-Zimmermann and Uhlenbeck, 1998). More specifically, ribozyme (CAT) and substrate (SUB) were separately heated at 95°C for 30 seconds in water in a thermal cycler, to destroy any aggregates that may form during storage, and than cooled to the reaction temperature (37°C). At such as temperature a "reaction buffer" (pH 7.5) with Mg^{2+} (10 mM final concentration) was added to both the ribozyme and substrate. After 10 minutes of pre-incubation in reaction buffer, ribozyme and substrate solution were mixed to start the reaction (see also section 5.6).

At different time-points, the cleavage reaction was stopped and samples were loaded on a denaturant 10% polyacrylamide gel. After electrophoresis run and ethidium bromide staining, the efficiency of cleavage, and the relative percentage at each time-point were calculated by the formula $E = [I_2/(I_1+I_2)]x100$, where E is the efficiency of cleavage, I_1 and I_2 are the intensities of the gel bands corresponding respectively to the entire substrate and to the 5' fragment of cleavage. The 3' fragment of cleavage was run out from gel in order to well separate the other fragments (Fig. 3.45). Cleavage percentage was plotted versus time (Fig. 3.46).

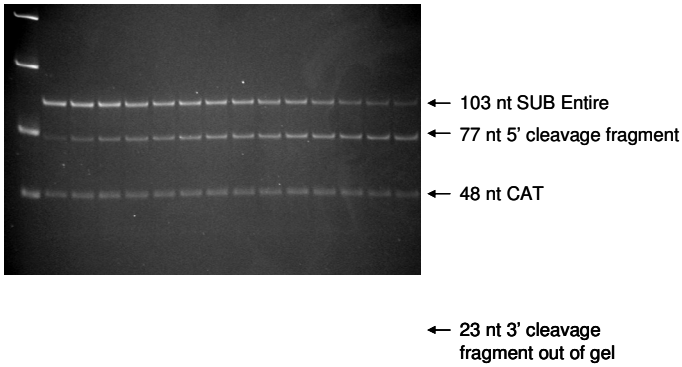

Fig. 3.45. Electrophoresis run on denaturant 10 % polyacrylamide gel of the trans cleaving kinetic reaction performed at 37°C, pH 7.5, 10 mM Mg^{2+}. From the left: RNA ladder, different time points at which the reaction was stopped (0, 0.2, 0.47, 0.75, 1, 1.25, 1.5, 1.75, 2, 2.5, 3, 5, 10, 20 minutes).

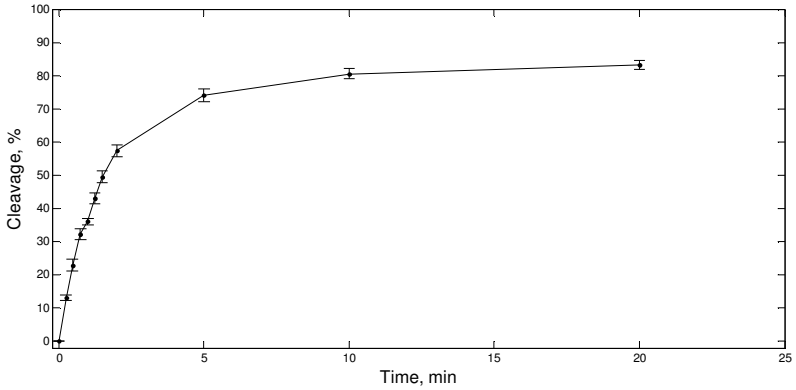

Fig. 3.46. Plot of cleavage percentage versus time. The percentage of cleavage reached at plateau is 83% ±1.3.

In these conditions the ribozyme is active. This reflects the formation of the right hammerhead structure after subunits annealing, as the theoretical secondary structure of the ribozyme shows (see Fig. 3.47). The secondary structure of the constructed system was analyzed with RNAcofold software (Bernhart *et al.*, 2006; I.L. Hofacker, 1994), that allowed us to predict the RNA secondary structure of two separated RNA sequences, which are then allowed to form a dimer structure.

The annealing of the substrate (SUB) with the ribozyme (CAT) was not the only possible. In fact, in solution SUB and CAT could also assemble separately or a substrate molecule could anneal with another substrate, as well as catalytic subunit with another catalytic subunit. In Fig. 3.48 and Fig. 3.49 all the possible different structures with their respective free energies are shown.

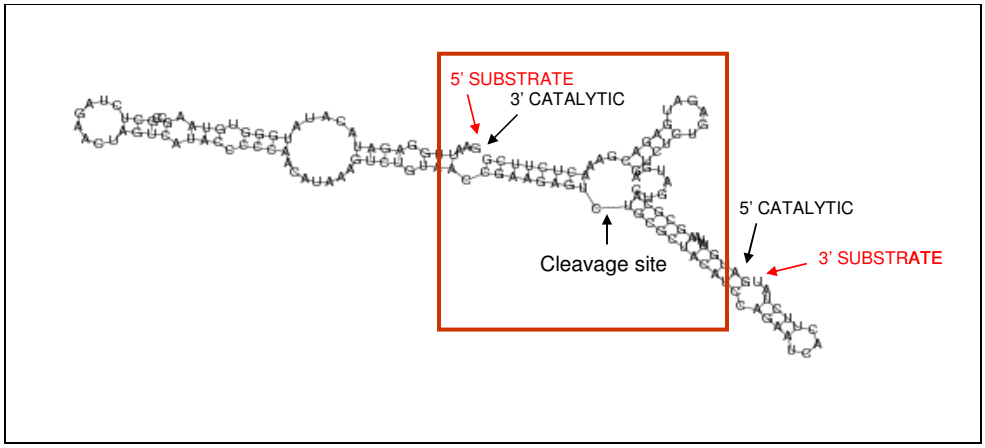

Fig. 3.47. Predicted secondary structure at 37°C of the two subunits (CAT and SUB) assembled obtained with RNAcofold software. In the box is shown the hammerhead structure. ΔG = -45.2 kcal/mol.

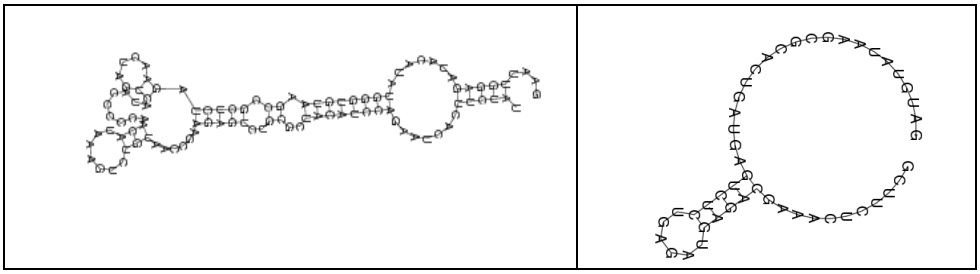

Fig. 3.48. Predicted secondary structure of SUB (left) and CAT (right) obtained at 37°C with RNAcofold software. ΔG SUB = -22.4 kcal/mol. ΔG CAT= -9.58 kcal/mol.

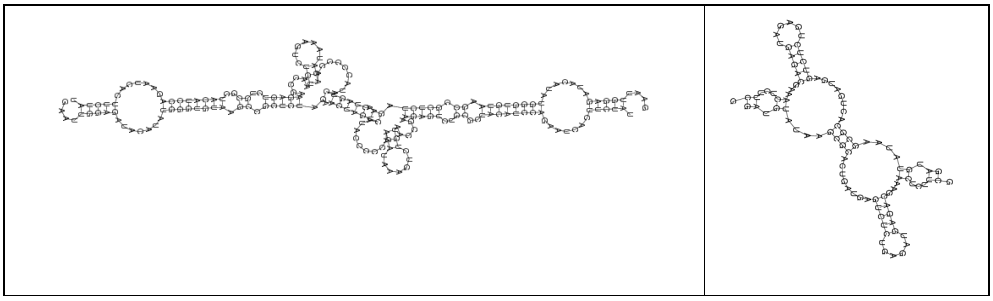

Fig. 3.49 Predicted secondary structure of SUB-SUB (left) and CAT-CAT (right) obtained at 37°C with RNAcofold software. ΔG SUB-SUB = -53 kcal/mol. ΔG CAT= -27 kcal/mol.

3.2.3. Studies of the activity of the trans-acting ribozyme following high temperature stress

To verify the effect of the high temperature on the activity of the trans acting ribozyme the catalytic subunit was stressed at 80°C for 0, 4, 6 and 12 hours in presence of water or in presence of the dipeptyde Lys-Lys. For each experiment a control that did not undergo any stress was made. The experiments were made as described in section 5.7. The catalytic subunit, after heating (30 seconds at 95°C) and slow cooling up to 37°C, was divided into four tubes. In two of them Lys-Lys (Lys-Lys control and stress) was added, in order to have 1 Lys-Lys molecule for each nucleotide of RNA. In the other two tubes the same volume of water (water control and stress) was added. After 15 minutes, tubes with CAT in presence of water/or Lys-Lys which should undergo stress ("S"), were put at 80°C. The other two negative controls (CAT water/or Lys-Lys "C") were left at 37°C for all the period during which the stress was applied. Molecules were stressed for 0h (any stress), 4h, 6h, and 12h. Then, all the tubes (CAT in water/or Lys-Lys, "C" and "S") were put into ice for 5 sec and trans-cleaving kinetics were performed by mixing CAT ("C" and "S", in water/or Lys-Lys) with SUB, as previous described. Results obtained are shown in Fig. 3.50, Fig. 3.51, Fig. 3.52 and Fig. 3.53.

The residual activity of the catalytic molecules after stress was compared with the activity of respective controls. The residual activity was calculated on the basis of the percentage of cleavage reached at plateau (Table 3.6, Table 3.7). The ratio between the percentage of cleavage reached at plateau by the stressed catalytic molecules and their respective controls was plot versus the stress time. This graphic gives us an idea of the loss of the activity of the ribozyme in the considered conditions (Fig. 3.54).

As a result, we observed that, after stress at 80°C, molecules in presence of Lys-Lys remained slightly more active than molecules in water without the dipeptyde. In fact, after 12h at 80°C the activity of the molecules in presence of Lys-Lys (one molecule for each nucleotide of CAT) was around 7% higher than the one observed for molecules without Lys-Lys. This result suggest a slight protection by Lys-Lys.

We wanted to test whether this protection could be enhanced by increasing the ratio Lys-Lys/ribozyme, i.e., two Lys-Lys molecules each nucleotide of CAT. In this experiment we stressed the catalytic subunit for 17h at 80°C, in order to enhance,

if any, the difference between water and Lys-Lys. In this case (see Fig. 3.55) the percentage of cleavage achieved at plateau after 60' was about 78 % for water control, 76% for Lys-Lys control, 49% for water stress and 70% for Lys-Lys stress. Thus, we observed a protection of 29% given by Lys-Lys, calculated by the difference between the residual activity of the ribozyme in presence of Lys-Lys (92%) and the one in water (63%).

Thus, from these preliminary results, it seems that Lys-Lys could have had a protection role of a primordial catalytic RNA against high temperature degradation.

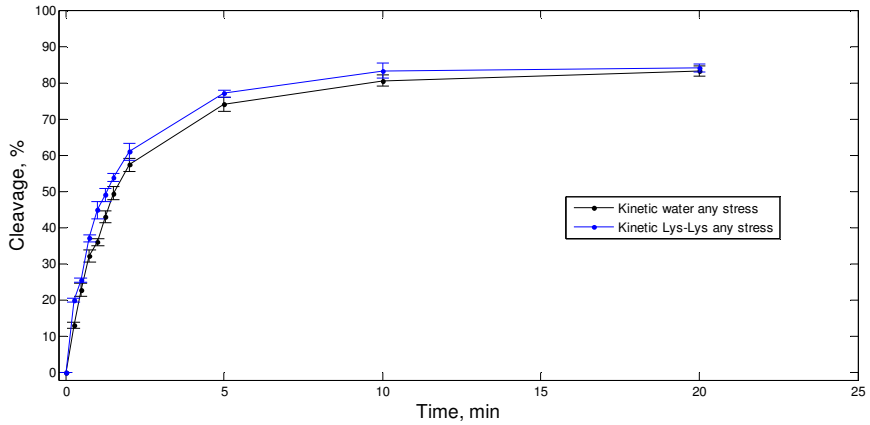

Fig. 3.50. Trans cleavage reaction in water (black line) and Lys-Lys (blue line) performed at 37°C after 0 hours of stress.

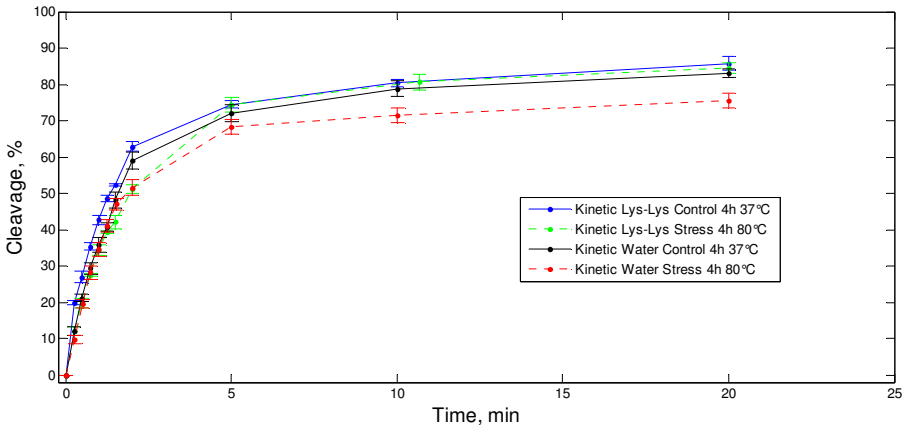

Fig. 3.51. Trans-cleavage kinetic reaction performed at 37°C after 4h hours of stress at 80°C in water (red line) and in presence of Lys-Lys (green line).
Black and blue lines are the kinetics control stayed at 37°C in presence of water or Lys-Lys respectively for all the stress time.

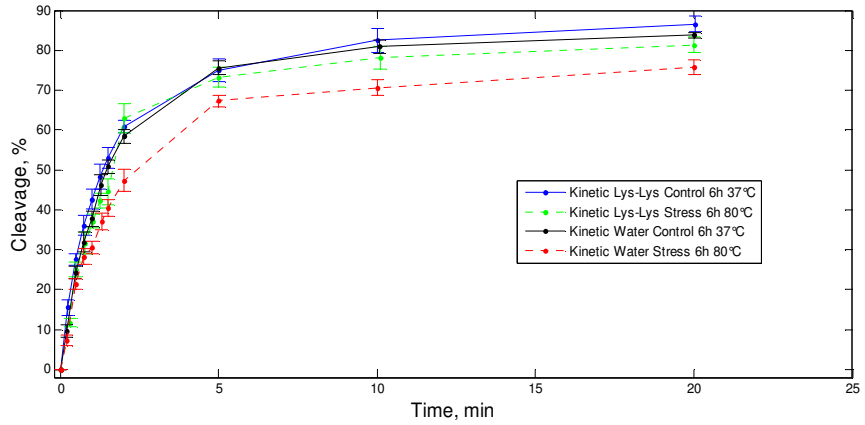

Fig. 3.52. Trans-cleavage kinetic reaction performed at 37°C after 6h hours of stress at 80°C in water (red line) and in presence of Lys-Lys (green line). Black and blue lines are the kinetics control stayed at 37°C in presence of water or Lys-Lys respectively for all the stress time.

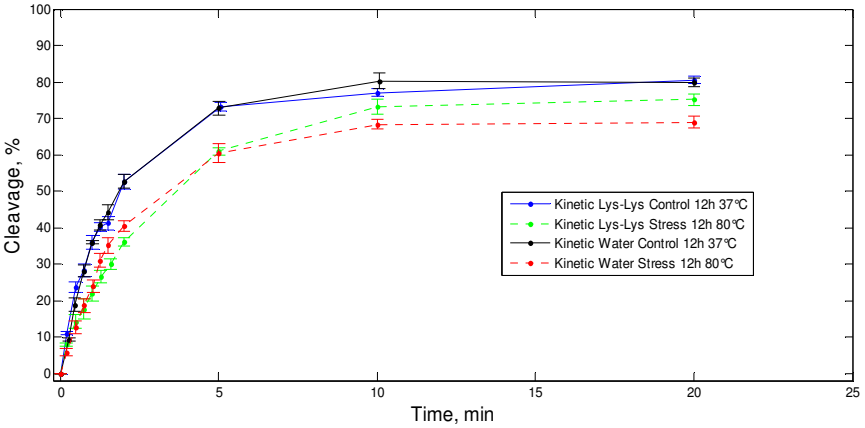

Fig. 3.53. Trans-cleavage kinetic reaction performed at 37°C after 12h hours of stress at 80°C in water (red line) and in presence of Lys-Lys (green line). Black and blue lines are the kinetics control stayed at 37°C in presence of water or Lys-Lys respectively for all the stress time.

Time stress	Cleavage percentage at Plateau. Water C^+	Error	Cleavage percentage at Plateau. Water Stress	Error	**Stress/C+**
0	83.18213	1.3	83.18213	1.3	**1**
4h	83.05694	1.2	75.48342	2	**0.908815**
6h	83.75049	0.7	75.78205	1.8	**0.904855**
12h	79.91617	1	68.95129	1.5	**0.862795**

Table 3.6. Cleavage percentage calculated at plateau (after 20') of the trans cleavage kinetics performed in presence of water.

Time stress	Cleavage percentage at Plateau. Lys-Lys C^+	Error	Cleavage percentage at Plateau. Lys-Lys Stress	Error	**Stress/C+**
0	84.06789	1.2	84.06789	1.2	**1**
4h	85.72559	1.9	84.44704	1.5	**0.985086**
6h	86.54262	2	81.31761	1.9	**0.939625**
12h	80.55707	1	75.08911	1.5	**0.932123**

Table 3.7. Cleavage percentage calculated at plateau (after 20') of the trans cleavage kinetics performed in presence of Lys-Lys.

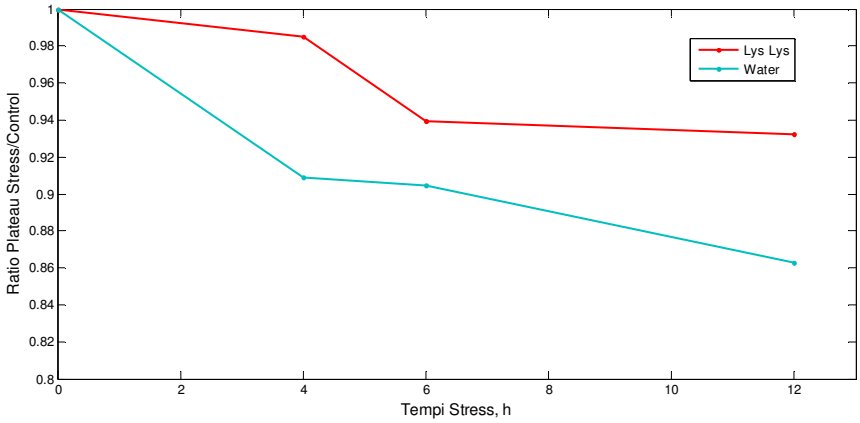

Fig. 3.54. Ratio between percentage of cleavage reached at plateau after stress and control in water (blue line) and in presence of Lys-Lys (red line) plotted versus time stress. After 12h of stress at 80°C the ratio for the ribozyme in presence of water is 0.86, while in presence of Lys-Lys is 0.93.

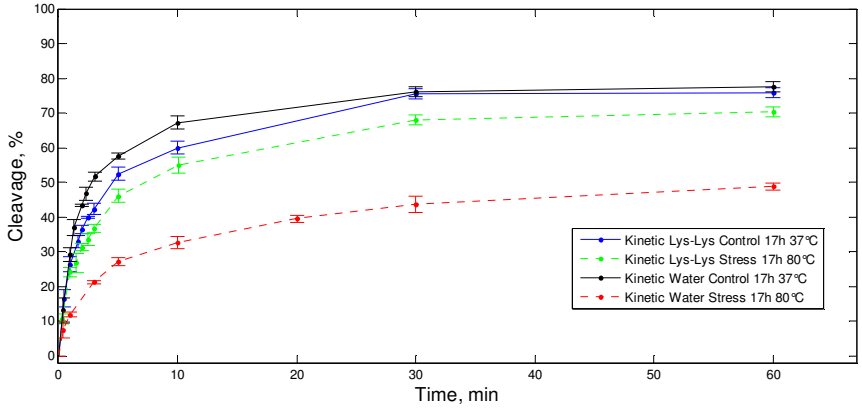

Fig. 3.55. Trans cleavage kinetic reaction performed at 37°C after 17h hours of stress at 80°C in water (red line) and in presence of Lys-Lys (2 molecules each CAT nucleotide, green line).
Black and blue lines are the kinetics control stayed at 37°C in presence of water or Lys-Lys respectively for all the stress time.

4. Conclusions and Discussions

The present thesis deals with the study of the structure, activity and protection of primordial catalytic RNA molecules, with the aim of understanding how they could have evolved in the supposed primitive RNA world.

4.1. Studies on ASBVd

In the first part of the work, we studied the *in vitro* self-cleavage activity and the structural organization of the monomeric and linear form of (+) and (-) ASBVd (*Avsunviroidae* family) in different conditions, obtained by varying the temperature and the Mg^{2+} concentrations.

Self-cleavage activity

The self-cleavage activity of (+) and (-) mASBVd was analyzed by performing *in vitro* self-cleavage kinetics at several different Mg^{2+} concentrations and temperatures. For both strands an increase in the activity with the increase of Mg^{2+} and of temperature is observed. Moreover, we found that the (-) strand is more active than the (+) strand and that it is more resistant to degradation at higher temperatures.

For these reasons we analyzed in detail the *in vitro* self-cleavage activity of (-) mASBVd under different conditions.

The results concerning the kinetic reactions performed in physiological conditions (25°C, 2 mM of Mg^{2+}, 150 mM of K^+, pH 7.5) show that *in vitro* the viroid is not active. It is likely that the concentration of Mg^{2+} and/or the temperature are too low and as a result not sufficient to shift the chemical equilibrium between the inactive (C_I) and the active conformations (C_A) of the monomers towards C_A. The formation of the active structures is in fact the rate-limiting step of the self-cleavage reaction. Therefore, we can hypothesize that *in vivo* the folding of the viroid in the catalytic structure may be helped by other ions and/or factors present inside the chloroplasts.

However, kinetic reactions carried out by changing Mg^{2+} concentration and temperature (same pH and K^+ concentration of physiological conditions) allowed us

to find favourable conditions for cleavage. Kinetic parameters (K_{obs} and F_{∞}), were calculated for each kinetic carried out. Data show that K_{obs} increases by increasing both the Mg^{2+} concentration and the temperature, while F_{∞} increases with the temperature, reaching a plateau at about 10 mM of Mg^{2+} at every analyzed temperature. These experiments indicate that the best temperature and Mg^{2+} concentration for the cleavage of (-) mASBVd are 55°C and 50 mM respectively.

Negative controls (carried out without Mg^{2+} at all the tested temperatures) show that (-) mASBVd is unable to self-cleave in the absence of Mg^{2+}, despite the presence of 150 mM of a monovalent cation (K^+). These results represent further evidence of the fundamental importance of divalent cations for viroid *in vitro* self-cleavage reaction.

Structural analysis

The structural organization of (-) mASBVd was characterized by Circular Dichroism (CD) and Raman spectroscopy.

This work allowed us to evaluate the structural changes leading to an inactive or an active structure, and to understand if a correlation between the cleavage efficiency and the structural changes of viroid was present. In fact, we investigated the relation between the cleavage reaction and the structures produced by Mg^{2+} and/or buffer-K^+. As already mentioned, our results suggest that Mg^{2+} is of fundamental importance for the *in vitro* self-cleavage of the (-) mASBVd, while K^+ does not allow the cleavage process.

CD results indicate that buffer-K^+, and Mg^{2+}, involve different structural organizations in the stacking of bases of the viroid. However, all measured CD spectra, with and without Mg^{2+} and/or buffer-K^+, represent a typical A-RNA form geometry.

Raman results show that the presence of buffer and K^+ mainly leads to a loss of structural rigidity and to a slackening of the structure of organized ribose phosphate backbone, as indicated by the decrease of the band at 813 cm^{-1} (marker of organized A-RNA backbone). A decrease of the ordered backbone implies a less homogeneous RNA population. Moreover, it is possible that the relaxation of conformational constraints on the backbone may allow a greater freedom for the stacking of bases. In contrast, the presence of Mg^{2+} increases the content and probably the constraints of the A-helix organized backbones, as displayed by the

increase of the Raman band at 813 cm^{-1}. Therefore, the Mg^{2+} leads the RNA molecules to take an A-helix form and increases the structural rigidity of the ribose phosphate backbones. The increase of organized A-RNAs means a more homogeneous population distribution of viroid. In addition, the conformational constraints of the backbone enhanced by Mg^{2+} could restrain the freedom of the bases, slightly impeding their stacking.

In the light of what stated above, we may postulate that the viroid presents two different structure types: an organized and constrained backbone structure favoured by Mg^{2+}, and a less organized and less constrained structure favoured by buffer-K^+. Thus, the population distribution between both structures is inversely shifted by Mg^{2+} and/or buffer-K^+.

As a further consideration we observe that both CD and Raman experiments show a correlation between the Mg^{2+} concentration and its effect. In fact, the effect of Mg^{2+} is enhanced by increasing Mg^{2+} concentration, which in turn results in an increased viroid activity, as demonstrated by kinetic reactions. Moreover, the presence of this cation is essential, at least *in vitro*, for the self-cleavage of the viroids, probably promoting the correct folding of their hammerhead ribozyme (Davies *et al.*, 1991). On the contrary, the viroid is inactive in presence of buffer-K^+ without Mg^{2+}. In view of this, we can suppose that the structure induced by buffer-K^+ could be associated with an inactive viroid conformation, while the structure induced by Mg^{2+} may be associated with an active viroid conformation. As Raman results suggest, an ordered and constrained A-helix form could be the correct structure that the viroid needs to cleave itself. Probably, the greater the number of molecules that take this conformation, the greater the cleavage efficiency.

Time-dependent studies during cleavage reaction

CD data obtained by monitoring the viroid spectra at different times after Mg^{2+} addition show that cleavage does not have any effect on the signal evidenced by CD. In fact no change in CD spectra was observed over time, neither in the presence nor in the absence of cleavage.

Differently, Raman signal involves time-dependent multistep processes and the three different analyzed conditions have different time-dependent windows.

However, the time-dependent Raman process is not directly linked to the cleavage. In fact, changes in Raman spectra compare over time in the absence of

cleavage (physiological conditions). In the cases where cleavage occurs (20 and 100 mM of Mg^{2+}), the time lapse during which Raman changes can be observed ends before the kinetic plateau is reached. Thus, in active cleavage conditions, the Raman temporal evolution is much faster than the kinetic of cleavage, suggesting that they do not depict identical processes. Moreover, once the viroid RNAs population is stabilized, no other spectral changes are observed, even if cleavage is still taking place. The Raman changes observed, therefore, are not related with the cleavage itself and with the formation of 2',3'-cyclic phosphate.

Nevertheless, there is a relationship between the velocity of the stabilization of Raman spectra and the efficiency of cleavage: the more efficient the kinetic of cleavage, the faster the time evolution of Raman signal and its stabilization. No stabilization was observed in the case of viroid inactivity.

In conclusion, the time dependence of the Raman signal does not originate from the cleavage; however, it could depict a step having an influence upon the cleavage. In fact, Mg^{2+} shifts the viroid populations from a slackened to a more constrained helical secondary structure. The time-dependent Raman process mostly results in a relaxation of constraints (lost of structural rigidity). We can hypothesize that it represents the attainment of a new equilibrium between both structural types. Thus, this process could arise from dynamic equilibrium perturbation between the constrained and slackened structures of the viroid. We may therefore conclude that the more quickly the new equilibrium is reached, the more efficient the cleavage.

Differences between Raman and CD spectroscopy signals

CD and Raman spectroscopy do not give the same information. CD depends on the coupling of electronic transition involving many bases along the most organized and constrained viroid domains. Therefore, the signal comes mostly from helical structured domains. Conversely, Raman scattering sums the vibrational modes of the individual signals of all backbone and base residues of the viroid. Thus, CD shows a more restricted domain of the viroid than Raman scattering.

However, cleavage does not have any straight effect neither on the CD nor on Raman spectra of viroid. Hence, the breaking of one ribose phosphate bonding over 249 (the length of entire viroid) involves a small perturbation of signal that is not detectable by the considered spectroscopy techniques.

Effect of temperature on CD spectra of viroid

CD experiments performed at different temperatures allowed us to understand the effect of this important parameter upon the viroid structure. Moreover, they allowed us to verify the reversibility of the viroid structure following exposition at high temperatures, which are considered a possible degrading agent in a primordial environment.

The obtained results demonstrate that the increase of temperature from 4°C to 95°C causes a decrease in the intensity and a red-shift of the main peak of the CD spectra (at about 260 nm). The effect is smooth up to 50°C, probably reflecting small variations in the coupling between bases, while it is steeper between 50 and 75°C, suggesting a melting of the structure at such as temperatures. Over 75°C, perhaps, the structure is completely melted, since no changes in CD spectra are observed by increasing temperature from 75°C to 95°C. These conclusions are also supported by theoretical structural analysis performed with Mfold software at different temperatures, which reflect the trend observed in CD spectra by increasing the temperature.

Experiments carried out to test the reversibility of the process show that a decrease in temperature from 95°C to 4°C causes an increase and a blue shift of the peak at about 260 nm, suggesting that the viroid does not lose its ability to acquire a closed structure starting by a melted one. Probably, the structural proprieties of viroid exhibit hysteresis, i.e. a "rate-independent memory".

Therefore, a decrease in intensity and a red-shift and of the main peak of CD spectra could be related to the passage of molecules from a closed status (with an extended base-paring) to a more relaxed conformation. The opposite is indicated by an increase in intensity and a blue shift of the same peak.

Further experiments, aimed at determining the optimal temperature for cleavage, are currently being performed.

4.2. Studies of trans-acting ribozyme

In the second part of our work we tested the effect of high temperatures on the catalytic activity of a hammerhead trans-acting ribozyme, constructed starting with the sequence of the hammerhead ribozyme of PLMVd. Trans-cleaving reactions were performed following a stress at 80°C in the presence or absence of the dipeptide

Lys-Lys, to simulate a scenario where both RNA molecules and amino acids, or short polypeptides, could have been present at the same time. Data obtained show that RNA molecules maintain their ability to interact with each other and to undergo a trans-cleaving reaction in presence of the dipeptide Lys-Lys. Moreover, preliminary results suggest that Lys-Lys protects RNA catalytic molecules against high temperatures. The greater stability of RNA/Lys-Lys as compared to the RNA in water (without Lys-Lys) suggests that a crucial step for evolution could have been the interaction between the first nucleic acid molecules and primordial peptides: a sort of primordial nucleosome-like structure.

5. Material and Methods

5.1. Preparation of linear and monomeric plus (+) and minus (-) Avocado Sunblotch viroid (ASBVd) RNA

5.1.1. Plasmid templates

The template DNA (cDNA) for the in *vitro* production of ASBVd RNA in its monomeric form (mASBV) was kindly provided by Dr. Flores, Universidad Politécnica de Valencia-CSIC, Spain. The cDNA was previous cloned into a plasmid (pKSmASBVd) and inserted into E.coli strain by Clementine Delan Florino (PhD student in the laboratory of Prof. Maurel, Acides Nucléiques et Biophotonique, Université Paris VI).

5.1.2. Sample preparation

After a MIDI-preparation of pKSmASBVd, the cDNA corresponding to mASBVd was amplified by PCR using the two couples of primers designed to obtain, after transcription with T7 RNA polymerase, (+) and (-) strand of mASBVd RNA. Primers containing the T7 promoter sequence, synthesized by MGW Biotech, are showed in Table 5.1 and Table 5.2.

Name	Sequence	Lenght	Tm
Pr Fw ASBVd (+)	5'-AAGAGATTGAAGACGAGTG-3'	19 nt	54°C
Pr Rev T7 ASBVd (-)	5'-**TAATACGACTCACTATAGG** GATCACTTCGTCTCTTCAGG-3'	39 nt	60°C

Table 5.1. Primers used for the obtainment of the (+) strand of mASBVd

Name	Sequence	Lenght	Tm
Pr Fw T7 ASBVd (-)	5'-**TAATACGACTCACTATAGG** AAGAGATTGAAGACGAGTG-3'	38 nt	54°C
Pr Rev ASBVd (+)	5'-GATCACTTCGTCTCTTCAGG-3'	20 nt	60°C

Table 5.2. Primers used for the obtainment of the (-) strand of mASBVd

All the PCR were performed in a reaction volume of 50 µl. The mix of reaction was composed by 20 ng of plasmidic DNA (pKSmASBVd), 0.2 mM of dNTPs, 1 µM of each primer, 2.5 units of Taq DNA polymerase, 1 X Taq-buffer. After an initial heating at 94°C for 5 min, the amplification profile (25 cicles) was 1 min at 94°C, 45 sec at 60 °C, 45 sec at 72°C, with a final extention of 10 min at 72°C. After performing reactions, PCR products were controlled on 1 % agarose gels, ethanol-precipitated, and resuspended in sterile ddH2O. Taq polymerase with relevant 10X buffer and dNTPs were all from Qbiogene.

Both the PCR products of (+) and (-) mASBVd RNAs were 266 nucleotides long: 247 nucleotides of cDNA corresponding to the length of the natural monomer viroid, plus 19 nucleotides corresponding to the T7-RNA polymerase (mettere figura 2/12/08 o 8/10/2008 per le PCR).

PCR products were in *vitro* transcribed by T7 RNA polymerase, in order to obtain (+) and (–) mASBVd RNAs. The reaction was carried out at 37°C for 5h in a final volume of 5 ml, containing 30ng/µl of DNA template, 1.2 U/µl of T7 RNA polymerase, 2 mM of NPTs (ROCHE), 0.5 U/µl of RNase-Inhibitor, 1X transcription buffer. Template DNA was enzimatically removed by 2U of DNase I each µg of DNA (1h at 37°C). T7 RNA polymerase with relevant 10X buffer, NPTs, RNase-Inhibitor and DNase I were all from ROCHE.

The transcription product was ethanol precipitated and resuspended in 300 µl of sterile ddH2O. (+) and (-) mASBVd RNAs were purified by polyacrylamide gel extraction, following the protocol described below.

After the addition of one volume of a "stop solution" (80% formamide, 30 mM EDTA pH 8, 0.0125% Xylene Cyanol), the sample was heated 5 min at 70°C to be completely denatured, and loaded on a denaturing polyacrylamide gel. Gels for mASBVd analysis and extraction were 7 M urea, 10% (w/v) polyacrylamide (19:1

mixture of acrylamide:bisacrylamide), and 1X TBE, with dimensions of 20x20x1.5 mm (WxHxD). All gels were run for about 2.5h at alternate constant amperes and power of 50 mA, 20-21 W. After than, the viroid band was cut out of gel, broken into 2-3 peaces and put it in a 5-10 ml syringe without the needle. The gel was crushed in a 50 ml tube containing 5 ml of 0.3 M Na-acetate, pH 5.2. After 15'-30' of gently vortex, the tube was left O/N at 4°C in slow motion (elution of RNA). The content of the tube was transferred in a 10 ml syringe without the needle, and the mixture passed into a new tube through a 0.45 μm filter. The mixture was filtered again through a 0.2 μm filter, to well remove all the polyacrylamide. The eluate was precipitated with 2.5 volumes of EtOH at -20°C for 30 min, centrifugated at 14000 rpm at 4°C for 30 min (or more), and the pellet resuspended in 2 ml of sterile ddH2O. The precipitation was repeated four or more times. Finally, the pellet was resuspended in 200-500 μl of sterile ddH2O.

RNA concentration was checked by UV-adsorption at 260 nm.

5.2. mASBVd *in vitro* self-cleavage reaction

All the in *vitro* self-cleavage kinetics were performed in a thermal cycler. Every time, before the buffer addition, the purified transcription products were heated 30 sec at 95°C (to destroy any possible aggregates that may form during storage) and slowly cooled (3°C/min) to the reaction temperature. This step was carried out in water in a volume of 1.25 less than the final volume of reaction.

5.2.1. Analysis of the activity of (+) and (-) mASBVd strands at different Mg^{2+} concentrations and at different temperatures

(+) and (-) mASBVd in *vitro* self-cleavage kinetics at several different Mg2+ concentration were performed at 37°C by incubating RNA (final concentration 955 nM) in 10 mM sodium cacodylate at pH 7.5 and 10, 20, 50 or 100 mM of Mg2+.

Buffer sodium cacodylate was chosen for different reasons. Firstly, because its pKa does not change with temperature (ΔpKa/Δt = -0.0015 °C-1); secondly, because it is compatible with Mg2+. The pH at 7.5 was adjusted by addition of HCl.

Reactions were stopped after the addition of Mg2+ (5 sec) and after 5h by mixing 5μl of the reaction in 35 μl of a "stop solution" (80% formamide, 30 mM

EDTA pH 8, 0.0125% Xylene Cyanol). The reactions were analyzed by denaturing (7M urea) polyacrylamide (10%) gel electrophoresis (PAGE) followed by Ethidium Bromide (EtBr) staining. The percentage of cleavage was analyzed with Image J software calculated as $E=[(I_1+I_2)/(I_1+I_2+I_i)] \times 100$, where I_i is the intensities of the band corresponding to the full-length molecule and I_1 and I_2 its 5' and 3' fragments of cleavage, respectively.

Self-cleavage kinetics at several different temperatures (25, 37, 45°C) were performed in the same way. Two Mg^{2+} concentration were checked for each temperature: 100 mM and 50 mM for the (+) strand, and 50 mM and 10 mM for the (-) strand.

5.2.2. Study of the *in vitro* self-cleavage activity of (–) mASBVd

In vitro mASBVd self-cleavage reactions were performed at 25, 35, 45, and 55°C following this protocol: as usually the purified transcription products were heated and slowly cooled up to the chosen reaction temperature. This step was carried out in water in a final volume of 40 µl. Once arrived at the chosen temperature, 5µl of a first buffer (9X "buffer 1"), containing cacodylate pH 7.5 (10 mM final concentration) and K^+ (150 mM final concentration), was added. After 10 min of stabilization in "buffer 1", 5µl of a second buffer containing Mg^{2+} (10X), cacodylate pH 7.5 (1X) and K^+ (1X) , was added to start the cleavage reaction ("cleavage buffer"). In the final 50 µl there were 955 nM RNA, 10 mM cacodylate pH 7.5, 150 mM of K^+, and 2, 10, 20, 50, or 100 mM of Mg^{2+}. Aliquots of 5 µl were taken at different time points and mixed with 35µl of "stop solution" in order to stop the kinetic.

Negative controls with 10 mM of cacodylate pH 7.5 and 150 mM of K^+ were made adding 10µl of the 5X "buffer 1", while the ones with the only cacodylate were made adding a 5X "buffer 3" with sodium cacodylate at pH 7.5. Negative controls were performed at every tested temperatures.

The reactions were analyzed as described above in section 5.2.1. Data of the percentage of cleavage were plotted and fitted with the equation $F_t = F_0 + F_\infty(1-e^{-k_{obs}t})$, where F_t, F_0 and F_∞ are the fractions of products cleaved at time t, at time 0 and at the plateau, respectively, and k_{obs} is the observed kinetic constant of the reaction.

5.3. Circular Dichroism

Circular dichroism (CD) is a phenomenon originating from interactions of chiral molecules with circularly polarized electromagnetic rays (Woody, 1995).

This spectroscopic method depends on the fact that certain molecules interact differently with right and left circularly polarized light (CPL). Chiral molecules occur in two nonsuperimposable forms which are mirror images of another. To discriminate between the two circular forms of light, a molecule must be chiral, which includes the cast majority of biological molecules. A method which can discern the subtle differences between nonsuperimposable mirror image molecules (enantiomers) must be highly sensitive to the three-dimensional features of molecules, that is, to conformation. This expectation has been amply verified and forms the basis for the many applications of CD in biochemistry.

5.3.1. Phenomenon of CD

Linearly polarized light can be shown to consist of two opposite CPL of equal amplitude and phase. A projection of the combined amplitudes perpendicular to the propagation direction yields a line (Fig. 5.1 a). When this light passes through an optically active sample with a different absorbance for the two components of CPL, the amplitude of the stronger absorbed component will be smaller than the one of the less absorbed component (Fig. 5.1 b and Fig. 5.2). The consequence is that a projection of the resulting amplitude is an ellipse instead of the usual line. The occurrence of ellipticity is related to optical activity.

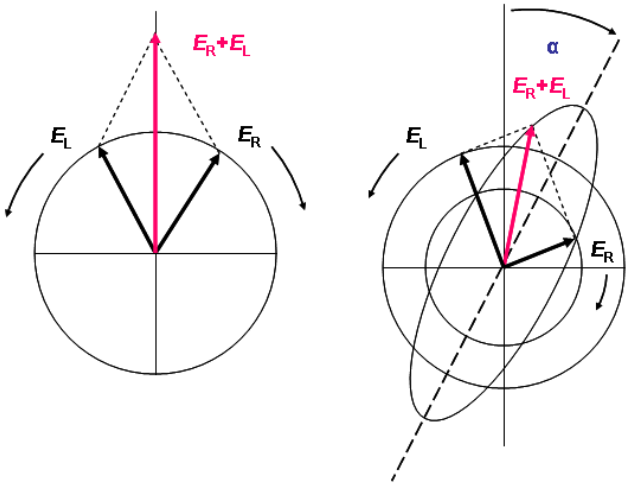

Fig. 5.1. (a) Linear polarized light can be viewed as a superposition of opposite circular polarized light of equal amplitude and phase. (b): different absorption of the left- and right hand polarized component leads to ellipticity (CD)

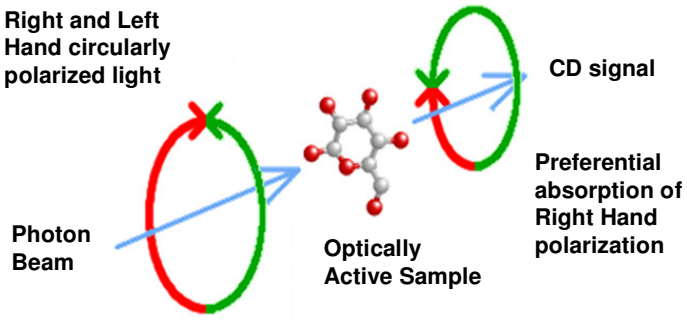

Fig. 5.2. Fig. 2. Schematic illustration of CD phenomenon

5.3.2. Application of CD spectroscopy in biochemistry

The phenomenon of CD is very sensitive to the secondary structure of chiral biological molecules. For this reason CD technique is largely used to study secondary structure formation in both proteins and nucleic acids and to monitor their conformational changes (Ivanov *et al.*, 1973).

Therefore, the alpha helix of proteins and the double helix of nucleic acids have CD spectral signatures representative of their structures. Historically, CD spectroscopy has been used to observe thermal or chemical denaturation, ligand binding, and conformational changes in nucleic acids as a function of salt

concentration, level of hydration, and pH (Woody, 1995). For a very recent review on the studies that provided important information about conformational properties of DNA using CD spectroscopy see (Kypr *et al.*, 2009). With the discovery of ribozymes the CD spectroscopy has been used to characterize the RNA structure and secondary and tertiary RNA folding transitions (Pan and Sosnick, 1997; Sosnick, 2001; Sosnick *et al.*, 2000).

5.3.3. Structural analysis of viroid with CD spectroscopy

Circular dichroism spectra for mASBVd were recorded on a Jasco model J-810 spectropolarimeter equipped with a thermoelectrically controlled cell holder. A 0.1 cm quartz cell was used. Each spectrum, monitored between 210 and 310 nm by steps of 1 nm, represents an average of 3 · 5 scans. In the region above 200 nm, the maximal absorbance is due to the nucleotide bases, which have a broad maximum in the region around 260 nm (Sosnick, 2001). Results are presented in molar circular dichroism (Δε, defined as the difference between the extinction coefficients for the two types of circularly polarized light) as a function of wavelength (nm).

Ellipticity was converted in Δε as in the equation

$\Delta\varepsilon\ (mol^{-1}.dm^{3}.cm^{-1}) = \theta/(32.980xCxLxN)$

where θ is the measured CD amplitude (ellipticity) in millidegrees, C is the sample concentration in mol/litre, L is the optical pathlength in centimetres, and N is the RNA nucleotides number (Sonsnick *et al.*, 2000).

Before to perform each experiment, the spectrum of water, of buffer cacodylate-K^+, and of buffer cacodylate-K^+ + Mg^{2+}, were measured at each tested temperature, in order to have all the baselines.

All CD experiments were done in duplicate or triplicate to ensure consistent results.

5.3.4. CD experiments during a self-cleavage kinetic

All CD experiments following a kinetic reaction were performed in the same way than *in vitro* self-cleavage kinetics (1.2.2.). Firstly, sample were diluted in water (200 µl), heated at 95°C for 30 sec and slowly cooled (3°C/min) up to the chosen temperature. This step was performed in a thermal cycler. Once arrived at the given temperature, the viroid RNA was put in a quartz cell previously heated at the same

temperature. The spectrum of the RNA in water was measured. Then, cacodylate buffer (10 mM, pH 7.5) with K^+ (150 mM), and finally the Mg^{2+} (2, 20 or 100 mM) were mixed to RNA in water. The final concentration of the RNA was 3.34µM in a final volume of 250 µl . The spectrum of the RNA was measured after the addition of each component. When Mg^{2+} comes in contact with RNA, the reaction starts; thus, the first spectrum, measured after Mg^{2+} addition, was called "spectrum at time 0". Spectra were monitored at different time points after Mg^{2+} addition (every 10'), in order to follow the variations in the structure of the RNA during the self-cleavage. Aliquots of the solution (1.5µl) were taken at different time points before each measure, and the reaction was stopped in "stop solution" in order to verify the kinetic of cleavage by denaturant PAGE.

5.3.5. Investigation of RNA structural changes at different Mg^{2+} concentrations by CD spectroscopy

CD experiments at different Mg^{2+} concentration were performed at 45°C and pH 7.5. As before, after that viroid was heated and slowly cooled, its spectrum in water at 45°C was measured. Buffer cacodylate (10 mM, pH 7.5) and K^+ (150 mM) were added and 5 µl of the solution were immediately taken and mixed with 35 µl of the

"stop solution" to be controlled on gel. The spectrum in buffer cacodylate-K^+ was measured. Mg^{2+} was gradually increased from 0.5 to 10 mM (0.5 mM each step) adding 5µl of a stock solution previously prepared with buffer cacodylate, K^+ and Mg^{2+}. Each of the 20 stock solutions contained the same concentration of buffer cacodylate and K^+ in the way that they did not change at each addition. In contrast, the concentration of Mg^{2+} varied in order that, each time, it increased of 0.5 mM. After each addition, 5 µl of the solution were mixed with the "stop solution" to be loaded on gel and the viroid spectrum was measured.

5.3.6. Investigation of RNA structural changes at different temperatures by CD spectroscopy

CD experiments at different temperatures were performed with 10 mM of Mg^{2+}, pH 7.5. After viroid was heated and slowly cooled up to 4 °C, its spectrum was measured. Buffer cacodylate and K^+ (same concentrations of the other

experiments), and finally Mg^{2+} (10 mM) were added. Spectra at 4°C was monitored. After that, in a first step, the temperature was increased from 4°C to 95°C (5°C/time). After each temperature variation, viroid was stabilized 5 minutes at the given temperature, and then the spectrum measured. As usually, a little aliquot of the solution was taken to be controlled on PAGE. Once arrived at 95°C, in a second step the temperature was increased from 95°C to 4°C (5°C/time). Following the same protocol than the first step, the spectrum of viroid was measured at each temperature.

5.4. Raman spectroscopy

Raman is a spectroscopic technique used to study vibrational and/or rotational modes in a molecular system.

5.4.1. Raman principle

Raman spectroscopy is based on inelastic scattering of photons interacting with the analyzed sample.

When monochromatic light is directed on a molecule, the light can be scattered or absorbed. Most of the scattered light will be at the same frequency as the incident light. This is known as Rayleigh scattering or elastic scattering (the emitted photon has the same wavelength as the absorbing photon). However, a small fraction of the light [about 1 in 10^5 photons (Ferraro *et al.*, 2003)] will be inelastically scattered at frequencies different from the incident photons. The energy difference between the incident and scattered light corresponds to a variation in the energy of the analyzed atom or molecule (i. e. to the passage from a certain energy level to another one) and it is proportional to the vibrational or rotational energy of the scattered molecules.

This process of energy exchange between scattering molecules and the incident light is the Raman effect (Raman C.V., 1928). In Raman scattering, the energies of the incident and scattered photons are different. A simplified energy diagram that illustrates these concepts is given in Fig. 5.3.

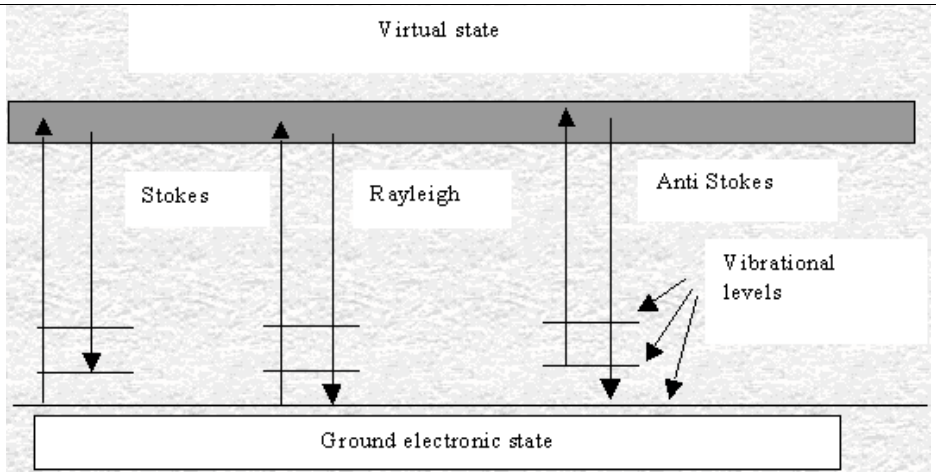

Fig. 5.3. Schematic representation of Rayeling scattering and Raman scattering (Stokes and Anti-Stokes)

When inelastic scattering happens two cases are possible:

1) the photon loses energy and the molecule changes from a lower to an upper energy level (Stokes scattering);

2) the photon gains energy and the molecule changes from an upper to a lower energy level (anti-Stokes scattering).

Both processes are simultaneously possible. However Stokes peaks are more intense than anti-Stokes peaks. Raman scattering is proportional to the population of the initial energy level. In fact, when the molecules of the target sample are in thermal equilibrium, the populations are given by the Boltzmann distribution, which states that lower energy levels are more populated.

5.4.2. Application of Raman spectroscopy in biochemistry

Raman spectroscopy is commonly used in chemistry, since vibrational information is specific to the chemical bonds and symmetry of molecules. It therefore provides a fingerprint by which the molecule can be identified (chemical identification). Functional groups of a molecule have vibrational frequencies, characteristic for each group, in well defined frequency regions of the spectrum. The fingerprint region of organic molecules is in the range 500-2000 cm^{-1}.

Raman spectroscopy is a well-established technique, successfully utilized in the structural characterization of nucleic acids. Laser Raman spectroscopy was first demonstrated as an effective experimental probe of nucleic acid constituents by

Richard C. Lord and co-workers (Lord RC, 1997). Thereafter, Raman methods were implemented in many laboratories to study native and model nucleic acid structures (Ashikawa *et al.*, 1983; Hartman *et al.*, 1973). Applications of Raman spectroscopy for investigation of nucleic acids and their biological complexes have continued to increase in number and diversity up to the present time (Benevides and Thomas, 2005; Benevides *et al.*, 1984; Murza *et al.*, 2003; Overman *et al.*, 1998; Reipa *et al.*, 2007; Thomas and Prescott, 1977; Vachousek J., 2008). For a recent review see (Benevides J. M., 2005).

Earlier studies have established the relationship between double-helical structures and Raman band frequencies (Benevides and Thomas, 1983; Thomas G. A., 1983), providing the basis for conformational marker bands. Experiments with model compounds and theoretical normal-mode calculations have enabled Raman band assignment to specific regions of the double helix. Subsequent studies have confirmed this method as a sensitive probe of phosphodiester torsion angles, sugar pucker, stacking geometry, and hydrogen bonding (Thomas, 1999). Investigations of ultrastable RNA tetraloops have established a Raman marker database that can be used for analysis of other structures such as internal loops or bulges (Baumruk *et al.*, 2001; Leulliot *et al.*, 1999).

5.4.3. Structural analysis of viroid with Raman spectroscopy

Raman spectra of the viroid have been recorded using a Raman setup home-built at AnBioPhy (UPMC, Paris). Excitation light at 780 nm was provided by a continuous-wave Ti:Sapphire laser (Spectra Physics, model 3900S) pumped by an argon-ion laser (Spectra Physics Stabilite 2017). Excitation power was attenuated by a neutral density filter to 300 mW in the sample compartment. Laser light was focused into the sample thermostabilized cell (2x2x4 mm) by an objective (Olympus MA10, $10^{\times}$, NA=0.25), which also collected the back-scattered Raman signal and delivered it onto the spectrograph (Acton SpectraPro 2500i) coupled with a deep-depletion back-illuminated CCD camera with liquid nitrogen cooling (Princeton Instruments SPEC-10 400BR/LN). Raman light was focused into the spectrometer's entrance slit (30 µm) by an achromatic lens with f = 75 mm. Spectral resolution was around 5 cm^{-1}. Raman signal was separated from laser light by two Semrock RazorEdge long pass filters (grade "U"). One filter, with λ_{laser}=780 nm, was placed

perpendicularly to the optical beam just before the focusing lens; another one, with λ_{laser} =830 nm, was used as a dichroic beamsplitter at an angle of incidence 45º: it reflected laser light at 780 nm and transmitted all the wavelengths longer than 785 nm. Raman spectra were acquired with WinSpec software; further treatment was performed using Igor Pro for Windows software. Raman spectra were accumulated with an exposure time of 1-3 sec each, and 100-300 spectra were normally averaged to produce the final spectrum at accumulation time of 5 minutes. The resulting spectra were then corrected for the signal originating from PBS, quartz cell and all the optical elements located along the detection pathway.

Viroid Raman spectra were measured during a self-cleavage reaction.

Raman experiments were performed by following the same protocol as CD experiments (1.3.4). In this case, the final concentration of the RNA was 300µM (25µg/µl) in a final volume of 20µl.

5.5. Preparation of trans-acting hammerhead ribozyme

5.5.1. Ribozyme and substrate template

Oligonucleotides for the *in vitro* transcription of catalytic (CAT) and substrate (SUB) subunits were synthetically prepared by Biomers. The cDNA sequences corresponding to SUB and CAT, preceded by the T7 promoter sequence (in bold), and the respective primers for their amplification are shown below.

Oligonucleotide DNA SUB: 125nt
5'-CCG**TAATACGACTCACTATAGG**GAATTGGAGATACATATGGGTGTAA GCCGCTCTAGAACTAGTCATACCCCCAACATAAAGTCTGTAACCGAAGAG TCTGCGCTACATCCAGAATCACTTCTAT -3'

Table 5.3. DNA sequence of SUB. In bold the T7 promoter sequence

Name	Sequence	Lenght	Tm	GC
Pr Fw **Rbz-Fwd**	5'- CCG**TAATACGACTCAC** -3'	16 mer	48°C	50%
Pr Rev **Sub-rev**	5'- ATAGAAGTGATTCTGG -3'	16 mer	44°C	37.5%

Table 5.4. Primers used for the amplification of SUB

Oligonucleotide DNA CAT (Rbz): 70nt
5'-CCG**TAATACGACTCACTATAGG**GATGTATAAGCGCACTGATGAGTCTCT GAGATGAGACGAAACTCTTCG-3'

Table 5.5. DNA sequence of CAT. In bold the T7 promoter sequence

Name	Sequence	Lenght	Tm	GC
Pr Fw **Rbz-Fwd**	5'- CCG**TAATACGACTCAC** -3'	16 mer	48°C	50%
Pr Rev **Rbz-rev**	5'- CGAAGAGTTTCGTCTC -3'	16 mer	48°C	50%

Table 5.6. Primers used for the amplification of CAT

5.5.2. PCR and *in vitro* transcription reactions

To generate templates for *in vitro* transcription, PCR reactions were performed in a final reaction volume of 50 µl. The mix of reaction was composed by 50 ng of DNA template, 0.2 mM of dNTPs, 0.4 µM of each primer, 1.5 mM of Mg^{2+}, 1.25 units of Taq DNA polymerase, 1 X Taq-buffer. After an initial heating at 95°C for 2 min, the amplification profile (25 cicles) was 30 sec at 95°C, 30 sec at 44 °C, 1 min at 72°C, with a final extention of 10 min at 72°C. After performing reactions, PCR products were controlled on 1.5 % agarose gels, ethanol-precipitated, and

resuspended in sterile ddH_2O. Taq polymerase with relevant 10X buffer and dNTPs were all from FERMENTAS.

PCR products were *in vitro* transcribed by T7 RNA polymerase. The reaction was carried out at 37°C for 2h in a final volume of 20 µl, containing the following components: 500 ng of PCR product, 40 units of T7 RNA polymerase, 2 mM of NPTs, 20 units of RNase-Inhibitor, 1X transcription buffer. Template DNA was enzimatically removed by 2 U of DNase I (1 h at 37°C, followed by 10 min at 65°C and quickly at 4°C to inactivate the enzyme). T7 RNA polymerase with relevant 10X buffer, NPTs, RNase-Inhibitor and DNase I were all from ROCHE.

Several transcriptions were joined to obtain a final volume of about 1 ml, ethanol precipitated, and resuspended in 100 µl of sterile ddH_2O. Following the addition of one volume of a 2X "stop solution" (50% formamide, 8 M Urea, 50 mM EDTA pH 8, 0.025% bromophenol blue), both CAT and SUB transcription products were gel purified on denaturing (7M urea) polyacrylamide (10%) gels and eluted over night at 4°C in 0.3M Na-acetate pH 5.2 and 10mM EDTA. Polyacrylamide gels for CAT and SUB analysis and extraction were the same than previous described for ASBVd. The RNA was separated from polyacrylamide passing the mixture through a 0.2 µm filter. After the addition of glycogen (10µg/µl), RNA was ethanol precipitated and resuspended in water. RNA concentration was than checked by UV-adsorption at 260 nm.

5.6. Trans-acting cleavage reaction

Trans-acting cleavage reactions were performed following a standard protocol (Zimmermann and Ohlenbeck, 1998; Fedor, 2004). Ribozyme and substrate were heated separately at 95°C for 30 sec and then cooled to the reaction temperature of 37°C. This step was performed in water in a final volume of 20 µl, were both CAT and SUB concentrations were 2.5X the final desiderated concentration. At this temperature, 5 µl of 5X "reaction buffer" (final concentration 50 mM NaHEPES pH 7.5, 0.1 mM EDTA, 10 mM Mg^{2+}) were added to both the ribozyme and substrate solutions. After 10 min of pre-incubation in 1X "reaction buffer", a little aliquot of substrate (1 µl) was mixed with the "stop solution" for a sample at time-point "t=0". After than, ribozyme and substrate solutions were mixed to start the reaction. In the

final volume of 50 µl the concentration of CAT and SUB were respectively 923 nM and 6 µM in (CAT=6.5 fold lower than SUB).

At different time-points the cleavage reaction was stopped mixing 5 µl of the reaction solution with 35 µl of the stop solution. Samples were loaded on a denaturant 10% acrylamide gel and run for 2.5 hours in order to separate well substrate and products. After ethidium bromide staining the efficiency, and the relative percentage, of cleavage at each time point were calculated by the formula $E = [I_2/(I_1+I_2)]x100$ where E was the efficiency of cleavage, I_1 and I_2 the intensity of the gel bands corresponding to the entire substrate and to the 5' fragment of cleavage respectively, quantified with Quantity One software (BioRad). The 3' fragment of cleavage was run out from gel in order to separate well the other fragments.

5.7. Study on the effect of high temperature in presence/absence of Lys-Lys

To verify the effect of the high temperature on the activity of the trans-acting ribozyme the catalytic subunit was stressed at 80°C for 0, 4, 6 and 12 hours in presence of water or in presence of the dipeptyde Lys-Lys. Catalytic subunit was heated at 95°C for 30 sec and then slowly cooled to 37°C. After than, it was divided in four tubes (10 µl each tube). In two of them (Lys-Lys control and stress) 10 µl of a 2X solution of Lys-Lys were added, in order to have a final Lys-Lys concentration of 110.4 µM in 20 µl. Thus, there was 1 Lys-Lys molecule for each nucleotide of RNA, whose concentration in 20 µl was 2.3 µM. In the experiments performed with 2 Lys-Lys molecules for each nucleotide of RNA 10 µl of a solution 4X of Lys-Lys was added to CAT. In the other two tubes (water control and stress) the same volume of water was added. After 15 min of RNA CAT incubation in Lys-Lys or water, the tubes "stress" (Lys-Lys/S and water/S) were put at 80°C. The tubes "control" (Lys-Lys/C and water/C) were maintained at 37°C for all the time of the stress. The time of stress chosen were 0h (any stress), 4h, 6h, 12h, 17h. After the stress, all the tubes (water and Lys-Lys, C and S) were put in ice for 5 sec and trans-cleaving kinetics were performed as previous described.

The residual activity of the catalytic molecules after stress were compared with the activity of the respective control. The residual activity of the ribozyme were

calculated on the base of the percentage of cleavage reached at plateau, in particular by the ratio between the percentage of cleavage reached at plateau by the stressed catalytic molecules and their respective control:

(Cleavage % at plateau CAT Stress)/ (Cleavage % at plateau CAT Control)

5.8. Analysis of predicted RNA secondary structures

Analysis of the theoretical structures of (+) and (-) mASBVd transcripts and calculation of the relative energies were performed with the Mfold software (Mathews *et al.*, 1999; Zuker, 2003). The secondary structure of CAT and SUB of the trans-acting constructed system was analyzed with RNAcofold software (Bernhart *et al.*, 2006; I.L. Hofacker, 1994), that allow us to predict the RNA secondary structure of two separated RNA sequences.

5.9. Statistics

All experiments were performed at least in triplicate. Error bars indicate standard deviation from mean of three independent measurements.

6. References

Abdelkafi, M., N. Leulliot, V. Baumruk, L. Bednarova, P.Y. Turpin, A. Namane, C. Gouyette, T. Huynh-Dinh, and M. Ghomi. 1998. Structural features of the UCCG and UGCG tetraloops in very short hairpins as evidenced by optical spectroscopy. Biochemistry 37:7878-84.

Amari, K., G. Gomez, A. Myrta, B. Di Terlizzi, and V. Pallas. 2001. The molecular characterization of 16 new sequence variants of Hop stunt viroid reveals the existence of invariable regions and a conserved hammerhead-like structure on the viroid molecule. J Gen Virol 82:953-62.

Ambros, S., C. Hernandez, J.C. Desvignes, and R. Flores. 1998. Genomic structure of three phenotypically different isolates of peach latent mosaic viroid: implications of the existence of constraints limiting the heterogeneity of viroid quasispecies. J Virol 72:7397-406.

Ashikawa, I., K. Kinosita, Jr., A. Ikegami, Y. Nishimura, M. Tsuboi, K. Watanabe, K. Iso, and T. Nakano. 1983. Internal motion of deoxyribonucleic acid in chromatin. Nanosecond fluorescence studies of intercalated ethidium. Biochemistry 22:6018-26.

Bachmann, P.A., P.L. Luisi, and J. Lang. 1991. Self-replicating Reverse Micelles. CHIMIA International Journal for Chemistry 45:266-268.

Bartel, D.P., and J.W. Szostak. 1993. Isolation of new ribozymes from a large pool of random sequences [see comment]. Science 261:1411-8.

Bashan, A., and A. Yonath. 2008. Correlating ribosome function with high-resolution structures. Trends Microbiol 16:326-35.

Baulcombe, D. 2004. RNA silencing in plants. Nature 431:356-63.

Baumruk, V., C. Gouyette, T. Huynh-Dinh, J.S. Sun, and M. Ghomi. 2001. Comparison between CUUG and UUCG tetraloops: thermodynamic stability and structural features analyzed by UV absorption and vibrational spectroscopy. Nucleic Acids Res 29:4089-96.

Baumstark, T., A.R. Schroder, and D. Riesner. 1997. Viroid processing: switch from cleavage to ligation is driven by a change from a tetraloop to a loop E conformation. EMBO J 16:599-610.

Bean, H.D., Y. Sheng, J.P. Collins, F.A. Anet, J. Leszczynski, and N.V. Hud. 2007. Formation of a beta-pyrimidine nucleoside by a free pyrimidine base and ribose in a plausible prebiotic reaction. J Am Chem Soc 129:9556-7.

Beaudry, D., F. Busiere, F. Lareau, C. Lessard, and J.P. Perreault. 1995. The RNA of both polarities of the peach latent mosaic viroid self-cleaves in vitro solely by single hammerhead structures. Nucleic Acids Res 23:745-52.

Bell AF, H.L., Barron LD (1997) 1997. J am Chem Soc 119:6006-6013.

Benevides J. M., O.S.A., George T.J. Jr. 2005. Raman, polarized Raman and ultraviolet resonance Raman spectroscopy of nucleic acids and their complexes. J. Raman Spectrosc. 36:279-299.

Benevides, J.M., and G.J. Thomas, Jr. 1983. Characterization of DNA structures by Raman spectroscopy: high-salt and low-salt forms of double helical poly(dG-dC) in H2O and D2O solutions and application to B, Z and A-DNA. Nucleic Acids Res 11:5747-61.

Benevides, J.M., and G.J. Thomas, Jr. 2005. Local conformational changes induced in B-DNA by ethidium intercalation. Biochemistry 44:2993-9.

Benevides, J.M., M. Tsuboi, J.K. Bamford, and G.J. Thomas, Jr. 1997. Polarized Raman spectroscopy of double-stranded RNA from bacteriophage phi6: local Raman tensors of base and backbone vibrations. Biophys J 72:2748-62.

Benevides, J.M., A.H. Wang, G.A. van der Marel, J.H. van Boom, A. Rich, and G.J. Thomas, Jr. 1984. The Raman spectra of left-handed DNA oligomers incorporating adenine-thymine base pairs+. Nucleic Acids Res 12:5913-25.

Benevides, J.M., A.H. Wang, A. Rich, Y. Kyogoku, G.A. van der Marel, J.H. van Boom, and G.J. Thomas, Jr. 1986. Raman spectra of single crystals of r(GCG)d(CGC) and d(CCCCGGGG) as models for A DNA, their structure transitions in aqueous solution, and comparison with double-helical poly(dG).poly(dC). Biochemistry 25:41-50.

Bernal, (ed.) 1951. The Physical Basis of Life, London.

Bernhart, S.H., H. Tafer, U. Muckstein, C. Flamm, P.F. Stadler, and I.L. Hofacker. 2006. Partition function and base pairing probabilities of RNA heterodimers. Algorithms Mol Biol 1:3.

Biondi, E., S. Branciamore, M.C. Maurel, and E. Gallori. 2007a. Montmorillonite protection of an UV-irradiated hairpin ribozyme: evolution of the RNA world in a mineral environment. BMC Evol Biol 7 Suppl 2:S2.

Biondi, E., S. Branciamore, L. Fusi, S. Gago, and E. Gallori. 2007b. Catalytic activity of hammerhead ribozymes in a clay mineral environment: implications for the RNA world. Gene 389:10-8.

Blount, K.F., and O.C. Uhlenbeck. 2005. The structure-function dilemma of the hammerhead ribozyme. Annu Rev Biophys Biomol Struct 34:415-40.

Boller, T., and S.Y. He. 2009. Innate immunity in plants: an arms race between pattern recognition receptors in plants and effectors in microbial pathogens. Science 324:742-4.

Boots, J.L., M.D. Canny, E. Azimi, and A. Pardi. 2008. Metal ion specificities for folding and cleavage activity in the Schistosoma hammerhead ribozyme. RNA 14:2212-22.

Branch, A.D., and H.D. Robertson. 1984. A replication cycle for viroids and other small infectious RNA's. Science 223:450-5.

Breaker, R.R., and G.F. Joyce. 1995. Self-incorporation of coenzymes by ribozymes. J Mol Evol 40:551-8.

Briones, C., M. Stich, and S.C. Manrubia. 2009. The dawn of the RNA World: toward functional complexity through ligation of random RNA oligomers. RNA 15:743-9.

Brodersen, P., and O. Voinnet. 2006. The diversity of RNA silencing pathways in plants. Trends Genet 22:268-80.

Bruening, G. 1989. Compilation of self-cleaving sequences from plant virus satellite RNAs and other sources. Methods Enzymol 180:546-58.

Bryant, D.E., and T.P. Kee. 2006. Direct evidence for the availability of reactive, water soluble phosphorus on the early Earth. H-phosphinic acid from the Nantan meteorite. Chem Commun (Camb):2344-6.

Buzayan, J.M., W.L. Gerlach, and G. Bruening. 1986. Satellite tobacco ringspot virus RNA: A subset of the RNA sequence is sufficient for autolytic processing. Proc Natl Acad Sci U S A 83:8859-8862.

Cairns-Smith, A.G. 1966. The origin of life and the nature of the primitive gene. J Theor Biol 10:53-88.

Canny, M.D., F.M. Jucker, and A. Pardi. 2007. Efficient ligation of the Schistosoma hammerhead ribozyme. Biochemistry 46:3826-34.

Canny, M.D., F.M. Jucker, E. Kellogg, A. Khvorova, S.D. Jayasena, and A. Pardi. 2004. Fast cleavage kinetics of a natural hammerhead ribozyme. J Am Chem Soc 126:10848-9.

Carbonell, A., A.E. Martinez de Alba, R. Flores, and S. Gago. 2008. Double-stranded RNA interferes in a sequence-specific manner with the infection of representative members of the two viroid families. Virology 371:44-53.

Carthew, R.W., and E.J. Sontheimer. 2009. Origins and Mechanisms of miRNAs and siRNAs. Cell 136:642-55.

Cech, T.R., A.J. Zaug, and P.J. Grabowski. 1981. In vitro splicing of the ribosomal RNA precursor of Tetrahymena: involvement of a guanosine nucleotide in the excision of the intervening sequence. Cell 27:487-96.

Chan, S.W.L., Henderson, I. R., and Jacobsen, S. E. 2004. Gardening the genome: DNA methylation in Arabidopsis thaliana. Nat. Rev. Genet. 6:351-360.

Chen, X., N. Li, and A.D. Ellington. 2007. Ribozyme catalysis of metabolism in the RNA world. Chem Biodivers 4:633-55.

Cochrane, J.C., and S.A. Strobel. 2008. Catalytic strategies of self-cleaving ribozymes. Acc Chem Res 41:1027-35.

Cochrane, J.C., S.V. Lipchock, and S.A. Strobel. 2007. Structural investigation of the GlmS ribozyme bound to Its catalytic cofactor. Chem Biol 14:97-105.

Coleman, T.M., and F. Huang. 2002. RNA-catalyzed thioester synthesis. Chem Biol 9:1227-36.

Costanzo, G., S. Pino, F. Ciciriello, and E. Di Mauro. 2009. Generation of long RNA chains in water. J Biol Chem.

Costanzo, G., R. Saladino, C. Crestini, F. Ciciriello, and E. Di Mauro. 2007. Formamide as the main building block in the origin of nucleic acids. BMC Evol Biol 7 Suppl 2:S1.

Cote, F., and J.P. Perreault. 1997. Peach latent mosaic viroid is locked by a 2',5'-phosphodiester bond produced by in vitro self-ligation. J Mol Biol 273:533-43.

Cote, F., D. Levesque, and J.P. Perreault. 2001. Natural 2',5'-phosphodiester bonds found at the ligation sites of peach latent mosaic viroid. J Virol 75:19-25.

Crick, F. 1970. Central dogma of molecular biology. Nature 227:561-3.

Crick, F.H. 1968. The origin of the genetic code. J Mol Biol 38:367-79.

Curtis, E.A., and D.P. Bartel. 2001. The hammerhead cleavage reaction in monovalent cations. RNA 7:546-52.

Daros, J.A., and R. Flores. 2002. A chloroplast protein binds a viroid RNA in vivo and facilitates its hammerhead-mediated self-cleavage. EMBO J 21:749-59.

Daros, J.A., J.F. Marcos, C. Hernandez, and R. Flores. 1994. Replication of avocado sunblotch viroid: evidence for a symmetric pathway with two rolling circles and hammerhead ribozyme processing. Proc Natl Acad Sci U S A 91:12813-7.

Davies, C., C.C. Sheldon, and R.H. Symons. 1991. Alternative hammerhead structures in the self-cleavage of avocado sunblotch viroid RNAs. Nucleic Acids Res 19:1893-8.

De la Pena, M., and R. Flores. 2002. Chrysanthemum chlorotic mottle viroid RNA: dissection of the pathogenicity determinant and comparative fitness of symptomatic and non-symptomatic variants. J Mol Biol 321:411-21.

de la Pena, M., B. Navarro, and R. Flores. 1999. Mapping the molecular determinant of pathogenicity in a hammerhead viroid: a tetraloop within the in vivo branched RNA conformation. Proc Natl Acad Sci U S A 96:9960-5.

De la Pena, M., S. Gago, and R. Flores. 2003. Peripheral regions of natural hammerhead ribozymes greatly increase their self-cleavage activity. EMBO J 22:5561-70.

Delgado, S., A.E. Martinez de Alba, C. Hernandez, and R. Flores. 2005. A short double-stranded RNA motif of Peach latent mosaic viroid contains the initiation and the self-cleavage sites of both polarity strands. J Virol 79:12934-43.

Demmig, B., and H. Gimmler. 1983. Properties of the Isolated Intact Chloroplast at Cytoplasmic K Concentrations : I. Light-Induced Cation Uptake into Intact Chloroplasts is Driven by an Electrical Potential Difference. Plant Physiol 73:169-174.

Dickson, E., H.D. Robertson, C.L. Niblett, R.K. Horst, and M. Zaitlin. 1979. Minor differences between nucleotide sequences of mild and severe strains of potato spindle tuber viroid. Nature 277:60-62.

Diener, T.O. 1989. Circular RNAs: relics of precellular evolution? Proc Natl Acad Sci U S A 86:9370-4.

Diener, T.O. 2001. The viroid: biological oddity or evolutionary fossil? Adv Virus Res 57:137-84.

Diener, T.O. 2003. Discovering viroids--a personal perspective. Nat Rev Microbiol 1:75-80.

Ding, B. 2009a. The biology of viroid-host interactions. Annu Rev Phytopathol 47:105-31.

Ding, B., and A. Itaya. 2007. Viroid: a useful model for studying the basic principles of infection and RNA biology. Mol Plant Microbe Interact 20:7-20.

Ding, B., M.O. Kwon, R. Hammond, and R. Owens. 1997. Cell-to-cell movement of potato spindle tuber viroid. Plant J 12:931-6.

Ding, B., X. Zhong. 2009b. Viroids/Virusoids Elsevier, Amsterdam.

Ding, D. 2004. A simplified algorithm for second-order sound beams with arbitrary source distribution and geometry. J Acoust Soc Am 115:35-7.

Ding, S.W., and O. Voinnet. 2007. Antiviral immunity directed by small RNAs. Cell 130:413-26.

Dunoyer, P., and O. Voinnet. 2005. The complex interplay between plant viruses and host RNA-silencing pathways. Curr Opin Plant Biol 8:415-23.

Ekland, E.H., and D.P. Bartel. 1996. RNA-catalysed RNA polymerization using nucleoside triphosphates. Nature 382:373-6.

Ekwall, K. 2004. The RITS complex-A direct link between small RNA and heterochromatin. Mol Cell 13:304-5.

Ellington, A.D., and J.W. Szostak. 1990. In vitro selection of RNA molecules that bind specific ligands. Nature 346:818-22.

Erfurth, S.C., E.J. Kiser, and W.L. Peticolas. 1972. Determination of the backbone structure of nucleic acids and nucleic acid oligomers by laser Raman scattering. Proc Natl Acad Sci U S A 69:938-41.

Evans, D., S.M. Marquez, and N.R. Pace. 2006. RNase P: interface of the RNA and protein worlds. Trends Biochem Sci 31:333-41.

Fadda, Z., J.A. Daros, R. Flores, and N. Duran-Vila. 2003a. Identification in eggplant of a variant of citrus exocortis viroid (CEVd) with a 96 nucleotide duplication in the right terminal region of the rod-like secondary structure. Virus Res 97:145-9.

Fadda, Z., J.A. Daros, C. Fagoaga, R. Flores, and N. Duran-Vila. 2003b. Eggplant latent viroid, the candidate type species for a new genus within the family Avsunviroidae (hammerhead viroids). J Virol 77:6528-32.

Fedor, M.J. 2000. Structure and function of the hairpin ribozyme. J Mol Biol 297:269-91.
Fedor, M.J., and J.R. Williamson. 2005. The catalytic diversity of RNAs. Nat Rev Mol Cell Biol 6:399-412.
Fels, A., K. Hu, and D. Riesner. 2001. Transcription of potato spindle tuber viroid by RNA polymerase II starts predominantly at two specific sites. Nucleic Acids Res 29:4589-97.
Ferris, J.P. 2002. Montmorillonite catalysis of 30-50 mer oligonucleotides: laboratory demonstration of potential steps in the origin of the RNA world. Orig Life Evol Biosph 32:311-32.
Ferris, J.P. 2006. Montmorillonite-catalysed formation of RNA oligomers: the possible role of catalysis in the origins of life. Philos Trans R Soc Lond B Biol Sci 361:1777-86; discussion 1786.
Ferris, J.P., and G. Ertem. 1993. Montmorillonite catalysis of RNA oligomer formation in aqueous solution. A model for the prebiotic formation of RNA. J Am Chem Soc 115:12270-5.
Fish, S.R., K.A. Hartman, G.J. Stubbs, and G.J. Thomas, Jr. 1981. Structural studies of tobacco mosaic virus and its components by laser Raman spectroscopy. Biochemistry 20:7449-57.
Flores, R. 1989. Synthesis of RNAs Specific to Citrus Exocortis Viroid by a Fraction Rich in Nuclei from Infected Gynura aurantiaca: Examination of the Nature of the Products and Solubilization of the Polymerase-Template Complex. J Gen Virol 70:2695-2706.
Flores, R., J.A. Daros, and C. Hernandez. 2000. Avsunviroidae family: viroids containing hammerhead ribozymes. Adv Virus Res 55:271-323.
Flores, R., C. Hernandez, M. de la Pena, A. Vera, and J.A. Daros. 2001. Hammerhead ribozyme structure and function in plant RNA replication. Methods Enzymol 341:540-52.
Flores, R., C. Hernandez, A.E. Martinez de Alba, J.A. Daros, and F. Di Serio. 2005. Viroids and viroid-host interactions. Annu Rev Phytopathol 43:117-39.
Flores, R., S. Delgado, M.E. Gas, A. Carbonell, D. Molina, S. Gago, and M. De la Pena. 2004. Viroids: the minimal non-coding RNAs with autonomous replication. FEBS Lett 567:42-8.
Forster, A.C., and R.H. Symons. 1987. Self-cleavage of plus and minus RNAs of a virusoid and a structural model for the active sites. Cell 49:211-20.
Forster, A.C., C. Davies, C.C. Sheldon, A.C. Jeffries, and R.H. Symons. 1988. Self-cleaving viroid and newt RNAs may only be active as dimers. Nature 334:265-7.
Franchi, M., and E. Gallori. 2005. A surface-mediated origin of the RNA world: biogenic activities of clay-adsorbed RNA molecules. Gene 346:205-14.
Fuller, W.D., R.A. Sanchez, and L.E. Orgel. 1972. Studies in prebiotic synthesis: VII. Solid-state synthesis of purine nucleosides. J Mol Evol 1:249-57.
Gallori, E., E. Biondi, and S. Branciamore. 2006. Looking for the primordial genetic honeycomb. Orig Life Evol Biosph 36:493-9.
Gallori, E., M. Bazzicalupo, L.D. Canto, R. Fani, P. Nannipieri, C. Vettori, and G. Stotzky. 1994. Transformation of Bacillus subtilis by DNA bound on clay in non-sterile soil. FEMS Microbiology Ecology 15:119-126.
Gesteland, R.F., T.R., Cech, J.F. Atkins. 2006. The RNA World Cold Spring Harbor Laboratory Press, New York.
Gilbert, W. 1986. Origin of life: The RNA world. Nature 319:618-618.

Gomez, G., G. Martinez, and V. Pallas. 2008. Viroid-induced symptoms in Nicotiana benthamiana plants are dependent on RDR6 activity. Plant Physiol 148:414-23.

Gomez, G., G. Martinez, and V. Pallas. 2009. Interplay between viroid-induced pathogenesis and RNA silencing pathways. Trends Plant Sci 14:264-9.

Gora-Sochacka, A. 2004. Viroids: unusual small pathogenic RNAs. Acta Biochim Pol 51:587-607.

Guerrier-Takada, C., K. Gardiner, T. Marsh, N. Pace, and S. Altman. 1983. The RNA moiety of ribonuclease P is the catalytic subunit of the enzyme. Cell 35:849-57.

Günter von, K. 1986. A Self-Replicating Hexadeoxynucleotide. Angewandte Chemie International Edition in English 25:932-935.

Haldane, J.B.S. 1929. The Origin of Life. Rationalist Annu. :148-169.

Ham, B.K., J.L. Brandom, B. Xoconostle-Cazares, V. Ringgold, T.J. Lough, and W.J. Lucas. 2009. A polypyrimidine tract binding protein, pumpkin RBP50, forms the basis of a phloem-mobile ribonucleoprotein complex. Plant Cell 21:197-215.

Hanczyc, M.M., and J.W. Szostak. 2004. Replicating vesicles as models of primitive cell growth and division. Curr Opin Chem Biol 8:660-4.

Hanczyc, M.M., S.M. Fujikawa, and J.W. Szostak. 2003. Experimental models of primitive cellular compartments: encapsulation, growth, and division. Science 302:618-22.

Hansen, J.L., T.M. Schmeing, P.B. Moore, and T.A. Steitz. 2002. Structural insights into peptide bond formation. Proc Natl Acad Sci U S A 99:11670-5.

Hanus, J.S., J., Turpin, P.Y., Bok, J. 1999. Formation and stability of nucleotide complexes: Raman titration investigation. J. Mol. Struct. 480/481:437-442.

Hartman, K.A., N. Clayton, and G.J. Thomas, Jr. 1973. Studies of viral structure by Raman spectroscopy. I. R17 virus and R17 RNA. Biochem Biophys Res Commun 50:942-9.

Hartmann, E., and R.K. Hartmann. 2003. The enigma of ribonuclease P evolution. Trends Genet 19:561-9.

Haseloff, J., and W.L. Gerlach. 1988. Simple RNA enzymes with new and highly specific endoribonuclease activities. Nature 334:585-91.

Hayden, E.J., and N. Lehman. 2006. Self-assembly of a group I intron from inactive oligonucleotide fragments. Chem Biol 13:909-18.

Heckman, J.E., D. Lambert, and J.M. Burke. 2005. Photocrosslinking detects a compact, active structure of the hammerhead ribozyme. Biochemistry 44:4148-56.

Hernandez, C., and R. Flores. 1992. Plus and minus RNAs of peach latent mosaic viroid self-cleave in vitro via hammerhead structures. Proc Natl Acad Sci U S A 89:3711-5.

Hobro, A.J., M. Rouhi, E.W. Blanch, and G.L. Conn. 2007. Raman and Raman optical activity (ROA) analysis of RNA structural motifs in Domain I of the EMCV IRES. Nucleic Acids Res 35:1169-77.

Huang, F., and M. Yarus. 1997. 5'-RNA self-capping from guanosine diphosphate. Biochemistry 36:6557-63.

Huang, W., and J.P. Ferris. 2003. Synthesis of 35-40 mers of RNA oligomers from unblocked monomers. A simple approach to the RNA world. Chem Commun (Camb):1458-9.

Huang, W., and J.P. Ferris. 2006. One-step, regioselective synthesis of up to 50-mers of RNA oligomers by montmorillonite catalysis. J Am Chem Soc 128:8914-9.

Hutchins, C.J., P.D. Rathjen, A.C. Forster, and R.H. Symons. 1986. Self-cleavage of plus and minus RNA transcripts of avocado sunblotch viroid. Nucleic Acids Res 14:3627-40.

I.L. Hofacker, W.F., P.F. Stadler, S. Bonhoeffer, M. Tacker, P. Schuster 1994. Fast Folding and Comparison of RNA Secondary

Structures. Monatshefte f. Chemie 125.

Igamberdiev, A.U., and L.A. Kleczkowski. 2001. Implications of adenylate kinase-governed equilibrium of adenylates on contents of free magnesium in plant cells and compartments. Biochem J 360:225-31.

Illangasekare, M., G. Sanchez, T. Nickles, and M. Yarus. 1995. Aminoacyl-RNA synthesis catalyzed by an RNA. Science 267:643-7.

Ingar, A.A., R.W. Luke, B.R. Hayter, and J.D. Sutherland. 2003. Synthesis of cytidine ribonucleotides by stepwise assembly of the heterocycle on a sugar phosphate. Chembiochem 4:504-7.

Itaya, A., A. Folimonov, Y. Matsuda, R.S. Nelson, and B. Ding. 2001. Potato spindle tuber viroid as inducer of RNA silencing in infected tomato. Mol Plant Microbe Interact 14:1332-4.

Itaya, A., X. Zhong, R. Bundschuh, Y. Qi, Y. Wang, R. Takeda, A.R. Harris, C. Molina, R.S. Nelson, and B. Ding. 2007. A structured viroid RNA serves as a substrate for dicer-like cleavage to produce biologically active small RNAs but is resistant to RNA-induced silencing complex-mediated degradation. J Virol 81:2980-94.

Johansen, S., and V.M. Vogt. 1994. An intron in the nuclear ribosomal DNA of Didymium iridis codes for a group I ribozyme and a novel ribozyme that cooperate in self-splicing. Cell 76:725-34.

Johansen, S., C. Einvik, and H. Nielsen. 2002. DiGIR1 and NaGIR1: naturally occurring group I-like ribozymes with unique core organization and evolved biological role. Biochimie 84:905-12.

Johnston, W.K., P.J. Unrau, M.S. Lawrence, M.E. Glasner, and D.P. Bartel. 2001. RNA-catalyzed RNA polymerization: accurate and general RNA-templated primer extension. Science 292:1319-25.

Jones-Rhoades, M.W., D.P. Bartel, and B. Bartel. 2006. MicroRNAS and their regulatory roles in plants. Annu Rev Plant Biol 57:19-53.

Joshi, P.C., S. Pitsch, and J.P. Ferris. 2007. Selectivity of montmorillonite catalyzed prebiotic reactions of D, L-nucleotides. Orig Life Evol Biosph 37:3-26.

Joyce, G.F. 2004. Directed evolution of nucleic acid enzymes. Annu Rev Biochem 73:791-836.

Keese, P., and R.H. Symons. 1985. Domains in viroids: evidence of intermolecular RNA rearrangements and their contribution to viroid evolution. Proc Natl Acad Sci U S A 82:4582-6.

Khvorova, A., A. Lescoute, E. Westhof, and S.D. Jayasena. 2003. Sequence elements outside the hammerhead ribozyme catalytic core enable intracellular activity. Nat Struct Biol 10:708-12.

Kikovska, E., S.G. Svard, and L.A. Kirsebom. 2007. Eukaryotic RNase P RNA mediates cleavage in the absence of protein. Proc Natl Acad Sci U S A 104:2062-7.

Kim, D.E., and G.F. Joyce. 2004. Cross-catalytic replication of an RNA ligase ribozyme. Chem Biol 11:1505-12.

Kim, N.K., A. Murali, and V.J. DeRose. 2005. Separate metal requirements for loop interactions and catalysis in the extended hammerhead ribozyme. J Am Chem Soc 127:14134-5.

Kisseleva, N., A. Khvorova, E. Westhof, and O. Schiemann. 2005. Binding of manganese(II) to a tertiary stabilized hammerhead ribozyme as studied by electron paramagnetic resonance spectroscopy. RNA 11:1-6.

Kolb, V.M., J.P. Dworkin, and S.L. Miller. 1994. Alternative bases in the RNA world: the prebiotic synthesis of urazole and its ribosides. J Mol Evol 38:549-57.

Kolonko, N., O. Bannach, K. Aschermann, K.H. Hu, M. Moors, M. Schmitz, G. Steger, and D. Riesner. 2006. Transcription of potato spindle tuber viroid by RNA polymerase II starts in the left terminal loop. Virology 347:392-404.

Kun, A., Maurel, M.C., Santos, M., Szathmary, E. 2006. The Aptamer Handbook Wiley-VCH.

Kypr, J., I. Kejnovska, D. Renciuk, and M. Vorlickova. 2009. Circular dichroism and conformational polymorphism of DNA. Nucleic Acids Res 37:1713-25.

Lafleur, L., J. Rice, and G.J. Thomas, Jr. 1972. Raman studies of nucleic acids. VII. Poly A-poly U and poly G-poly C. Biopolymers 11:2423-37.

Lafontaine, D., D. Beaudry, P. Marquis, and J.P. Perreault. 1995. Intra- and intermolecular nonenzymatic ligations occur within transcripts derived from the peach latent mosaic viroid. Virology 212:705-9.

Lambowitz, A.M., and S. Zimmerly. 2004. Mobile group II introns. Annu Rev Genet 38:1-35.

Lee, D.H., J.R. Granja, J.A. Martinez, K. Severin, and M.R. Ghadri. 1996. A self-replicating peptide. Nature 382:525-8.

Lee, T.S., G.M. Giambasu, C.P. Sosa, M. Martick, W.G. Scott, and D.M. York. 2009. Threshold occupancy and specific cation binding modes in the hammerhead ribozyme active site are required for active conformation. J Mol Biol 388:195-206.

Leulliot, N., V. Baumruk, M. Abdelkafi, P.Y. Turpin, A. Namane, C. Gouyette, T. Huynh-Dinh, and M. Ghomi. 1999. Unusual nucleotide conformations in GNRA and UNCG type tetraloop hairpins: evidence from Raman markers assignments. Nucleic Acids Res 27:1398-404.

Levy, M., and A.D. Ellington. 2001. The descent of polymerization. Nat Struct Biol 8:580-2.

Li, H.W., and S.W. Ding. 2005. Antiviral silencing in animals. FEBS Lett 579:5965-73.

Li, N., and F. Huang. 2005. Ribozyme-catalyzed aminoacylation from CoA thioesters. Biochemistry 44:4582-90.

Lilley, D.M. 2004. The Varkud satellite ribozyme. RNA 10:151-8.

Lincoln, T.A., and G.F. Joyce. 2009. Self-sustained replication of an RNA enzyme. Science 323:1229-32.

Lord RC, T.G. 1997. Jr. Spectrochim. Acta Part A 23.

Lorsch, J.R., and J.W. Szostak. 1994. In vitro evolution of new ribozymes with polynucleotide kinase activity. Nature 371:31-6.

Luisi, P.L., and F.J. Varela. 1989. Self-replicating micelles — A chemical version of a minimal autopoietic system. Origins of Life and Evolution of Biospheres 19:633-643.

Machida, S., N. Yamahata, H. Watanuki, R.A. Owens, and T. Sano. 2007. Successive accumulation of two size classes of viroid-specific small RNA in potato spindle tuber viroid-infected tomato plants. J Gen Virol 88:3452-7.

Mansy, S.S., J.P. Schrum, M. Krishnamurthy, S. Tobe, D.A. Treco, and J.W. Szostak. 2008. Template-directed synthesis of a genetic polymer in a model protocell. Nature 454:122-5.

Markarian, N., H.W. Li, S.W. Ding, and J.S. Semancik. 2004. RNA silencing as related to viroid induced symptom expression. Arch Virol 149:397-406.

Martick, M., and W.G. Scott. 2006. Tertiary contacts distant from the active site prime a ribozyme for catalysis. Cell 126:309-20.

Martinez de Alba, A.E., R. Flores, and C. Hernandez. 2002. Two chloroplastic viroids induce the accumulation of small RNAs associated with posttranscriptional gene silencing. J Virol 76:13094-6.

Mathews, D.H., J. Sabina, M. Zuker, and D.H. Turner. 1999. Expanded sequence dependence of thermodynamic parameters improves prediction of RNA secondary structure. J Mol Biol 288:911-40.

Matousek, J., L. Orctova, J. Ptacek, J. Patzak, P. Dedic, G. Steger, and D. Riesner. 2007a. Experimental transmission of pospiviroid populations to weed species characteristic of potato and hop fields. J Virol 81:11891-9.

Matousek, J., P. Kozlova, L. Orctova, A. Schmitz, K. Pesina, O. Bannach, N. Diermann, G. Steger, and D. Riesner. 2007b. Accumulation of viroid-specific small RNAs and increase in nucleolytic activities linked to viroid-caused pathogenesis. Biol Chem 388:1-13.

Matzke, M.A., and J.A. Birchler. 2005. RNAi-mediated pathways in the nucleus. Nat Rev Genet 6:24-35.

Meli, M., J. Vergne, and M.C. Maurel. 2003. In vitro selection of adenine-dependent hairpin ribozymes. J Biol Chem 278:9835-42.

Michel, F., and J.L. Ferat. 1995. Structure and activities of group II introns. Annu Rev Biochem 64:435-61.

Michel, F., A. Jacquier, and B. Dujon. 1982. Comparison of fungal mitochondrial introns reveals extensive homologies in RNA secondary structure. Biochimie 64:867-81.

Mittapalli, G.K., Y.M. Osornio, M.A. Guerrero, K.R. Reddy, R. Krishnamurthy, and A. Eschenmoser. 2007. Mapping the landscape of potentially primordial informational oligomers: oligodipeptides tagged with 2,4-disubstituted 5-aminopyrimidines as recognition elements. Angew Chem Int Ed Engl 46:2478-84.

Monnard, P.A. 2005. Catalysis in abiotic structured media: an approach to selective synthesis of biopolymers. Cell Mol Life Sci 62:520-34.

Motard, J., F. Bolduc, D. Thompson, and J.P. Perreault. 2008. The peach latent mosaic viroid replication initiation site is located at a universal position that appears to be defined by a conserved sequence. Virology 373:362-75.

Movileanu, L., J.M. Benevides, and G.J. Thomas, Jr. 2002. Temperature dependence of the Raman spectrum of DNA. II. Raman signatures of premelting and melting transitions of poly(dA).poly(dT) and comparison with poly(dA-dT).poly(dA-dT). Biopolymers 63:181-94.

Murray, J.B., A.A. Seyhan, N.G. Walter, J.M. Burke, and W.G. Scott. 1998. The hammerhead, hairpin and VS ribozymes are catalytically proficient in monovalent cations alone. Chem Biol 5:587-95.

Murza, A., S. Alvarez-Mendez, S. Sanchez-Cortes, and J.V. Garcia-Ramos. 2003. Interaction of antitumoral 9-aminoacridine drug with DNA and dextran sulfate studied by fluorescence and surface-enhanced Raman spectroscopy. Biopolymers 72:174-84.

Navarro, B., and R. Flores. 1997. Chrysanthemum chlorotic mottle viroid: unusual structural properties of a subgroup of self-cleaving viroids with hammerhead ribozymes. Proc Natl Acad Sci U S A 94:11262-7.

Navarro, B., V. Pantaleo, A. Gisel, S. Moxon, T. Dalmay, G. Bisztray, F. Di Serio, and J. Burgyan. 2009. Deep sequencing of viroid-derived small RNAs from grapevine provides new insights on the role of RNA silencing in plant-viroid interaction. PLoS One 4:e7686.

Navarro, J.A., and R. Flores. 2000. Characterization of the initiation sites of both polarity strands of a viroid RNA reveals a motif conserved in sequence and structure. EMBO J 19:2662-70.

Navarro, J.A., J.A. Daros, and R. Flores. 1999. Complexes containing both polarity strands of avocado sunblotch viroid: identification in chloroplasts and characterization. Virology 253:77-85.

Navarro, J.A., A. Vera, and R. Flores. 2000. A chloroplastic RNA polymerase resistant to tagetitoxin is involved in replication of avocado sunblotch viroid. Virology 268:218-25.

Nelsestuen, G.L. 1980. Origin of life: consideration of alternatives to proteins and nucleic acids. J Mol Evol 15:59-72.

Nelson, J.A., and O.C. Uhlenbeck. 2006. When to believe what you see. Mol Cell 23:447-50.

Nielsen, H., and S.D. Johansen. 2007. A new RNA branching activity: the GIR1 ribozyme. Blood Cells Mol Dis 38:102-9.

Nielsen, H., E. Westhof, and S. Johansen. 2005. An mRNA is capped by a 2', 5' lariat catalyzed by a group I-like ribozyme. Science 309:1584-7.

Nissen, P., J. Hansen, N. Ban, P.B. Moore, and T.A. Steitz. 2000. The structural basis of ribosome activity in peptide bond synthesis. Science 289:920-30.

O'Rear, J.L., S. Wang, A.L. Feig, L. Beigelman, O.C. Uhlenbeck, and D. Herschlag. 2001. Comparison of the hammerhead cleavage reactions stimulated by monovalent and divalent cations. RNA 7:537-45.

Oparin, A.I., (ed.) 1924. Proiskhozhdenie Zhizny, Moscow.

Oparin, A.I. 1965. The origin of life and the origin of enzymes. Adv Enzymol Relat Areas Mol Biol 27:347-80.

Orgel, L.E. 1968. Evolution of the genetic apparatus. J Mol Biol 38:381-93.

Orgel, L.E. 2004. Prebiotic chemistry and the origin of the RNA world. Crit Rev Biochem Mol Biol 39:99-123.

Overman, S.A., K.L. Aubrey, K.E. Reilly, O. Osman, S.J. Hayes, P. Serwer, and G.J. Thomas, Jr. 1998. Conformation and interactions of the packaged double-stranded DNA genome of bacteriophage T7. Biospectroscopy 4:S47-56.

Owens, R., and R. Hammond. 2009. Viroid Pathogenicity: One Process, Many Faces. Viruses 1:298-316.

Palukaitis, P. 1987. Potato spindle tuber viroid: Investigation of the long-distance, intra-plant transport route. Virology 158:239-41.

Pan, T., and T.R. Sosnick. 1997. Intermediates and kinetic traps in the folding of a large ribozyme revealed by circular dichroism and UV absorbance spectroscopies and catalytic activity. Nat Struct Biol 4:931-8.

Papaefthimiou, I., A. Hamilton, M. Denti, D. Baulcombe, M. Tsagris, and M. Tabler. 2001. Replicating potato spindle tuber viroid RNA is accompanied by short RNA fragments that are characteristic of post-transcriptional gene silencing. Nucleic Acids Res 29:2395-400.

Parsons, I., M.R. Lee, and J.V. Smith. 1998. Biochemical evolution II: origin of life in tubular microstructures on weathered feldspar surfaces. Proc Natl Acad Sci U S A 95:15173-6.

Pasek, M.A., and D.S. Lauretta. 2005. Aqueous corrosion of phosphide minerals from iron meteorites: a highly reactive source of prebiotic phosphorus on the surface of the early Earth. Astrobiology 5:515-35.

Paul, N., and G.F. Joyce. 2002. Inaugural Article: a self-replicating ligase ribozyme. Proc Natl Acad Sci U S A 99:12733-40.

Penedo, J.C., T.J. Wilson, S.D. Jayasena, A. Khvorova, and D.M. Lilley. 2004. Folding of the natural hammerhead ribozyme is enhanced by interaction of auxiliary elements. RNA 10:880-8.

Pino, S., F. Ciciriello, G. Costanzo, and E. Di Mauro. 2008. Nonenzymatic RNA ligation in water. J Biol Chem 283:36494-503.

Pley, H.W., K.M. Flaherty, and D.B. McKay. 1994. Three-dimensional structure of a hammerhead ribozyme. Nature 372:68-74.

Portis, A.R. 1981. Evidence of a Low Stromal Mg Concentration in Intact Chloroplasts in the Dark: I. STUDIES WITH THE IONOPHORE A23187. Plant Physiol 67:985-989.

Powner, M.W., B. Gerland, and J.D. Sutherland. 2009. Synthesis of activated pyrimidine ribonucleotides in prebiotically plausible conditions. Nature 459:239-42.

Powner, M.W., C. Anastasi, M.A. Crowe, A.L. Parkes, J. Raftery, and J.D. Sutherland. 2007. On the prebiotic synthesis of ribonucleotides: photoanomerisation of cytosine nucleosides and nucleotides revisited. Chembiochem 8:1170-9.

Prody, G.A., J.T. Bakos, J.M. Buzayan, I.R. Schneider, and G. Bruening. 1986. Autolytic Processing of Dimeric Plant Virus Satellite RNA. Science 231:1577-1580.

Pyle, A.M. 1993. Ribozymes: a distinct class of metalloenzymes. Science 261:709-14.

Pyle, A.M. 2005. Capping by branching: a new ribozyme makes tiny lariats. Science 309:1530-1.

Qi, Y., T. Pelissier, A. Itaya, E. Hunt, M. Wassenegger, and B. Ding. 2004. Direct role of a viroid RNA motif in mediating directional RNA trafficking across a specific cellular boundary. Plant Cell 16:1741-52.

Qu, F., X. Ye, G. Hou, S. Sato, T.E. Clemente, and T.J. Morris. 2005. RDR6 has a broad-spectrum but temperature-dependent antiviral defense role in Nicotiana benthamiana. J Virol 79:15209-17.

Rackwitz, H.R., W. Rohde, and H.L. Sanger. 1981. DNA-dependent RNA polymerase II of plant origin transcribes viroid RNA into full-length copies. Nature 291:297-301.

Raines, R.T. 1998. Ribonuclease A. Chem Rev 98:1045-1066.

Reanwarakorn, K., and J.S. Semancik. 1998. Regulation of pathogenicity in hop stunt viroid-related group II citrus viroids. J Gen Virol 79:3163-3171.

Reanwarakorn, K., and J.S. Semancik. 1999. Correlation of hop stunt viroid variants to cachexia and xyloporosis diseases of citrus. Phytopathology 89:568-74.

Reipa, V., G. Niaura, and D.H. Atha. 2007. Conformational analysis of the telomerase RNA pseudoknot hairpin by Raman spectroscopy. RNA 13:108-15.

Robart, A.R., and S. Zimmerly. 2005. Group II intron retroelements: function and diversity. Cytogenet Genome Res 110:589-97.

Rocheleau, G.A., and S.A. Woodson. 1994. Requirements for self-splicing of a group I intron from Physarum polycephalum. Nucleic Acids Res 22:4315-20.
Rocheleau, L., and M. Pelchat. 2006. The Subviral RNA Database: a toolbox for viroids, the hepatitis delta virus and satellite RNAs research. BMC Microbiol 6:24.
Rodio, M.E., S. Delgado, A. De Stradis, M.D. Gomez, R. Flores, and F. Di Serio. 2007. A viroid RNA with a specific structural motif inhibits chloroplast development. Plant Cell 19:3610-26.
Rodriguez, M.J., and J.W. Randles. 1993. Coconut cadang-cadang viroid (CCCVd) mutants associated with severe disease vary in both the pathogenicity domain and the central conserved region. Nucleic Acids Res 21:2771.
Rogers, J., and G.F. Joyce. 2001. The effect of cytidine on the structure and function of an RNA ligase ribozyme. RNA 7:395-404.
Roth, A., and R.R. Breaker. 1998. An amino acid as a cofactor for a catalytic polynucleotide. Proc Natl Acad Sci U S A 95:6027-31.
Roth, B.M., G.J. Pruss, and V.B. Vance. 2004. Plant viral suppressors of RNA silencing. Virus Res 102:97-108.
Ruffner, D.E., G.D. Stormo, and O.C. Uhlenbeck. 1990. Sequence requirements of the hammerhead RNA self-cleavage reaction. Biochemistry 29:10695-702.
Ruiz-Ferrer, V., and O. Voinnet. 2009. Roles of plant small RNAs in biotic stress responses. Annu Rev Plant Biol 60:485-510.
Saladino, R., C. Crestini, V. Neri, F. Ciciriello, G. Costanzo, and E. Di Mauro. 2006. Origin of informational polymers: The concurrent roles of formamide and phosphates. Chembiochem 7:1707-14.
Saladino, R., C. Crestini, F. Ciciriello, S. Pino, G. Costanzo, and E. Di Mauro. 2009. From formamide to RNA: the roles of formamide and water in the evolution of chemical information. Res Microbiol 160:441-8.
Salehi-Ashtiani, K., A. Luptak, A. Litovchick, and J.W. Szostak. 2006. A genomewide search for ribozymes reveals an HDV-like sequence in the human CPEB3 gene. Science 313:1788-92.
Sanchez, R.A., and L.E. Orgel. 1970. Studies in prebiotic synthesis. V. Synthesis and photoanomerization of pyrimidine nucleosides. J Mol Biol 47:531-43.
Sano, T., T. Candresse, R.W. Hammond, T.O. Diener, and R.A. Owens. 1992. Identification of multiple structural domains regulating viroid pathogenicity. Proc Natl Acad Sci U S A 89:10104-8.
Scappini, F., F. Casadei, R. Zamboni, M. Franchi, E. Gallori, and S. Monti. 2004. Protective effect of clay minerals on adsorbed nucleic acid against UV radiation: possible role in the origin of life. International Journal of Astrobiology 3:17-19.
Schindler, I.M., and Mühlbach, H. P. . 1992. Involvement of nuclear DNAdependent RNA polymerases in potato spindle tuber viroid replication: A reevaluation. Plant Sci. 84.
Schnell, R.J., Kuhn, D.N., Olano, C.T., Quintanilla, W.E. 2002. Sequence diversity among avocado sunblotch viroid isolated from single avocado trees. Phytoparasitica 29.
Schnolzer, M., B. Haas, K. Raam, H. Hofmann, and H.L. Sanger. 1985. Correlation between structure and pathogenicity of potato spindle tuber viroid (PSTV). EMBO J 4:2181-90.
Schrader, O., T. Baumstark, and D. Riesner. 2003. A mini-RNA containing the tetraloop, wobble-pair and loop E motifs of the central conserved region of

potato spindle tuber viroid is processed into a minicircle. Nucleic Acids Res 31:988-98.
Schutz, S., and P. Sarnow. 2006. Interaction of viruses with the mammalian RNA interference pathway. Virology 344:151-7.
Scott, W.G., J.T. Finch, and A. Klug. 1995. The crystal structure of an all-RNA hammerhead ribozyme: a proposed mechanism for RNA catalytic cleavage. Cell 81:991-1002.
Segre, D., D. Ben-Eli, D.W. Deamer, and D. Lancet. 2001. The lipid world. Orig Life Evol Biosph 31:119-45.
Semancik, J.S., and J.A. Szychowski. 1994. Avocado sunblotch disease: a persistent viroid infection in which variants are associated with differential symptoms. J Gen Virol 75 (Pt 7):1543-9.
Sheldon, C.C., and R.H. Symons. 1989. RNA stem stability in the formation of a self-cleaving hammerhead structure. Nucleic Acids Res 17:5665-77.
Sheng, Y., H.D. Bean, I. Mamajanov, N.V. Hud, and J. Leszczynski. 2009. Comprehensive Investigation of the Energetics of Pyrimidine Nucleoside Formation in a Model Prebiotic Reaction. Journal of the American Chemical Society 131:16088-16095.
Shih, I.H., and M.D. Been. 2002. Catalytic strategies of the hepatitis delta virus ribozymes. Annu Rev Biochem 71:887-917.
Sioud, M., (ed.) 2004. Ribozymes and siRNA Protocols, Vol. 252, pp. 1-19-32. Humana Press, Totowa.
Smith, J.V. 1998. Biochemical evolution. I. Polymerization On internal, organophilic silica surfaces of dealuminated zeolites and feldspars. Proc Natl Acad Sci U S A 95:3370-5.
Sosnick, T.R. 2001. Characterization of tertiary folding of RNA by circular dichroism and urea. Curr Protoc Nucleic Acid Chem Chapter 11:Unit 11 5.
Sosnick, T.R., X. Fang, and V.M. Shelton. 2000. Application of circular dichroism to study RNA folding transitions. Methods Enzymol 317:393-409.
Stage-Zimmermann, T.K., and O.C. Uhlenbeck. 1998. Hammerhead ribozyme kinetics. RNA 4:875-89.
Stahley, M.R., and S.A. Strobel. 2005. Structural evidence for a two-metal-ion mechanism of group I intron splicing. Science 309:1587-90.
Steitz, T.A., and P.B. Moore. 2003. RNA, the first macromolecular catalyst: the ribosome is a ribozyme. Trends Biochem Sci 28:411-8.
Stepanek, J., M. Vincent, P.Y. Turpin, D. Paulin, S. Fermandjian, B. Alpert, and C. Zentz. 2007. C-->G base mutations in the CArG box of c-fos serum response element alter its bending flexibility. Consequences for core-SRF recognition. FEBS J 274:2333-48.
Stern, D.S., Higgs, D.C., and Yang, J. . 1997. Transcription and translation in chloroplasts. Trends Plant Sci. 2:308-315.
Stotzky, G., E. Gallori, M. Khanna. 1996. Molecular Microbial Ecology Manual, Dordrecht.
Strobel, S.A., and J.C. Cochrane. 2007. RNA catalysis: ribozymes, ribosomes, and riboswitches. Curr Opin Chem Biol 11:636-43.
Symons, J.P., M.F. Sowers, and S.D. Harlow. 1997. Relationship of body composition measures and menstrual cycle length. Ann Hum Biol 24:107-16.
Symons, R.H. 1989. Self-cleavage of RNA in the replication of small pathogens of plants and animals. Trends Biochem Sci 14:445-50.
Szathmary, E. 1993. Coding coenzyme handles: a hypothesis for the origin of the genetic code. Proc Natl Acad Sci U S A 90:9916-20.

Szathmary, E. 1999. The origin of the genetic code: amino acids as cofactors in an RNA world. Trends Genet 15:223-9.
Tabler, M., and M. Tsagris. 2004. Viroids: petite RNA pathogens with distinguished talents. Trends Plant Sci 9:339-48.
Takeda, R., and B. Ding. 2009. Viroid Intercellular Trafficking: RNA Motifs, Cellular Factors and Broad Impacts. Viruses 1:210-221.
Teixeira, A., A. Tahiri-Alaoui, S. West, B. Thomas, A. Ramadass, I. Martianov, M. Dye, W. James, N.J. Proudfoot, and A. Akoulitchev. 2004. Autocatalytic RNA cleavage in the human beta-globin pre-mRNA promotes transcription termination. Nature 432:526-30.
Thaddeus, P. 2006. The prebiotic molecules observed in the interstellar gas. Philos Trans R Soc Lond B Biol Sci 361:1681-7.
Thomas G. A., a.P.W.L. 1983. Fluctuations in nucleic acid conformations 2. Raman spectroscopic evidence of varying ring pucker in A-T Polynucleotides. J. Am. Chem. Soc. 105:993-996.
Thomas, G.J., Jr. 1999. Raman spectroscopy of protein and nucleic acid assemblies. Annu Rev Biophys Biomol Struct 28:1-27.
Thomas, G.J., Jr., and K.A. Hartman. 1973. Raman studies of nucleic acids. 8. Estimation of RNA secondary structure from Raman scattering by phosphate-group vibrations. Biochim Biophys Acta 312:311-32.
Thomas, G.J., Jr., and B. Prescott. 1977. Secondary structure of histones and DNA in chromatin. Science 197:385-8.
Thomas, J.M., and D.M. Perrin. 2009. Probing general acid catalysis in the hammerhead ribozyme. J Am Chem Soc 131:1135-43.
Tjivikua, T., P. Ballester, and J. Rebek. 2002. Self-replicating system. Journal of the American Chemical Society 112:1249-1250.
Tsagris, M., M. Tabler, and H.L. Sanger. 1987a. Oligomeric potato spindle tuber viroid (PSTV) RNA does not process autocatalytically under conditions where other RNAs do. Virology 157:227-31.
Tsagris, M., M. Tabler, H.P. Muhlbach, and H.L. Sanger. 1987b. Linear oligomeric potato spindle tuber viroid (PSTV) RNAs are accurately processed in vitro to the monomeric circular viroid proper when incubated with a nuclear extract from healthy potato cells. EMBO J 6:2173-2183.
Tuerk, C., and L. Gold. 1990. Systematic evolution of ligands by exponential enrichment: RNA ligands to bacteriophage T4 DNA polymerase. Science 249:505-10.
Ueda, T., K. Ushizawa, and M. Tsuboi. 1993. Depolarization of Raman scattering from some nucleotides of RNA and DNA. Biopolymers 33:1791-802.
Vachousek J., S.J. 2008. Raman study of HIV TAR structural stability. Spectroscopy 22:267-277.
Vader, A., H. Nielsen, and S. Johansen. 1999. In vivo expression of the nucleolar group I intron-encoded I-dirI homing endonuclease involves the removal of a spliceosomal intron. EMBO J 18:1003-13.
Valadkhan, S. 2007. The spliceosome: a ribozyme at heart? Biol Chem 388:693-7.
Vettori, C., D. Paffetti, G. Pietramellara, G. Stotzky, and E. Gallori. 1996. Amplification of bacterial DNA bound on clay minerals by the random amplified polymorphic DNA (RAPD) technique. FEMS Microbiology Ecology 20:251-260.
Vicens, Q., and T.R. Cech. 2009. A natural ribozyme with 3',5' RNA ligase activity. Nat Chem Biol 5:97-9.

Visvader, J.E., and R.H. Symons. 1985. Eleven new sequence variants of citrus exocortis viroid and the correlation of sequence with pathogenicity. Nucleic Acids Res. 13:2907–2920.

Vitreschak, A.G., D.A. Rodionov, A.A. Mironov, and M.S. Gelfand. 2004. Riboswitches: the oldest mechanism for the regulation of gene expression? Trends Genet 20:44-50.

Vogt, U., T. Pelissier, A. Putz, F. Razvi, R. Fischer, and M. Wassenegger. 2004. Viroid-induced RNA silencing of GFP-viroid fusion transgenes does not induce extensive spreading of methylation or transitive silencing. Plant J 38:107-18.

Voinnet, O. 2005. Induction and suppression of RNA silencing: insights from viral infections. Nat Rev Genet 6:206-20.

Walde, P., R. Wick, M. Fresta, A. Mangone, and P.L. Luisi. 2002. Autopoietic Self-Reproduction of Fatty Acid Vesicles. Journal of the American Chemical Society 116:11649-11654.

Wang, M.B., X.Y. Bian, L.M. Wu, L.X. Liu, N.A. Smith, D. Isenegger, R.M. Wu, C. Masuta, V.B. Vance, J.M. Watson, A. Rezaian, E.S. Dennis, and P.M. Waterhouse. 2004. On the role of RNA silencing in the pathogenicity and evolution of viroids and viral satellites. Proc Natl Acad Sci U S A 101:3275-80.

Warrilow, D., and R.H. Symons. 1999. Citrus exocortis viroid RNA is associated with the largest subunit of RNA polymerase II in tomato in vivo. Arch Virol 144:2367-75.

Wassenegger, M., S. Heimes, L. Riedel, and H.L. Sanger. 1994. RNA-directed de novo methylation of genomic sequences in plants. Cell 76:567-76.

Weinberg, M.S., and J.J. Rossi. 2005. Comparative single-turnover kinetic analyses of trans-cleaving hammerhead ribozymes with naturally derived non-conserved sequence motifs. FEBS Lett 579:1619-24.

White, H.B. 1982. The Pyridine Nucleotide Coenzymes Academic Press, New York.

Williams, A.L., Jr., C. Cheong, I. Tinoco, Jr., and L.B. Clark. 1986. Vacuum ultraviolet circular dichroism as an indicator of helical handedness in nucleic acids. Nucleic Acids Res 14:6649-59.

Winkler, W.C., A. Nahvi, A. Roth, J.A. Collins, and R.R. Breaker. 2004. Control of gene expression by a natural metabolite-responsive ribozyme. Nature 428:281-6.

Wise, R.P., M.J. Moscou, A.J. Bogdanove, and S.A. Whitham. 2007. Transcript profiling in host-pathogen interactions. Annu Rev Phytopathol 45:329-69.

Woese. 1967. The Genetic Code Harper & Row, New York.

Woody, R.W. 1995. Circular dichroism. Methods Enzymol 246:34-71.

Yarus, M. 1993. How many catalytic RNAs? Ions and the Cheshire cat conjecture. FASEB J 7:31-9.

Young-Min, W., I. Asuka, A.O. Robert , T. Li, W.H. Rosemarie , C. Huei-Chi, M.C.L. Michael , and D. Biao. 1999. Characterization of nuclear import of potato spindle tuber viroid RNA in permeabilized protoplasts. The Plant Journal 17:627-635.

Zaher, H.S., and P.J. Unrau. 2007. Selection of an improved RNA polymerase ribozyme with superior extension and fidelity. RNA 13:1017-26.

Zanchetta, G., T. Bellini, M. Nakata, and N.A. Clark. 2008. Physical polymerization and liquid crystallization of RNA oligomers. J Am Chem Soc 130:12864-5.

Zhao, Y., R.A. Owens, and R.W. Hammond. 2001. Use of a vector based on Potato virus X in a whole plant assay to demonstrate nuclear targeting of Potato spindle tuber viroid. J Gen Virol 82:1491-7.

Zhong, X., A.J. Archual, A.A. Amin, and B. Ding. 2008. A genomic map of viroid RNA motifs critical for replication and systemic trafficking. Plant Cell 20:35-47.

Zhong, X., X. Tao, J. Stombaugh, N. Leontis, and B. Ding. 2007. Tertiary structure and function of an RNA motif required for plant vascular entry to initiate systemic trafficking. EMBO J 26:3836-46.

Zhu, Y., L. Green, Y.M. Woo, R. Owens, and B. Ding. 2001. Cellular basis of potato spindle tuber viroid systemic movement. Virology 279:69-77.

Zhu, Y., Y. Qi, Y. Xun, R. Owens, and B. Ding. 2002. Movement of potato spindle tuber viroid reveals regulatory points of phloem-mediated RNA traffic. Plant Physiol 130:138-46.

Zubay, G., and T. Mui. 2001. Prebiotic synthesis of nucleotides. Orig Life Evol Biosph 31:87-102.

Zuker, M. 2003. Mfold web server for nucleic acid folding and hybridization prediction. . Nucleic Acids Res. 31:3406-15.

Ringraziamenti

Ringrazio...

Il Prof. Enzo Gallori

La Prof. Marie-Christine Maurel, per avermi dato la possibilità di lavorare nel suo laboratorio

Il Prof. Giuseppe Zaccai, per la sua disponibilità e per l'aiuto all' Institut Laue-Langevin

Il Prof. Josef Štepánek e soprattutto il Dr. Christian Zentz ed il Dr. Sergei Kruglik, esperti di spettroscopia Raman e Dicroismo Circolare.

Il Dr. Jacque Vergne e la Dr.ssa Claire Torchet, per la loro gentilezza ed i preziosi consigli scientifici

Tutti i collaboratori e gli studenti della Prof. Maurel, in particolar modo Clémentine Delan-Forino, Hussain Kaddour, Camil Cibot e Nizar El-Murr, amici parigini, oltre che colleghi...

Il Dr. Sergio Branciamore, per i preziosi suggerimenti, anche oltreoceano

Tutti coloro che, con un aiuto tecnico, scientifico,ma anche e soprattutto morale, hanno contribuito alla realizzazione di questa tesi.

In particolare...

Luca, per l'inglese e per tutti i "Giulia respira"

Lorenzo, per la perfezione nell'uso di Photoshop

Tutto Arcetri ed in particolar modo il Prof. Emanuele Pace

Alessandro, Maurizio e Mauro, per aver reso più "leggeri" questi giorni con le (sempre più lunghe) "pause caffè"

Giacomo, compagno di avventure Parigine e di "stress tesi" (la stufina è tutta tua!)

Tutti i ragazzi e i ricercatori del Laboratorio del Prof. Buiatti (ex e non)

Marta e Martina, sempre presenti…

...Un GRAZIE infinito alla mia famiglia, per la forza, l'incoraggiamento, il sostegno, e l'aiuto…mai mancato!